



5-2008

## **Approaches to Generating Selectivity in Microcantilever Sensors**

Peter J. Chapman

*University of Tennessee - Knoxville*

Follow this and additional works at: [https://trace.tennessee.edu/utk\\_graddiss](https://trace.tennessee.edu/utk_graddiss)

 Part of the [Chemistry Commons](#)

---

### **Recommended Citation**

Chapman, Peter J., "Approaches to Generating Selectivity in Microcantilever Sensors. " PhD diss., University of Tennessee, 2008.  
[https://trace.tennessee.edu/utk\\_graddiss/336](https://trace.tennessee.edu/utk_graddiss/336)

This Dissertation is brought to you for free and open access by the Graduate School at TRACE: Tennessee Research and Creative Exchange. It has been accepted for inclusion in Doctoral Dissertations by an authorized administrator of TRACE: Tennessee Research and Creative Exchange. For more information, please contact [trace@utk.edu](mailto:trace@utk.edu).

To the Graduate Council:

I am submitting herewith a dissertation written by Peter J. Chapman entitled "Approaches to Generating Selectivity in Microcantilever Sensors." I have examined the final electronic copy of this dissertation for form and content and recommend that it be accepted in partial fulfillment of the requirements for the degree of Doctor of Philosophy, with a major in Chemistry.

Michael Sepaniak, Major Professor

We have read this dissertation and recommend its acceptance:

Panos Datskos, Ziling Xue, Frank Vogt

Accepted for the Council:

Carolyn R. Hodges

Vice Provost and Dean of the Graduate School

(Original signatures are on file with official student records.)

To the Graduate Council:

I am submitting herewith a dissertation written by Peter J. Chapman entitled “Approaches to Generating Selectivity in Microcantilever Sensors.” I have examined the final electronic copy of this dissertation for form and content and recommend that it be accepted in partial fulfillment of the requirements for the degree of Doctor of Philosophy, with a major in Chemistry.

Dr. Michael Sepaniak, Major Professor

We have read this dissertation  
and recommend its acceptance:

Dr. Panos Datskos

Dr. Ziling Xue

Dr. Frank Vogt

Acceptance for the Council:

Carolyn R. Hodges, Vice Provost and Dean  
of the Graduate School

(Original signatures are on file with official student records.)

# **APPROACHES TO GENERATING SELECTIVITY IN MICROCANTILEVER SENSORS**

A Dissertation  
Presented for the  
Doctor of Philosophy Degree  
The University of Tennessee, Knoxville

Peter J. Chapman  
May 2008

## **DEDICATION**

This dissertation is dedicated to my parents Darwin and Evelyn Chapman and my sisters Laura, Lisa and Linda. They provided a stable home environment for me to flourish and gave me a huge amount of love and support throughout my life.

This dissertation is also dedicated to my best friend and wife Joy. Her encouraging words kept me going at times when school became difficult. I am so thankful for her presence in my life.

## ACKNOWLEDGMENTS

I would like to take this opportunity to thank all of the people who helped make this work and my graduate career possible. I would like to first thank God, who is my ever present source of strength and direction. My relationship with Him has made me a much better person with the ability to accomplish great things for Him.

I would also like to thank my family. I would like to thank my wife Joy, who has provided constant encouragement and love. Additionally, my parents and sisters have provided an unwavering support.

I would also like to thank the people I have encountered throughout my graduate career here at the University of Tennessee. First and foremost to Dr. Sepaniak, whose constant guidance has not only enabled me to become a better scientist, but also has demonstrated to me how to be a professional. I would also like to thank Dr. Gilman, while working in his group my first year I developed a taste for research. I was able to develop close relationships with many fellow researchers at the University of Tennessee. Dr. Pampa Dutta, without your help in learning to use microcantilever sensors, I would not be at the point that I now find myself. A special thanks to the friends that I have met through my graduate career in Dr. Sepaniak's Group, Dr. Amber Wellman, Dr. Maggie Connatser, Kasey Hill, Matt Walworth, Nahla Abu-Hatab, Jenny Oran, Zhou Long, Deepak Bhandari, Joshy John, and Jim Patton. Without the entertainment, good conversation and help with experiments that you guys provided, my five years here at UT would have been very difficult, boring, and lonely. I wish each of you

the best as you move on in your careers. I would also like to thank Dr. Panos Datskos for his valuable input into this work, without his knowledge and assistance things would have been much more difficult. I would also like to thank Dr. Gerald DeVault, who provided me with the opportunity to collaborate with researchers outside of the University of Tennessee.

I would also like to thank Tim Free and Gary Wynn for their technical support. Tim your machining jobs and Gary your building of electrical components for our setups enabled me to progress through my research with a lot more speed than if I did not have both of your guys' help.

I wish to thank the chemistry department and the Science Alliance for providing financial support to enable me to complete this research.

Finally, I would like to thank my committee members: Dr. Vogt, Dr. Datskos, and Dr. Xue. Thank you for your willingness to serve on my committee.

## **ABSTRACT**

Microcantilever (MC) sensors have emerged as sensing transducers that offer greater sensitivity than comparable sensors due in large part to their very small dimensions. MCs have been utilized in many chemical sensing applications. Not only do MCs demonstrate greater sensitivity, but they also are relatively low in cost, they can be used in an array format, and they can be integrated into on-chip electronic circuitry.

While MC sensors demonstrate great sensitivity, an area of weakness that MC sensors must overcome is that of selectivity. The response of a MC sensor to analyte is mechanical; these mechanical responses lack the information rich spectral features like those found in vibrational spectroscopic techniques. Thus the underlying goal of this research is to develop approaches to enhancing selectivity in MC sensors.

The initial research focused simply on demonstrating that MC sensors could be functionalized with thiolated self-assembled monolayers (SAMs) and then used to detect metal ions in the liquid phase. The initial research not only demonstrated the moderate selectivity of SAMs to metal ions, but also the good sensitivity at which these metal ions could be detected.

The second phase of the research represented the first time that microcantilever array sensors (MCAs) were functionalized with SAMs having different ligand functionalities on one sensor chip. The MCA was exposed to different metal ions and the response signatures used in conjunction with pattern recognition algorithms to identify and quantitate the metal ion injected.



In an extension of the metal ion array research, the SAM MCA was coupled to an ion-exchange chromatography (IEC) column for the separation and detection of metal ions.

The second major division of research presented in this work involves improving the selectivity of detection of analytes in the gas phase. MCAs differentially coated with polymeric RPs by way of PVD were made. Experimental parameters were adjusted to determine if the parameters would impact the selectivity of the MCA.

The final project involved taking the former gas phase project a step further by invoking the use of gas chromatography (GC) to impart selectivity to the system.

## TABLE OF CONTENTS

<b>CHAPTER 1: INTRODUCTION TO CHEMICAL SENSORS AND MICROCANTILEVER SENSORS .....</b>	<b>1</b>
1.1 INTRODUCTION TO CHEMICAL SENSORS.....	1
1.2 MASS SENSORS .....	3
1.2.1 Quartz Crystal Microbalance Sensors.....	3
1.2.2 Surface Acoustic Wave Sensors .....	6
1.2.3 Flexural Plate Wave Sensors .....	8
1.3 MICROCANTILEVER SENSORS.....	10
1.3.1 Historical Background .....	10
1.3.2 Static Mode .....	14
1.3.3 Dynamic Mode.....	18
1.3.4 Readout Methods .....	19
<b>CHAPTER 2: CHARACTERIZATION OF LIGAND-FUNCTIONALIZED MICROCANTILEVERS FOR METAL ION SENSING .....</b>	<b>25</b>
2.1 INTRODUCTION .....	25
2.2 EXPERIMENTAL .....	29
2.3 RESULTS AND DISCUSSION .....	33
<b>CHAPTER 3: DIFFERENTIALY LIGAND-FUNCTIONALIZED MICROCANTILEVER ARRAYS FOR METAL ION IDENTIFICATION AND SENSING .....</b>	<b>49</b>
3.1 INTRODUCTION.....	49
3.2 EXPERIMENTAL .....	52

3.3 RESULTS AND DISCUSSION .....	61
3.4 FURTHER WORK: MICROCANTILEVER LC HYPHENATION .....	74
3.4.1 Introduction .....	74
3.4.2 Experimental .....	75
3.4.3 Results and Discussion .....	77
<b>CHAPTER 4: DIFFERENTIALLY POLYMER COATED</b>	
<b>MICROCANTILEVER ARRAYS FOR GAS PHASE SENSING AND</b>	
<b>IDENTIFICATION .....</b>	<b>95</b>
4.1 INTRODUCTION .....	95
4.2 EXPERIMENTAL .....	96
4.3 RESULTS AND DISCUSSION .....	100
<b>CHAPTER 5: FACILE HYPHENATION OF GAS CHROMATOGRAPHY</b>	
<b>AND A MICROCANTILEVER ARRAY SENSOR FOR ENHANCED</b>	
<b>SELECTIVITY .....</b>	<b>113</b>
5.1 INTRODUCTION .....	113
5.2 EXPERIMENTAL .....	115
5.3 RESULTS AND DISCUSSION .....	123
<b>CHAPTER 6: CONCLUSIONS .....</b>	<b>138</b>
<b>REFERENCES.....</b>	<b>141</b>
<b>VITA.....</b>	<b>149</b>

## LIST OF TABLES

TABLE	PAGE
<b>Table 1</b> List of Thiolated Ligands .....	30
<b>Table 2</b> List of Thiolated Ligands .....	53
<b>Table 3</b> Optimized concentrations of ligand solutions.....	55
<b>Table 4</b> The slope, r-squared value, and RSDs .....	69
<b>Table 5</b> Generalized prediction rates .....	72
<b>Table 6</b> RPs used for gas phase sensing array.....	98
<b>Table 7</b> Predicted vs. actual concentration for gas mixture. ....	105
<b>Table 8</b> List of compounds used as RPs.....	117
<b>Table 9</b> The reproducibility (%RSD) of peak heights and peak areas .....	130
<b>Table 10</b> The effects of column flow rate on GC-MCAD peak retention .....	135

## LIST OF FIGURES

FIGURE	PAGE
<b>Figure 1</b> Quartz crystal microbalance . . . . .	5
<b>Figure 2</b> Surface Acoustic Wave Sensor.....	7
<b>Figure 3</b> Flexural Plate Wave Sensor.....	9
<b>Figure 4</b> Microfabrication of MCs.....	13
<b>Figure 5</b> Static Mode Bending of MC.....	16
<b>Figure 6</b> Optical Detection Scheme . . . . .	20
<b>Figure 7</b> Schematic representation of the molecular structure of the SAM . . . . .	34
<b>Figure 8</b> Time trace of SAM coated MC on exposure to Cs <sup>+</sup> . . . . .	37
<b>Figure 9</b> Comparison of the bending responses . . . . .	40
<b>Figure 10</b> Effect of immersion time . . . . .	42
<b>Figure 11</b> Response (maximum bending) selectivity for metal ion . . . . .	44
<b>Figure 12</b> Concentration-based response curve of AET . . . . .	47
<b>Figure 13</b> The effect of dealloyed thickness . . . . .	62
<b>Figure 14</b> Surface thiolation studies . . . . .	64
<b>Figure 15</b> The ability to differentially functionalize.....	67
<b>Figure 16</b> The response diversity to each metal ion.....	71
<b>Figure 17</b> Cation Exchange Separation of metal ions.....	79
<b>Figure 18</b> Triplicate measurements of 0.1 mmol/L CoCl <sub>2</sub> . . . . .	81
<b>Figure 19</b> The separation of metal ions using a strong cation exchange column. 82	
<b>Figure 20</b> Effects of laser warm-up time on noise levels.....	86
<b>Figure 21</b> Peak tailing demonstrated . . . . .	88

<b>Figure 22</b>	Flow profiles in several different flow cell geometries are depicted. .	90
<b>Figure 23</b>	Flow rate study with new flow cell design. ....	92
<b>Figure 24</b>	FT-IR spectra of polymer PDPP before and after vapor deposition..	101
<b>Figure 25</b>	Response of 10 RP coated MCs to 10% TCE . ....	103
<b>Figure 26</b>	Temperature effects on response. ....	108
<b>Figure 27</b>	Humidity effects on the response. ....	110
<b>Figure 28</b>	Illustrations detailing the ease of instrumental hyphenation. ....	119
<b>Figure 29</b>	The response variability (selectivity) is displayed. ....	124
<b>Figure 30</b>	Singular values obtained from the full calibration set. ....	126
<b>Figure 31</b>	A separation of a VOC mixture. ....	128
<b>Figure 32</b>	Response of TBATS coated cantilever. ....	131

## ABBREVIATIONS AND SYMBOLS

$A_{cr}$	Cross-sectional Area
$A_s$	Peak Asymmetry
AB	Acetate Buffer
Ac $\beta$ CD	Acetyl- $\beta$ -cyclodextrin
AET	2-Aminoethanethiol
AFM	Atomic Force Microscopy
ANN	Artificial Neural Networks
ATP	4-Aminothiophenol
APTES	3-Amino propyl triethoxy silane
Cal-4	4-tert-Butylcalix[6]arene
Cal-6	4-tert-Butylcalix[4]arene
CCD	Charge-coupled Device
CuPC	Copper Phthalocyanine
$c_m$	Mass Sensitivity Factor
DA	Dealloyed
E	Young's Modulus
$f$	Frequency
$f_0$	Initial Frequency
HF	Hydrofluoric Acid
HPLC	High Performance Liquid Chromatography
ICA	Independent Component Analysis
IDT	Interdigital Transducer

IEC	Ion-exchange Chromatography
$k_f$	Frequency Constant of the Crystal
LPCVD	Low Pressure Chemical Vapor Deposition
MBA	o-Mercaptobenzoic Acid
MC	Microcantilever
MCA	Microcantilever Array
MCAD	Microcantilever Array Detector
Me $\beta$ CD	Methyl- $\beta$ -cyclodextrin
MEMS	Micro-electro-mechanical Systems
MP	3-Mercaptopropanol
MPA	3-Mercaptopropionic Acid
MRP	Molecular Recognition Phase
MUA	11-Mercaptoundecanoic Acid
MUD	11-Mercaptoundecanol
$\Delta m_a$	Change in Mass
$\Delta m_s$	Change in Surface Mass Density
$\eta$	Liquid Viscosity
$\eta_q$	Viscosity of Quartz
$\rho_m$	Density of Applied Chemical Film
$\rho_q$	Density of Quartz
PCA	Principal Component Analysis
PDPP	Poly(diphenoxyphosphazene)
PECH	Poly(epichlorohydrin)



PECVD	Plasma-enhanced Chemical Vapor Deposition
PEI	Poly(ethyleneimine)
PIB	Poly(isobutylene)
PSD	Position Sensitive Detector
PVD	Physical Vapor Deposition
QCM	Quartz Crystal Microbalance
REI	Reactive Ion Etching
RP	Responsive Phase
RSD	Relative Standard Deviation
SAM	Self-assembled Monolayer
SERS	Surface Enhanced Raman Spectroscopy
SVD	Singular Value Decomposition
TBATS	Tetrabutylammonium p-toluenesulfonate
TCD	Thermal Conductivity Detector
THPED	N,N,N',N'-Tetrakis(2-hydroxypropyl)ethylenediamine
VOC	Volatile Organic Compound
$\nu$	Poisson's Ratio
$\nu_0$	Acoustic Wave Phase Velocity
$\Delta\nu$	Change in Acoustic Wave Phase Velocity

# CHAPTER 1: INTRODUCTION TO CHEMICAL SENSORS AND MICROCANTILEVER SENSORS

## 1.1 INTRODUCTION TO CHEMICAL SENSORS

Chemical sensors have benefited very much from the information age in which we live. Handheld cellular devices allow us to receive phone calls, check our email, and surf the internet. Chemical sensors give us information about the world around us and have been applied to almost every area of life. The desire to know and to have access to information at our finger tips has undoubtedly aided the rise of chemical sensors. To further discuss chemical sensors, a good working definition of chemical sensors should be established. Bezegh and Janata have provided one of the most accepted definitions of a chemical sensor. In their definition they define a chemical sensor as *a transducer which provides direct information about the chemical composition of its environment; it is composed of a physical transducer and a chemically selective layer*[1].

In addition to a good working definition for chemical sensors, some ideal fundamental properties that all proper chemical sensors must possess should also be laid out. The first fundamental property that a chemical sensor must possess is the sensor response must be proportional to the amount or concentration of the analyte to be measured. A linear relationship of chemical sensor response over many orders of magnitude of analyte concentration is a desirable characteristic in chemical sensors. The linearity and dynamic range of this relationship between a sensor and the analyte goes along way in determining specific sensor applications and overall acceptance as a legitimate chemical sensor. The second fundamental

property related to an ideal chemical sensor is reversibility. If the sensor is not completely reversible and all of the analyte is not removed after exposure of the sensor to the sample, then the sensor will become saturated after multiple exposures and not allow for sensing of the analyte, rendering the sensor useless. The third fundamental property of an ideal chemical sensor is that the sensor exhibit fast response times. This property is very critical in processes where the sensor is placed in a flow cell and the sample is flowing by the sensor. If the sensor is slow to respond to an analyte present for only a short period of time, the sensor will give a false negative. In sensor applications such as biological warfare agent detectors, a false negative is the worst situation possible and could result in the loss of many innocent unsuspecting lives, simply because the sensor had a slow response time.

Additionally, it is important for sensors to be sensitive, reproducible and selective. Extremely sensitive sensors allow for detection of very small amounts of analyte. A reproducible sensor allows quantitative measurements to be made on an analyte. A selective sensor provides the ability to distinguish between analytes.

No perfect chemical sensor exists however. Some chemical sensors have fast response times, but poor dynamic ranges. Others are very reversible and show no hysteresis, but have slow response times. In each sensor application, there is generally a balance of the good with the bad. The quest to develop the perfect chemical sensor has enticed many to pursue chemical sensors as a research interest.

The range of types and applications of chemical sensors is too broad in scope to cover in this work. Therefore, the remainder of this work will focus on a specific type of chemical sensor, the microcantilever (MC) sensor, but first mass sensitive chemical sensors related to MCs will be discussed.

## 1.2 MASS SENSORS

### 1.2.1 Quartz Crystal Microbalance Sensors

Quartz crystal resonators were first used in radio-communication equipment to control frequency. A relationship between the resonant frequency of these quartz crystal resonators and the amount of foreign material deposited on them has been known for some time[2]. A quantitative relationship, equation 1, between resonance frequency of quartz crystal resonators and amount of material deposited was not established until the quartz crystal microbalance (QCM) was first introduced by Sauerbrey in 1959[3]

$$\Delta f = -\frac{1}{\rho_m k_f} f_0^2 \frac{\Delta m_a}{A_{cr}} \quad (1)$$

where  $\Delta f$  is the change in frequency,  $\rho_m$  is the density of the chemical film,  $k_f$  is the frequency constant,  $f_0$  is the fundamental resonance frequency of the crystal,  $\Delta m_a$  is the change in mass and  $A_{cr}$  is the cross-sectional area of the crystal. Sauerbrey demonstrated that the decrease in resonant frequency of a vibrating quartz crystal resonator was proportional to the added mass. Thus the first QCM was demonstrated.

QCM based sensors, shown in Figure 1, are coated with a metallic film to allow for electrical contact. The crystal can then be coated with a selective

sensing coating specific to the analyte to be detected. The coated QCM is then placed in an oscillation circuit where it resonates close to its fundamental frequency. As analyte adsorbs onto the surface of the QCM, through interaction with the sensing layer, the resonance frequency of the QCM is altered. The typical operational frequency range for QCM sensors is between 5-30 MHz, with measurable frequency changes as small as 1 Hz. Equation 1 can be used to determine the mass of the adsorbed analyte if the measurements are made in the gas phase. For liquid phase measurements, the equation must be altered (equation 2) to account for the dramatic change in the fundamental resonance frequency of the QCM

$$\Delta f = f_0^{3/2} \left[ \frac{\rho \eta}{\pi \eta_q \rho_q} \right] \quad (2)$$

where  $\Delta f$  is the change in frequency,  $f_0$  is the fundamental resonance frequency of the crystal,  $\rho$  is the density of the surrounding liquid,  $\eta$  is the viscosity of the surrounding liquid,  $\eta_q$  is the viscosity of the quartz crystal, and  $\rho_q$  is the density of the quartz crystal.

One of the limitations related to QCMs occurs when the sensors are used in viscous solutions, which dampen the resonance frequency of the QCM so much so that the sensitivity becomes limited. The dampening is demonstrated by equation 1, where the change in frequency  $\Delta f$  divided by the  $\Delta m_a$  is proportional

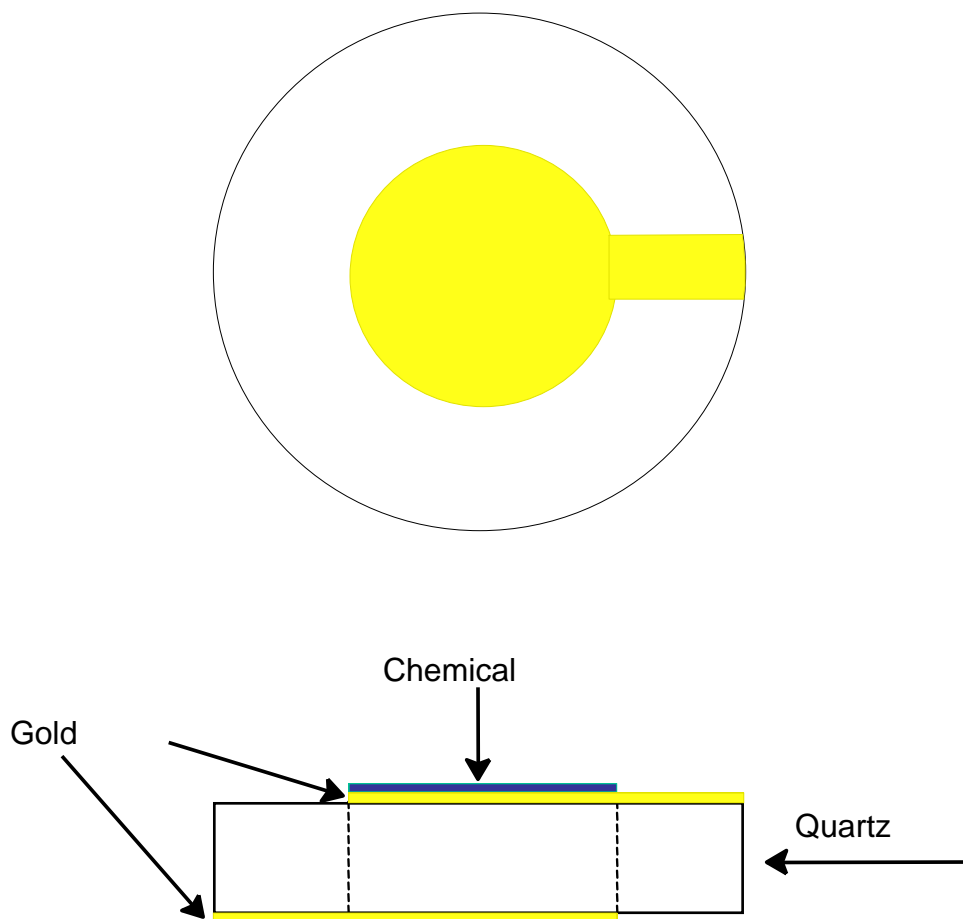


**Figure 1** Quartz crystal microbalance has a typical diameter of 1 cm and a thickness of 50  $\mu\text{m}$ .

to resonance frequency  $(f_0)^2$ . As the viscosity of the environment increases,  $\Delta m_a$  increases and the resonance frequency decreases.

### 1.2.2 Surface Acoustic Wave Sensors

Surface acoustic wave (SAW) sensors utilize a pair of interdigital transducers (IDT)[4, 5]. The IDTs are deposited onto a piezoelectric substrate in a configuration known as a delay line (Figure 2). An alternating voltage is applied to each interdigital pair, which in turn creates an electric field in the piezoelectric material. A surface wave travels along the surface of the sensor until it interacts with the second pair of digits, triggering an alternating voltage in the second pair of digits. The electrical signal can then be detected and quantified. When mass

loading in the region between the digit pairs occurs, the loading causes the surface wave to change velocity[6]. This change in the surface wave velocity causes a change in the frequency (1 Hz routinely measured), therefore the change in frequency is related to the mass of loading by equation 3[7]

$$\frac{\Delta v}{v_0} = -c_m f_0 \Delta m_s \quad (3)$$

where  $\Delta v$  is the change in acoustic wave velocity,  $v_0$  is the initial acoustic wave velocity,  $c_m$  is the mass sensitivity factor,  $f_0$  is the fundamental resonance frequency and  $\Delta m_s$  is the change in mass loading. SAW sensors operate at frequencies in the range of 30-300 MHz, higher than QCMs, rendering them more sensitive than QCM sensors. SAW sensors can also be used in an array format to

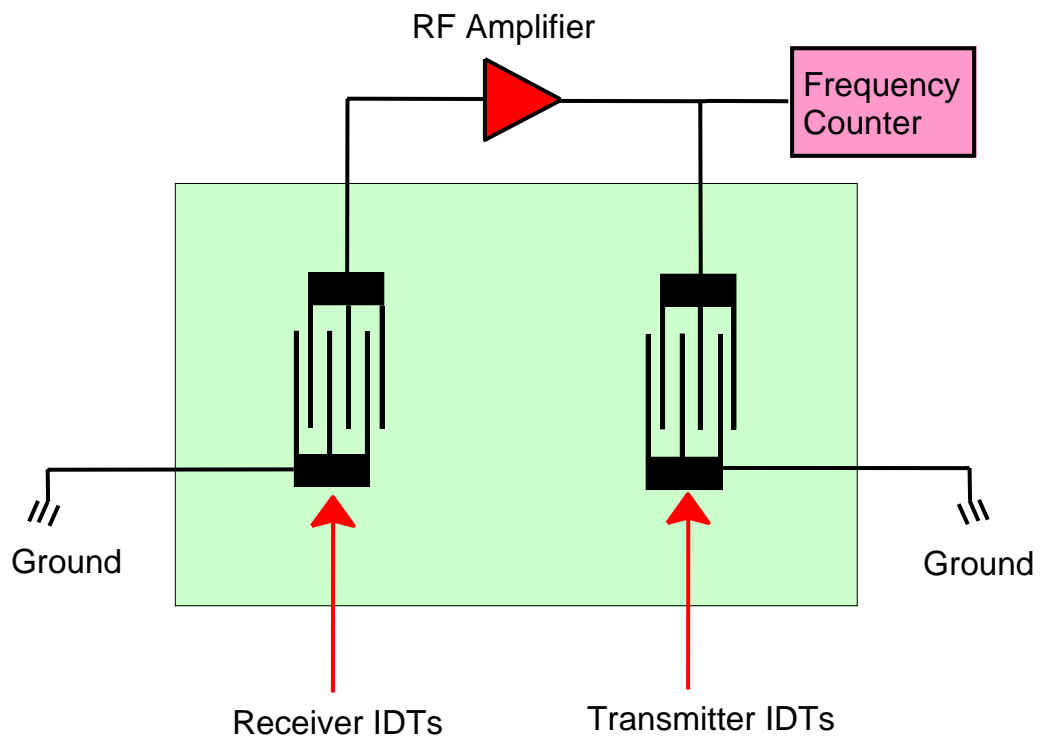


**Figure 2** Surface Acoustic Wave Sensor



enhance selectivity of the sensor. The current limitation for SAW sensors is that they are not very applicable in liquid environments. The surface waves are highly attenuated by the liquid phase which has limited SAW sensor's use in this environment.

### **1.2.3 Flexural Plate Wave Sensors**

Similar to SAW sensors flexural plate wave (FPW) sensors rely on the propagation of a wave along the sensor and its interaction with the analyte for sensing to occur (Figure 3). The waves in FPW devices are known as Lamb waves. Lamb waves travel through the entire width of a thin material. Therefore, the entire plate is utilized in propagation of the wave rather than the wave propagating on the sensor surface as in SAW sensors[6]. Propagation through the entire plate is enabled by the fact that the thickness of the plate used in FPWs is much smaller than those used in SAW sensors. The Lamb waves cause a mechanical flexing of the plate in FPW sensors, thus the name “flexural”[8]. The velocity of the wave decreases as the thickness of the plate decreases. Just as in SAW and QCM sensors, the resonance frequency of the FPW is related to the mass loading of the sensor.

The Lamb waves do not emit into the surrounding environment, therefore FPW sensors are easily adapted to liquid phase sensing[8]. FPW sensors are actually more sensitive than SAW sensors even though they oscillated at low frequencies. This is because the Lamb waves are confined to the plate and therefore are more impacted by mass loading. The drawback of FPW sensors is

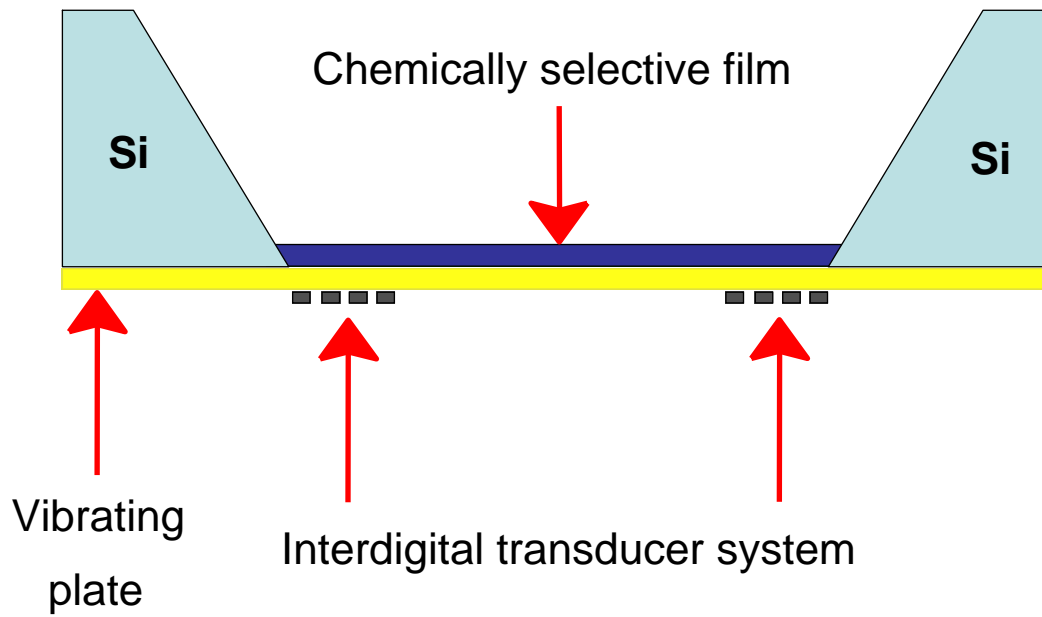


**Figure 3** Flexural Plate Wave Sensor

that preparation of the flexural plates involve a more complicated fabrication, thus the FPW sensors are more expensive than other comparable sensors.

The focal point of this work and the final sensor discussed in this chapter, in much greater detail compared to previous sensors, is the MC sensor. Cantilever sensors currently are routinely used on the micrometer size. However, cantilever sensors, compared to competing sensors, offer the ability to be further miniaturized to the nano-scale which will allow for the study of nano-mechanics.

### **1.3 MICROCANTILEVER SENSORS**

#### **1.3.1 Historical Background**

The foundations of MCs began to be laid in the mid 1920's. At that time, Meehan[9] observed that yellow pine charcoal would undergo adsorption-induced expansion when exposed to carbon dioxide vapors. Not only did he demonstrate these adsorption induced effects, but he also demonstrated that these effects were reversible. In 1954, Yates demonstrated that porous glass would expand when exposed to nonpolar gases such as argon, nitrogen, and oxygen[10]. The first mention of a cantilever mechanical transducer in the literature was detailed by Norton[11] in 1943. In 1969 Shaver[12] designed a bi-metallic hydrogen detector based on a cantilever mechanical transducer. In his work he was able to measure the presence of hydrogen gas at concentrations as low 50 ppm in a background of nitrogen gas. While the macrocantilever detectors described by Norton and Shaver were by no means on the micro scale, they did demonstrated that this sensor scheme could be employed for detection of various analytes.

The macrocantilever detectors were sensitive transducers at the time of their use, but they were limited by several difficulties. One problem that existed with the macrocantilever sensor was that the existing means of measuring the cantilever deflection could not provide the desired accuracy or sensitivity needed for the macrocantilever to be a viable sensor. Another inherent problem with the macrocantilever sensors was their large size, 100 mm long and 125  $\mu\text{m}$  thick[13], which made them vulnerable to external vibrations. Researchers believed that smaller micrometer sized cantilevers would be able to measure tiny surface stress changes[14-18], but the microfabrication technology did not exist to produce such a cantilever. The microfabrication technology needed to produce micrometer sized cantilevers was ushered in by the emergence of atomic force microscopy (AFM).

In AFM a flexible force-sensing cantilever is scanned over a surface in a raster pattern. The force acting between the cantilever and the sample surface causes deflection of the cantilever. Deflection of the cantilever is measured by a laser reflecting off the tip of the cantilever to a position sensitive detector (PSD)[19]. As the cantilever tip is deflected, a piezoelectric device moves the sample in x, y, and z directions to maintain a constant force between the tip and the sample. The movement of the piezoelectric device allows for topographic mapping of the sample surface. With AFM, displacements as small as  $10^{-5}$  nm can be detected resulting from forces as small as  $10^{-18}$  N[20] in extreme cases. Routinely, displacements as small as  $10^{-3}$  can be measured resulting from forces on the order of a few pN. The invention of AFM in 1986[20] necessitated the

mass production of cantilevers on the micrometer scale, which motivated many advancements in microfabrication techniques.

Some researchers took advantage of the advancements in microfabrication techniques and began using conventional microfabricated AFM tips as transducers[21-27]. Microfabrication of MCs is made possible through one of two micromachining techniques, either bulk micromachining or surface micromachining[13]. In bulk micromachining, removal of a large portion of the substrate occurs. Bulk micromachining is used to produce three dimensional suspended structures. Surface micromachining allows for much more of the original substrate to remain intact. From the original substrate a device is formed through deposition and etching processes. The most preferred substrate for microfabrication of MCs is single crystal silicon. A common microfabrication process for MCs begins with deposition of a sacrificial layer on a prepatterned substrate (Figure 4). A structural silicon nitride or polysilicon material layer is then deposited using low pressure chemical vapor deposition (LPCVD) or plasma-enhanced chemical vapor deposition (PECVD) on top of the sacrificial layer. The specific cantilever shapes can then be defined by patterning the silicon nitride or polysilicon structural layer using photolithography followed by reactive ion etching (REI). The silicon substrate is then etched away to produce free standing cantilevers on the micrometer scale. AFM ushered in micromachining technology which enabled mass production of micrometer sized cantilevers. Microfabrication technologies had now provided a gateway for theoretical MC calculations of years past to be tested empirically. The MC was no longer theory,

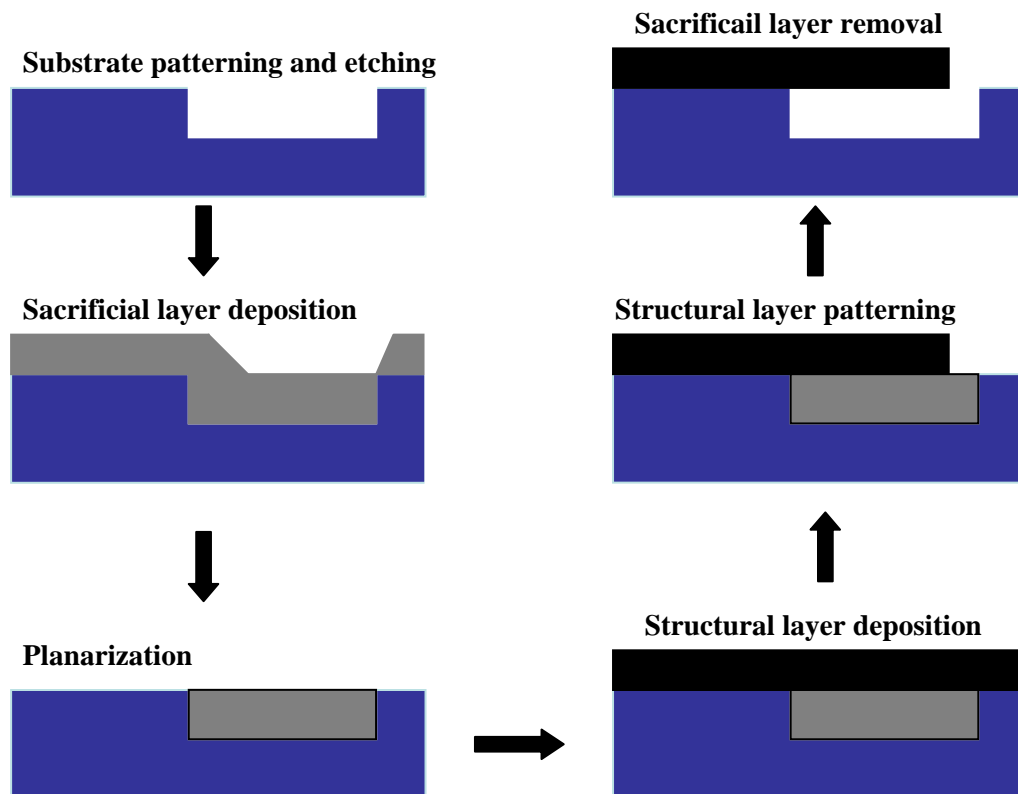


**Figure 4** Microfabrication of MCs

but a physical micromachined microtransducer and researchers began to test the tiny structure for its chemical sensing ability.

### 1.3.2 Static Mode

As a chemical sensor MCs respond to chemical stimuli by either of two physical means. MCs can undergo a static deformation or a change in resonance frequency due to environmental changes.

In the static deformation, also known as static mode operation, MCs are differentially coated with responsive phases (RPs). One surface of the MC is coated with a RP possessing an affinity for the analyte of interest. The opposing surface of the MC is passivated relative to the coated side, based on the fact that it remains uncoated. Since the 1960s it has been known that adsorption of chemicals on an atomically pure single crystal will induce significant surface stress changes. Based on the Shuttleworth equation[28], the surface stress can be related to surface free energy (equation 4)

$$\sigma = \gamma + \left( \frac{\partial \gamma}{\partial \varepsilon} \right) \quad (4)$$

where  $\sigma$  is the surface stress,  $\gamma$  is the surface free energy,  $\partial \gamma$  is the relative change in surface free energy and  $\partial \varepsilon$  is defined as the relative change in surface area. In many cases, the contribution from the surface strain term can be neglected and the surface stress change is approximately equal to the free energy change. Micrometer scale cantilevers can detect surface stress changes in the low mN/m range[13].

Three general models have been developed for understanding how chemical stimuli impart surface stress changes to a MC coated with a RP. The first model is applicable when the interactions between the chemical stimuli and the MC are localized to the cantilever surface. The model is relevant when the RP is only a monolayer. The chemical stimuli may physisorb through van der Waals forces to the surface monolayer or the chemical stimuli can chemisorb through chemical bonding to the surface monolayer. Physisorption can polarize the surface monolayer creating induced dipoles. The energy related to physisorption is very small, less than 0.1 eV, resulting in small surface stress changes. The process of chemisorption is a higher energy interaction, greater than 0.3 eV, causing larger surface stress changes. The surface stress can be attributed to the Gibbs free energy of the adsorption process. Therefore, spontaneous adsorption processes will occur when there is an excess of interfacial free energy, which typically results in the reduction of interfacial stress. This surface stress change is known as compressive because the possibility of the return of the surface to its original compressed state. Therefore, the largest static deformations will occur in cantilevers with high initial surface free energies (Figure 5). These deformations can accurately be predicted by using the relationships derived by Stoney[29]. With an understanding of the radius of curvature and the length of the cantilever, the bending of the MC (tip deflection,  $z_{\max}$ ) can be characterized and approximated by equation 5

$$z_{\max} = \frac{3l^2(1-\nu)}{Et^2} \Delta\sigma \quad (5)$$



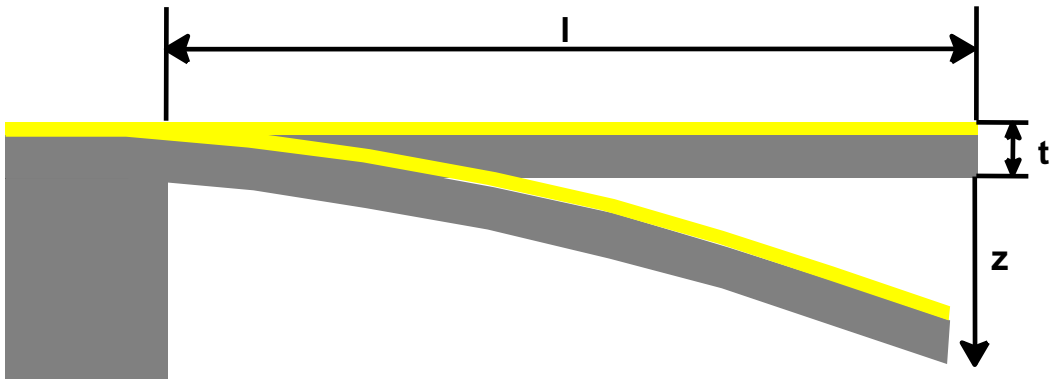


**Figure 5** Static Mode Bending of MC

where  $\nu$  and  $E$  are, respectively, the Poisson ratio and Young's modulus for the cantilever,  $t$  is the thickness of the MC,  $l$  is the cantilever effective length, and  $\Delta\sigma$  is analyte-induced differential surface stress ( $\Delta\sigma_{\text{active (i.e., RP) side}} - \Delta\sigma_{\text{passive side}}$ ).

The second model developed for static deformations of cantilevers is related to MCs having RPs thicker than a single monolayer such as a polymer coating ranging in thickness from 100 to 500 nm. The polymer RP coating is permeable to the analyte of interest. The interaction, therefore, is no longer limited to surface phenomena. As the analyte penetrates the thick RP, forces including dispersion, electrostatic, steric, osmotic, and solvation can be altered by the invading analyte molecules[30]. The alteration of these forces in the polymer coating can cause stress changes which are imparted to the cantilever causing deformations. The in-plane component of the RP stress can be multiplied by the coating thickness to give an apparent surface stress change, which can be applied to Stoney's model.

The third model developed for static deformations of cantilevers can be applied to cantilevers with nanostructured surfaces. These irregular amorphous nanostructured surfaces on cantilevers are desirable because it has been known for some time that disordered amorphous films have high intrinsic stresses[17]. In nanostructured RPs, analyte-induced stresses combine bulk, surface, and intersurface mechanisms resulting in large stress changes and large amounts of cantilever deformation. Recent studies have shown that nanostructured surfaces can enhance the cantilever response by two orders of magnitude[31, 32]. The static deformation of the nanostructured cantilever cannot be predicted with

previous models, but estimates of the mechanical energy produced by a cantilever can be calculated. The product of the energy associated with the binding site-analyte interaction and the number of interactions can be used to estimate the mechanical energy.

### 1.3.3 Dynamic Mode

Not only can chemical stimuli cause static deformations in a cantilever, but mass loading of an analyte onto the surface of a cantilever can impart a resonance frequency change. The very small size and mass of MCs allows them to be operated in resonant mode with or without external excitation. For a resonating cantilever, Hook's law can be applied to a rectangular leaf spring with an effective suspended mass  $m_0$  and a spring constant  $k$ . In the absence of damping the fundamental resonance frequency ( $f_0$ ) of the cantilever can be approximated as equation 6[33].

$$f_0 = \frac{1}{2\pi} \sqrt{\frac{k}{m_0}} \quad (6)$$

To more accurately calculate cantilever resonance frequencies the dissipation of the resonator energy must be taken into account. This is accomplished by introducing a  $Q$  factor as in equation 7[33, 34].

$$f_{0,Q} = \frac{1}{2^{3/2}\pi} \sqrt{\frac{k}{m_0}} \frac{\sqrt{2Q-1}}{Q} \quad (7)$$

The  $Q$  factor compares the frequency at which the cantilever oscillates to the rate at which it dissipates energy. The  $Q$  factor supplies the experimenter with an idea of mechanical friction. By invoking the  $Q$  factor, the change in the resonance

frequency can then be related several mechanisms; adsorbate-induced mass-loading, chemically induced changes in the cantilever stiffness, and mechanical damping by the viscous medium.

#### **1.3.4 Readout Methods**

Despite the limited number of operating modes, static and dynamic, there are many methods to make real-time measurements of cantilever deformations or resonance frequency changes. The readout methods include optical, piezoelectric, piezoresistive, capacitance, and electron tunneling schemes.

In the first optical readout method, known as the optical beam deflection, a laser is focused on the tip of the cantilever (Figure 6). The laser reflects from the tip of the cantilever to a PSD, just as in AFM. As cantilever deformation occurs, the position of the laser on the PSD changes. This optical arrangement allows for very small changes in cantilever tip deflection to be measured, up to  $10^{-14}$  m displacements have been reported[35] in the most stringent of experimental setups. However, displacements as small as of  $10^{-10}$  m are routinely measured. This readout scheme provides the advantages having no electrical connections to the cantilever, linear response, simplicity and reliability. However, if changes in the optical properties of the medium surrounding the cantilever occur, interferences with output can be seen.

The second optical readout method included interferometric measurements. A single visible laser source illuminates an entire array of cantilevers. The reflected light is either interferometrically coupled with a reference beam and detected by a charge-coupled device (CCD) or directly

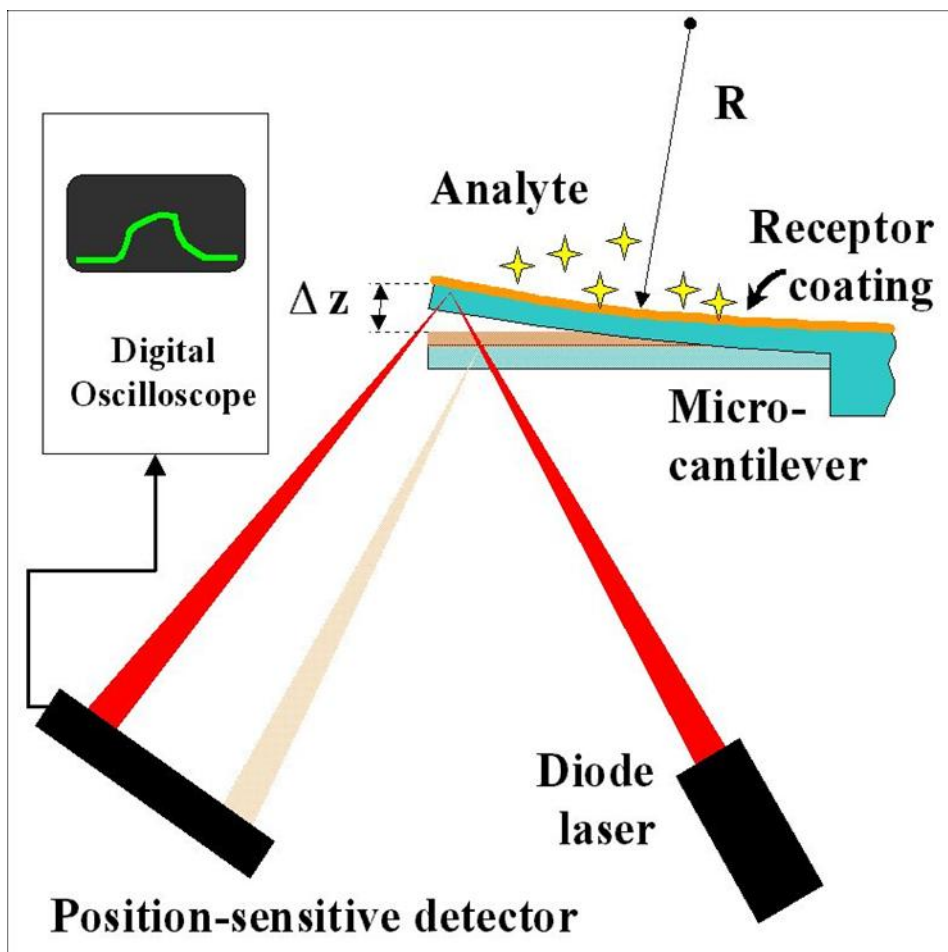


**Figure 6** Optical Detection Scheme

reflected onto the CCD. Interferometric detection readout schemes are important because they can be used to monitor deflections of large two-dimensional cantilever arrays.

Piezoresistive readout schemes are based on the phenomenon that as a stress is applied to a material, the bulk resistivity of that material will change. A material that exhibits strong piezoresistive effects is boron doped single crystal silicon, the material from which cantilevers are generally fabricated[36, 37]. Therefore, when analyte-induced stress manifests itself in cantilevers in the form of static deformations or changes in resonance frequency, the bulk resistivity of the cantilever changes. A portion of the silicon cantilever is doped with a boron channel. The cantilever is included with a dc-biased Wheatstone bridge having resistors of identical initial resistance. Changes in resistance occur as the cantilever deforms in response to external stimuli. The disadvantage of the technique is that it requires current to flow in the cantilever resulting in heating of the cantilever. If changes in the surrounding environment occur, heat will be dissipated at a different rate causing bending in the cantilever unrelated to chemical stimuli.

Piezoelectric readout techniques are based on the piezoelectric effect, in which transient charges are induced in the piezoelectric layer when it is deformed[38]. Therefore, a piezoelectric material must be deposited on the cantilever before it can be monitored by piezoelectric means. The disadvantage of this readout scheme is that it requires electrical connects directly to the MC. Additionally, in order to obtain large output signals the thickness of the

piezoelectric film must be increased. However, it is evident, when looking at the Stoney equation that as the total thickness of the cantilever increases, the tip deflection decreases. The increase in sensor thickness will ultimately decrease the sensitivity of the MC.

Another means of measuring MC responses to chemical stimuli is through capacitance. This detection scheme is based on measuring the capacitance between a conductor on the tip of the cantilever and a conductor on the surface of a substrate separated from the cantilever by a small gap[39-41]. As cantilever deformations occur, the capacitance between the two conductors changes. This capacitance change can be related to the change in distance. If the dielectric constant of the medium changes then accurate measurement of cantilever deformation becomes difficult. The major advantage for the capacitance detection scheme is that it can be envisioned as a means to provide a readout scheme for nanocantilevers.

The final readout scheme to be discussed herein is that of electron tunneling, which has been used to measure tip deflection in AFM[42]. In electron tunneling, a conducting tip and the cantilever are separated by a subnanometer gap. A bias voltage is applied between the conducting tip and cantilever resulting in a flow of electrons. The tunneling current is sensitive to the gap distance. Therefore, any cantilever deformation can be detected by this technique. Using this electron tunneling technique, cantilever displacements as small as  $10^{-4}$  nm can be detected[43].

Over the past 20 years there has been a steady growth in the use and application of MC sensors. As noted in this chapter, the fundamental theory, modes of operation and sensor readout schemes have been explored. Our previous research in the area of MC sensors focused on enhancing the sensitivity. Enhancements in sensitivity were accomplished by using various techniques to increase the surface area of the MC sensor. An increase in surface area provided more surface sites for analyte to interact thus an increase in sensitivity. The most successful approach to increasing MC surface area was a process known as dealloying, which created a gold nanostructured surface on the MC. The gold nanostructured surface increased the surface area of the MC sensor by 20 times. Enhancements in response to analytes with the nanostructured surface were as much as 10 times larger versus the smooth gold coated MC.

The current research presented in the following chapters will focus on enhancing the selectivity of the MC sensor. Attempts at enhancing the selectivity of the MC sensor were made with liquid and gas phase analytes. The main strategy used to increase the selectivity of the MC was to use the sensor in an array format. The microcantilever array sensor (MCA) allows for coating of each cantilever in the array with a different RP. Each phase responds differently to each analyte injected and a MCA gives a unique response signature for each analyte. Pattern recognition algorithms can then be applied to these unique analyte signatures to identify the analyte. To further enhance the selectivity of this strategy chromatographic techniques were applied to mixtures of analytes. The mixtures were separated before introduction into the MCA flow cell. The



chromatographic coupling to MCAs was invoked to provide an additional dimension of selectivity of to the system. These attempts at enhancing the selectivity of the MC sensor will be presented in the following chapters.

## **CHAPTER 2: CHARACTERIZATION OF LIGAND-FUNCTIONALIZED MICROCANTILEVERS FOR METAL ION SENSING**

Chapter 2 is an adaptation of a research article *Anal. Chem.* **2005**, *77*, (20), 6601-6608. The article demonstrated that thiolated ligand self-assembled monolayers could be formed on cantilevers that could subsequently be used to selectively detect metal ions.

### **2.1 INTRODUCTION**

The continued release of metal contaminants into the natural environment from different sources has prompted the development of practical detection schemes for metal ions present in different sample matrices. Heavy metals are highly toxic for biological organisms even at trace amounts. Moreover, as metals are non-degradable they tend to bioaccumulate as they move along the food chain. Traditional methods for metal ion detection include liquid or gas chromatography (GC)[44-46], atomic absorption[47], flow-injection systems[48], electrochemistry[49, 50], fluorescent sensors,[51] inhibition based enzymatic assays,[52] solid phase extraction[53], and immunoassay[54]. These methods, however, are either expensive or not useful when there is a need to detect metals at low concentrations.

In recent years, microfabricated cantilevers (MCs) have been demonstrated as platforms for novel physical, chemical, and biological sensing[55-68]. Due in part to their diminutive size, MCs typically offer approximately two orders of magnitude better sensitivity than other mass-based

sensors such as QCMs, FPW oscillators, and SAW devices[69]. In addition, MCs can be relatively low in cost, integrated with micromechanical components including on-chip electronic circuitry, and used in an array format. The MC array format can yield a good degree of selectivity and provide multiple analyte measurements when used in conjunction with multiple chemically selective coatings[58, 70-74].

The principles of MC operation can be quite simple. Intermolecular forces arising from analyte adsorption on surfaces or absorption into surface-immobilized thin films are known to induce surface stresses[69]. Static mechanical bending of the cantilever can occur if surface stresses on opposite sides of the cantilever are modulated by different degrees. Differential stress occurs when a molecular (or ionic) recognition phase (MRP) is immobilized on one side of the cantilever while the other side of the MC remains largely passive toward the target analyte(s). The cantilever response (displacement of the MC tip,  $z_{\max}$ ) resulting from this difference in surface stress can be approximated by Stoney's Equation[29, 75]

$$z_{\max} = \frac{3l^2(1-\nu)}{Et^2} \Delta\sigma \quad (5)$$

where  $\nu$  and  $E$  are, respectively, the Poisson ratio and Young's modulus for the cantilever,  $t$  is the thickness of the MC,  $l$  is the cantilever effective length, and  $\Delta\sigma$  is analyte-induced differential surface stress ( $\Delta\sigma_{\text{active side}} - \Delta\sigma_{\text{passive side}}$ ). Our recent studies[60, 66, 76-78] have focused on the design of MC sensors in which weak chemical or biochemical stimuli can be converted into mechanical

responses with very high efficiency. We have demonstrated that nanostructuring of the active side of the MCs can magnify analyte-induced responses by one or more orders of magnitude in both gaseous and liquid environments[60, 76, 77]. In addition to the analytical significance of increased responses with functionalized nanostructured MCs, complications arising from analyte interactions at non-treated cantilever surfaces are rendered negligible using this approach.

Despite their high sensitivity, unmodified MCs do not exhibit tunable chemical selectivity. In MC sensing, two approaches have been widely used to functionalize the MC surface with MRPs and impart selectivity. Thin films of MRPs have been used extensively wherein the analyte – MRP interaction is an absorption process. Many polymeric materials and macrocycle receptors have been used in this manner[58, 74, 77-80]. Although both gas phase and liquid phase sensing is possible, the stability of the phase in liquid environments can be an issue[60]. Conversely, MRPs as self-assembled monolayers (SAMs) have been proven successful for the detection of analytes in water[81-83]. The SAM molecule contains a functional group (e.g., a thiol moiety) to chemically attach it to the MC surface, which serves to provide stability. Tailoring of the molecular recognition terminal of SAM-forming molecules through the use of mono- and bi-functional molecules has led to many interesting possibilities for engineering the response characteristics of MCs[60, 81-83]. For example, Thundat and coworkers have demonstrated the use of SAMs of thiolated chelates on MCs for sensing of different metal ions such as cesium, calcium, and chromium[81-83]. They have

also demonstrated a protein functionalized MC sensor which exhibited large responses to multiple metal ions[84]. However, in these cases, the strong metal binding characteristics of the chelates or proteins tends to produce irreversible responses; e.g., even the use of EDTA was not enough to regenerate the protein functionalized MC[84].

In this chapter we report the use of single and binary mixtures of different thiolated ligands as SAMs on nanostructured MCs for the selective and sensitive sensing of multiple metal ions in aqueous solution. To our knowledge, this is the first report of the development of SAM-functionalized, nanostructured MC using different mono-dentated ligands for detection of monovalent, divalent, and trivalent metal ions. Cantilever tip deflections are monitored by optical beam bending technique commonly employed in AFM. Of the plethora of possible simple ligands that are expected to yield different affinities for metals, the ones used in our studies have hydroxyl, carboxyl, or amine functionalities, as well as different alkyl chain lengths separating the thiol and ligand functionalities. While it is likely that multiple ligands bind to a single metal ion, it is unlikely that the full coordination sphere of the metal is satisfied with our approach. Thus, overall binding strengths are less than that expected with binding to chelating ligands. This gives rise to reversible responses that are so important in true sensing applications. Moreover, we compensate for the expected lower responses with smaller binding strengths by using the more responsive nanostructured MC surfaces; good sensitivities are observed for several tested metal ions. Although we mentioned the potential use of differentially-functionalized MC arrays, in this

initial study we chemically treated all the cantilevers the same and simply recorded the response of a single randomly chosen MC within an array.

## **2.2 EXPERIMENTAL**

Experiments were performed using commercially available silicon arrays (five cantilevers per array) of MCs coated with aluminum and having dimensions 400  $\mu\text{m}$  length, 100  $\mu\text{m}$  width, and approximately 1  $\mu\text{m}$  thickness (Mikro Masch Co., Sunnyvale, CA). Chromium, gold, and silver metals deposited on the MCs were obtained from Kurt J. Lesker, Gatewest, and Alfa Aesar Co., respectively, at 99.9% purity. Different thiolated ligands used for functionalization are listed in Table 1. All the metal-chloride, -nitrate and -acetate salts, the salts employed for the preparation of buffer solutions, the solvent ethanol, and all other reagents were purchased from Sigma or Fisher at highest available purity and used as received. Water used to prepare solutions was obtained from a Barnstead E-Pure water filtration system.

For measurements using cantilevers coated with aluminum, the cantilevers were cleaned in a piranha bath (75%  $\text{H}_2\text{SO}_4$ , 25%  $\text{H}_2\text{O}_2$ ) for 30 minutes [Caution: piranha solution reacts violently with organics] after removal of thin aluminum layer by immersing them in aqua regia (75%  $\text{HCl}$ , 25%  $\text{HNO}_3$ ) for 3 minutes [Caution: aqua regia is very corrosive]. The cantilevers were then thoroughly rinsed in deionized water. The process of creating the nanostructured MCs having a dealloyed surface is described in detail elsewhere[77]. In order to create gold nanostructured surface on one side of the cantilevers, a composite metal coating was created using physical vapor deposition (PVD) in vacuum from tungsten

**Table 1** List of Thiolated Ligands

<b>Acronyms</b>	<b>Name of the thiolated ligand</b>
AET	2-Aminoethanethiol
MPA	3-Mercaptopropionic acid
MUA	11-Mercaptoundecanoic acid
MP	3-Mercaptopropanol
MUD	11-Mercaptoundecanol
Cysteine	Cysteine

boats (Cooke Vacuum Products, model CE 301, South Norwalk, CT). Evaporation of a 5 nm chromium adhesion layer was followed by evaporation of a 15 nm gold layer and, without stopping the evaporation of gold, by co-evaporation of gold and silver until a composite Au/Ag film of ~50 nm thickness was formed. Both the deposition rate and resulting coating thickness were monitored using a QCM. Silver was subsequently etched out of the composite film by placing the cantilevers in an aqueous solution of 0.2% w/v H<sub>2</sub>AuCl<sub>4</sub> for 2-3 minutes. Cantilevers were rinsed with copious amounts of water after etching. MCs with smooth gold surfaces were prepared by depositing 30 nm gold onto 5 nm chromium adhesion layer.

The nanostructured and smooth gold coated cantilevers used in our studies were chemically modified with SAMs of single and binary mixtures of bifunctional n-alkyl compounds possessing a thiol group for binding to the metallic MC surface on one end and a mono-dentated ligand group for the complexation of sample metal ions on the opposing end. In case of MC functionalization with single thiolated ligands, this modification was performed by immersion of the nanostructured MC into 10 mL solutions of 1 mM corresponding reagent in ethanol for up to 18 hrs. When the MCs were functionalized with binary mixtures of ligands, similar concentrations were mixed in 1:1 proportions by volume and then nanostructured MCs were dipped into 10 mL of ethanolic solution of that binary mixtures for up to 18 hrs. Upon removal from the ethanolic solution, the MCs were initially rinsed with ethanol and then copiously rinsed with water and stored in pH 5 acetate buffer (AB) at room temperature.



The bending responses of the MCs were monitored using an optical beam bending technique as previously described (see chapter 1)[60, 66]. The apparatus included a 5 mW diode laser (Coherent Laser Corp., Auburn, CA) operating at 632 nm, a focusing system, and an in-house-built position-sensitive optical detector. The amplified output signal of the detector was displayed and recorded with a multichannel digital recorder (Stanford Research Systems, Sunnyvale, CA). The signals in this work are reported in voltage output of the detector. Data were collected at 1 Hz and then running averaged over 32 data points to generate the figures presented herein. This smoothing did not alter the shape of the true response curves. The cantilever was mounted inside a 150  $\mu$ L volume Teflon flow cell that was imaged with a Watec CCD camera (Edmund Industrial Optics, Barrington, NJ) equipped with a microscope zoom lens. Analyte solutions were delivered to the flow cell via a system of vessels connected to three-way valves allowing for switching between different solutions (AB and samples) with minimal disturbances of the flow. The flow rate was adjusted to 0.2 mL/min. The entire apparatus was placed on a vibration isolation table (Newport Corp., RS2000) located in a thermally controlled environment. Measurement of pH was utilized an Orion SA 520 pH meter (Thermo Orion, Beverly, MA).

All metal-chloride, -nitrate, and -acetate solutions were prepared in pH 5 AB which was also used as a background buffer solution. Chemically modified cantilevers were allowed to equilibrate in the background solution until a stable baseline was achieved before any measurements. For our purposes, tensile (compression of the nanostructured surface) and compressive (expansion of the

nanostructured surface) responses involve bending away from and bending toward the bare silicon side of the MC, respectively.

## **2.3 RESULTS AND DISCUSSION**

Figure 7A is a depiction of the predicted surface structure of the SAM modified, nanostructured MC where SAM is represented by a mixture of different thiolated, mono-dentated ligands with variable chain length. Upon exposure to metal ion solutions, a limited number of the ligands bound to the functionalized MC are accessible to the metal ion of interest. Thus, the figure demonstrates that simple mono-dentated ligands will not satisfy the full coordination sphere of the metal, which gives rise to modest binding constants and reversible responses.

Different models have been proposed to describe the analyte induced changes in apparent surface stress ( $\Delta\sigma$ )[85]. In the case of charged cantilever surfaces, modified with ionizable ligand phases and interacting with aqueous metal ion electrolyte solutions, it is expected that changes in Columbic forces contribute significantly to MC response characteristics. In comparing smooth gold to dealloyed MCs we have often noted analyte induced responses that differ in direction, compressive (expansion of the active surface) versus tensile (contraction of the active surface). Based on observed responses, it appears that the smooth gold bares a negative charge (perhaps due to traces of gold oxides) while our fabricated dealloyed surface is positively charged (perhaps due to residual silver ions produced in the dealloying process). With extended use and modification the charge situation can change. Figure 7B depicts the effects of

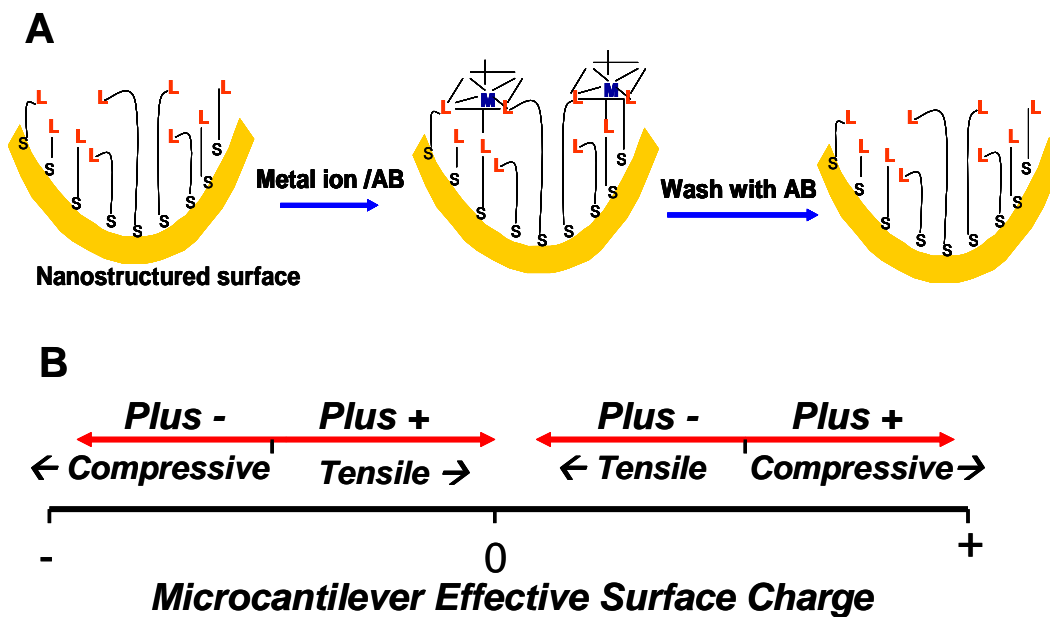


**Figure 7** (A) Schematic representation of the molecular structure of the SAM of mixture of thiolated ligands with variable chain length as ionic recognition phase for metal ions. (B) Depiction of the columbic based realization of changes in compressive or tensile surface stresses resulting in expansion or contraction, respectively, of the surface.

Coulombic forces on response characteristics. If changes in the local environment (e.g., injection of sample) cause the MC surface charge to diminish the surface will contract (tensile response), while increasing the charge, in either direction, will produce an expansion of the surface (compressive response).

While we did not perform the more demanding direct measurement of the double layer potential under varying local environments, we did conduct some independent experiments using our versions of MC surfaces to validate assertions regarding charge effects. Smooth and dealloyed gold surface MCs (no ligands) were exposed to 0.1 and 1.0 mM solutions of metal electrolyte in the presence of an excess of AB. The electrolytes were cobalt-acetate to study interactions of the metal ion with the surfaces, with the same counter anion as the buffer, and sodium-chloride to study anion effects, with the same counter cation as the buffer. With the doubly charged  $\text{Co}^{2+}$  metal, the dealloyed kinetic response rise was +4.4 and +11.8 mV/second for exposure to the dilute and concentrated solutions, respectively. It appears that a weak interaction between the cobalt cation and the gold surface occurs. The positive slope indicates a compressive response, which is consistent with an increasing positive surface charge. Conversely, when the expected negatively charged smooth gold surface MC was exposed to the dilute cobalt solution, the response was tensile (-5.0 mV/second) indicating a move toward zero charge. However the more concentrated cobalt solution produced a compressive +4.5 mV/second response rise following a very brief negative excursion as the  $\text{Co}^{2+}$  solution just reached the MC. This is consistent with the surface charge moving through the zero charge point. For the interaction with  $\text{Cl}^-$ ,

the smooth surface produced +0.40 and +1.4 mV/second compressive responses for the dilute and concentrated solutions, respectively. This is consistent with anion interactions with a negative surface. The responses were -0.40 (tensile) and + 0.30 (compressive) mV/second for the dealloyed surface, consistent with moving past the zero point charge for a surface that is initially positive in charge.

In another experiment, both the dealloyed and smooth gold surface MCs were exposed to dilute aqueous solution of MPA (1mM) in pH 5 AB, one of the ligands used in this work to form SAMs where the same buffer was the background solution. On exposure to this negatively charged reagent, negative smooth gold surface showed a rapid compressive response while the positive dealloyed surface experience a slower tensile bending. These results are again consistent with increasing and decreasing surface charges, respectively, as represented in Figure 7B.

In preliminary experiments, attempts were made to determine if SAMs (18 hrs. functionalization time to form the monolayer) comprised of mono-dentate ligands can actual detect metal ions in solution. Figure 8A shows the response behavior of a 3-Mercaptopropanol (MP) functionalized MC upon exposure to 1 mM Co and Cs metal ions in pH 5 AB solutions. An exposure time of 3 minutes produced a compressive response in the MP coated MC, which was reversed when the metal ion solution was replaced by background buffer solution. It is reasonable to expect that the weak complexation of the positive metal ions via the neutral MP ligand will cause an increasing positive surface charge and subsequent charge repulsion by metal ions produce the observed compressive responses. It

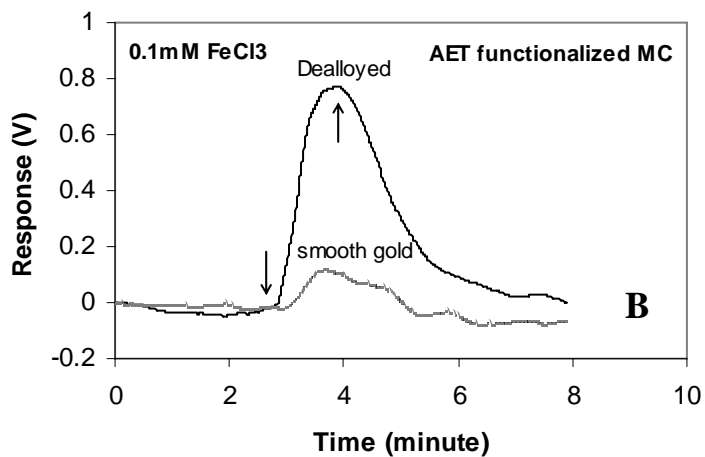
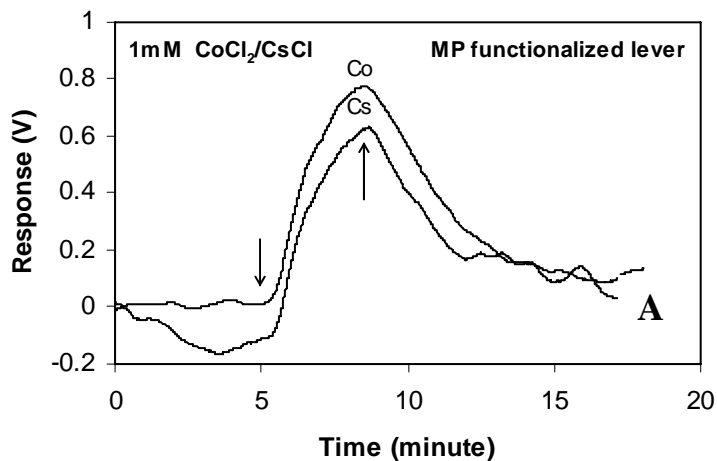


**Figure 8** Time trace of SAM coated MC on exposure to  $\text{Cs}^+$ ,  $\text{Co}^{2+}$  and  $\text{Fe}^{3+}$  metal ions in AB solution (pH 5), first arrow indicates injection of metal ions and the second one indicates the return to background AB (pH 5). **(A)** Response of MP coated MC and **(B)** comparison of bending responses of AET functionalized nanostructured (dealloyed) MC to similarly functionalized smooth gold MC.

should be mentioned, however, that unlike the experiments involving acetate counter ions described above, a couple of complications exist in this experiment. While freshly prepared dealloyed surfaces appear to possess a positive charge, the functionalized surface may not. Secondly, a different counter ion ( $\text{Cl}^-$ ) has been brought into the system.

SAMs of 2-Aminoethanethiol (AET) were formed on both 30 nm smooth gold and dealloyed MCs. Figure 8B shows the responses of the two different MC surfaces upon exposure to 0.1mM  $\text{FeCl}_3$  in AB solution. Though the kinetics of bending of the asymmetrically nanostructured MC was much faster than that of the cantilever with smooth surface, both the MCs showed reversible compressive responses to the metal ion. The compressive response of the AET coated nanostructured MC is nearly an order of magnitude larger than that of the smooth one. This enhancement in chemimechanical response of the dealloyed surface is also observed for other thiol SAMs as well as for other metal ions. In fact, enhancements are consistently observed in MC bending upon dealloying of previously smooth MC surfaces reaching orders of magnitude and sometimes exceeding the increase in surface area produced by the nanostructuring[60, 77]. Microscopic investigations of the surfaces that are nanostructured by the dealloying process reveal it's colloid like morphology[77]. Consistent with our MC observations, theoretical and experimental studies have shown that stresses caused by inter- and intra-molecular interactions in surface-confined colloids may exceed that on smooth surfaces by orders of magnitude[77, 86].

In another series of experiments, dealloyed MCs were functionalized with single short chain thiolated ligands (MPA and MP) and binary mixtures of either short and long chain ligands with the same functionality at the end (MPA-MUA, MP-MUD) or ligands with different functionalities at the other end (MPA-MP, AET-MPA). Upon exposure to 0.1mM CoCl<sub>2</sub> in buffer solution, all of the differently functionalized MCs showed reversible compressive responses. The response magnitude of the singularly functionalized MCs is 2-4 times larger than the dual functionalized MCs irrespective of similar or different functionalities (Figure 9A and 9B). The smaller response with the dual ligand systems was somewhat surprising as we felt the long and short chain system would provide greater geometric flexibility and the dual functional system would permit greater versatility to complex the metal ion. Nevertheless, Figures 8 and 9, demonstrate that the shapes and the magnitudes of the response profiles are characteristics of metal ions and ligands. This fact could have implications for selective metal ion recognition in an array format.

In addition to the impact of ligand type and the nanostructuring of the MC, optimization of the sensor's response is influenced by the uniformity and the density of the SAM and the pH of the working buffer. To optimize the SAM to obtain the highest sensitivity towards different metal ions, both the immersion time and the concentration of the ligand solution (single and dual ligand cases) were studied. Also, pH of the working buffer solution affects protonation of the functional group at the end of the thiol receptor molecule impacting sensor



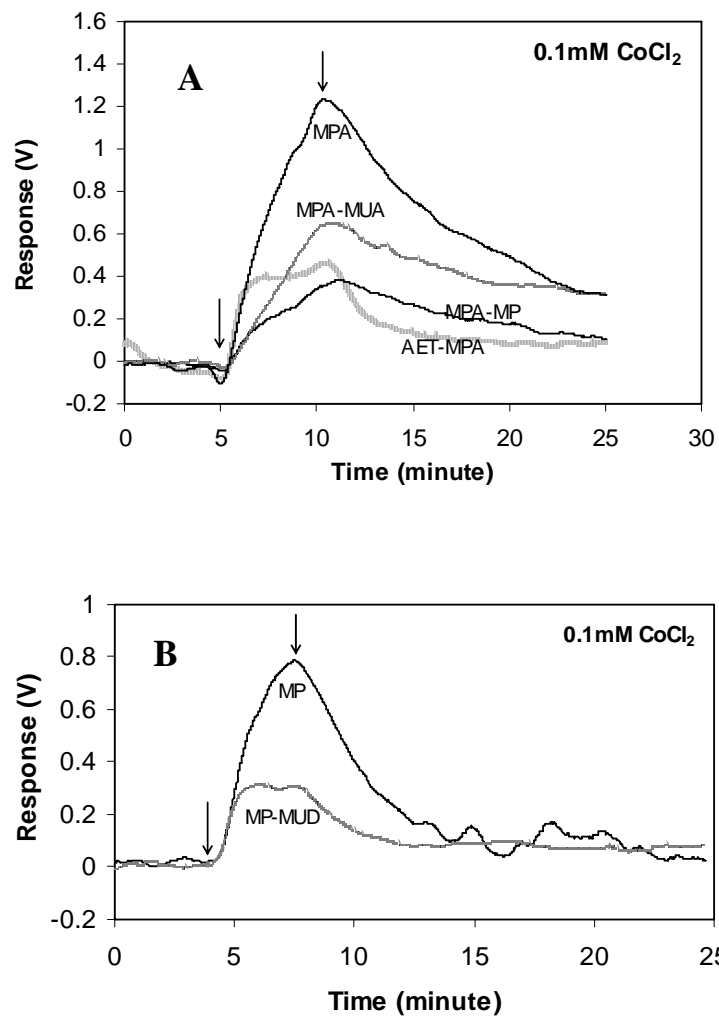


**Figure 9** Comparison of the bending responses of the single and dual thiolated ligand functionalized MCs as a function of time,  $t$ , upon exposure to 0.1 mM CoCl<sub>2</sub> in buffer solution (pH 5), first arrow indicates injection of metal ion and the second one indicates the return to background buffer (pH 5).

performance. In the present work, different mono-dentate single and binary mixtures of simple thiolated ligands were used for detection of monovalent, divalent, and trivalent metal ions. Optimization of different SAMs with respect to immersion time, concentration, and pH was performed using  $\text{CoCl}_2$  as the analyte.

Figure 10A shows the effect of immersion time in ligand solutions on the response magnitude of differently functionalized MCs with single mono-dentate ligands when exposed to 0.1mM  $\text{CoCl}_2$  in AB solutions. For immersion time experiments, dealloyed MCs were dipped into 1mM thiol solution in ethanol from 0.5 hr to 18 hrs. Comparison of the different immersion times for SAM formation showed that 2 hrs. functionalization yielded the maximum response for all the ligands. Although it may have formed a denser monolayer, longer incubation times did not result in an optimized MC surface for metal ion sensing. Note that some of our other experiments were performed prior to obtaining the data in Figure 10A and, hence, using systems that were not optimized in terms of SAM-formation time. The effect of immersion time when functionalizing the MC with 1:1 binary mixtures of short and long chain ligands with the same functionality was also studied. Substantially different results were observed when comparing the dual system to the singularly functionalized systems (compare Figures 9A & B). The required extended incubation time for efficient functionalization of surfaces with mixtures of thiolated compounds has been observed before[87]. The increased formation time (18 hours yield the best responses) may be due to the rearrangement of two different chain length thiols to the proper orientation for binding to the gold surface. The use of a lower concentration of ligand solution

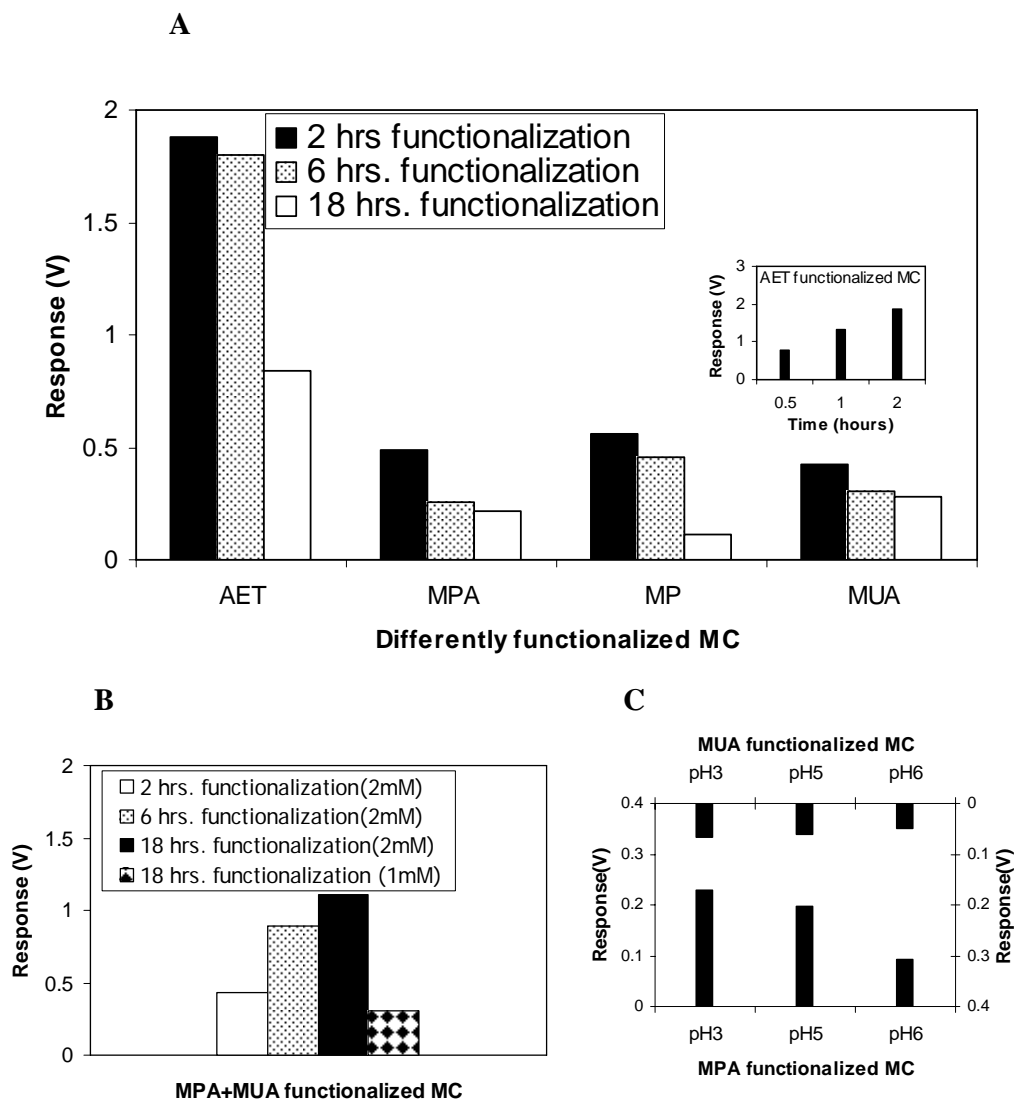


**Figure 10** Effect of immersion time on response (bending) to 0.1mM CoCl<sub>2</sub> for functionalization with single (**A**) thiolated ligand and (**B**) dual thiolated ligand systems. In (**C**) the effect of pH on the bending responses of SAM - MCs are shown when exposed to 0.1mM Co<sup>2+</sup> solutions.

for functionalization also resulted in a 3-fold lower response for 0.1mM CoCl<sub>2</sub> at the 18 hour incubation time (Figure 10B).

The impact of pH on the sensor response is demonstrated in Figure 10C for the test CoCl<sub>2</sub> solution on the MPA and MUA functionalized MC. As the pH is lower from 6 to 3 and the acidic group neutralized, both conditional complexation constants and ion exchange capacity are expected to decrease. Nevertheless, the response in terms of bending increases with lowering of pH. It is conceivable that rearrangement of the SAM on the dealloyed surface as the MPA and MUA are neutralized influences the ability to complex the metal. Also it is possible that even smaller binding can produce a greater surface stress depending on the surface charge changes that occur as depicted by Figure 7B. It is appropriate to note here that the static bending of MC, unlike traditional mass sensing transducers, is an apparent surface stress phenomenon that is only loosely related to the mass loading of the sensing surface with analyte.

Metal ion recognition using differently functionalized MCs is based upon selective binding of ions with specific coordination and geometric requirements to the ligand molecules on the sensing surface. Thus designing and varying binding sites in the SAM can enhance the selectivity of the sensor. Figure 11 shows response selectivity for metal ion recognition with variation of functionality and chain length of the thiolated ligands in combination with the variation of counter anion of metal salt solutions. All responses are based on 3 minute exposures to a single moderate concentration (0.1mM) of the salt solutions in buffer. The selectivity factors for the various metal ions for a particular ligand can be

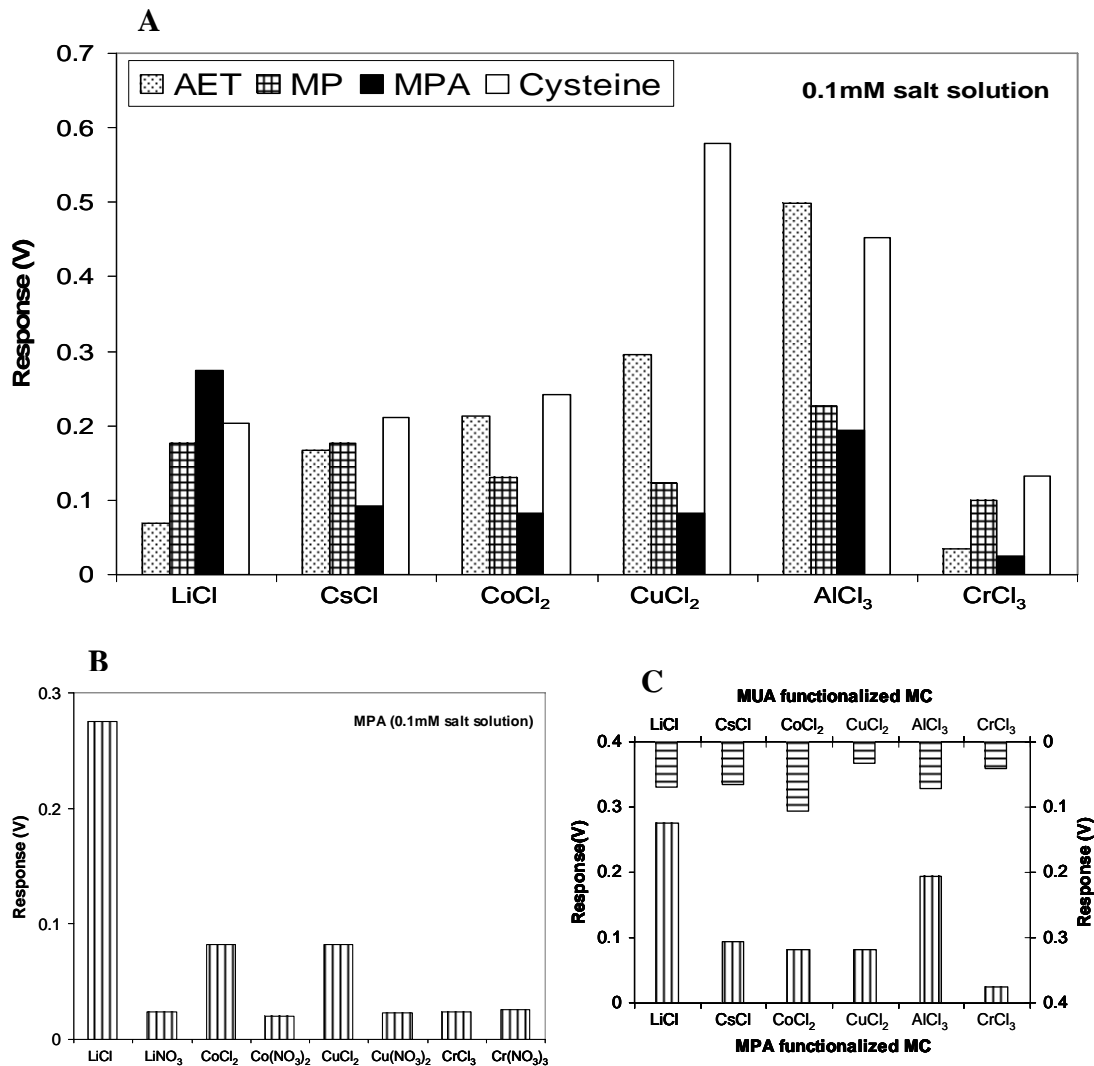


**Figure 11** Response (maximum bending) selectivity for metal ion detection (A) with different thiol functionalized MC, (B) with different counter anion, and (C) with different chain length thiol using 0.1 mM metal ion solutions in buffer.

determined from the ratio of the response magnitudes of two similarly charged metal ions. As stated above the response ratios are not strictly a matter of ionic recognition. Moreover, the response ratios could change with concentration. Figure 11A demonstrates the selectivity pattern for differently functionalized MCs for six different metal ions. Trivalent metal ions are more selectively sensed relative to each other than the divalent and monovalent metal cations, a trend common to each ligand. This trend has also been observed by Zugle et al. in the electrochemical detection of metal ions using ion-channel sensor based on a SAM of thioctic acid[87]. The MP functionalized MC showed no response selectivity for both the divalent and monovalent metal ions whereas the AET coated MC showed better selectivity in sensing monovalent metal cations than the divalent cations. Selectivity patterns for MPA and Cysteine functionalized MCs are opposite in sensing monovalent and divalent metal cations.

To study the counter ion effect, an MPA functionalized MC was exposed to chloride and nitrate salts of four different metal ions. The greater response of chloride salts over the nitrate salts was demonstrated for all metal cations except Cr (Figure 11B). This may indicate the simple chloride anion has less interference with the ligand and metal cation interaction than the larger, more complex nitrate ion. Figure 11C shows the comparison of selectivity pattern for MCs functionalized with different chain lengths (MPA and MUA). It is obvious in the figure that short chain functionalized MC shows better selectivity in sensing monovalent and trivalent metal ions than the divalent ions. However, the long chain thiol coated MC shows better selectivity in sensing divalent cations.

Our prior work [60, 66, 69, 77, 78] shows that calibration plots are generally linear for two or more orders of magnitude while coefficients of variation for measurements using a given MC-MRP are generally 10% or better. Repeated exposure of the same 0.1mM CoCl<sub>2</sub> to the same single cantilever in the MC array functionalized with AET caused similar response amplitudes and bending rates indicating good single day measurement reproducibility with CV values of 9%. Inter-day reproducibility studies using MUA functionalized MC showed the average value of bending response from day 2 was ~90% of the average value from day 1 when stored in AB at room temperature. Thus, reasonable reproducibility can be achieved with this sensor which, nevertheless, requires calibration on at least a daily basis.

Linear dynamic range in MC applications can be limited by instrumental factors (e.g., an eventual non-linear relationship between tip displacement and PSD output) or fundamental relationships between the magnitude of stress modulation and analyte concentration. As an example of the latter, in the current application it is reasonable to expect that as the SAM becomes saturated with metal ion both the absence of available ligands and charge repulsion will diminish the tendency for further metal complexation. Figure 12 provides calibration plot of an AET functionalized MCs exposed to CoCl<sub>2</sub> in AB. Here the response magnitude of MCs was plotted against the concentration of CoCl<sub>2</sub> during a 3 minute exposure time. The two inserts provide real response curves of AET functionalized MC (2 hrs. functionalization) on exposure to 1×10<sup>-7</sup>M CoCl<sub>2</sub> with (32 data points averaging) and without

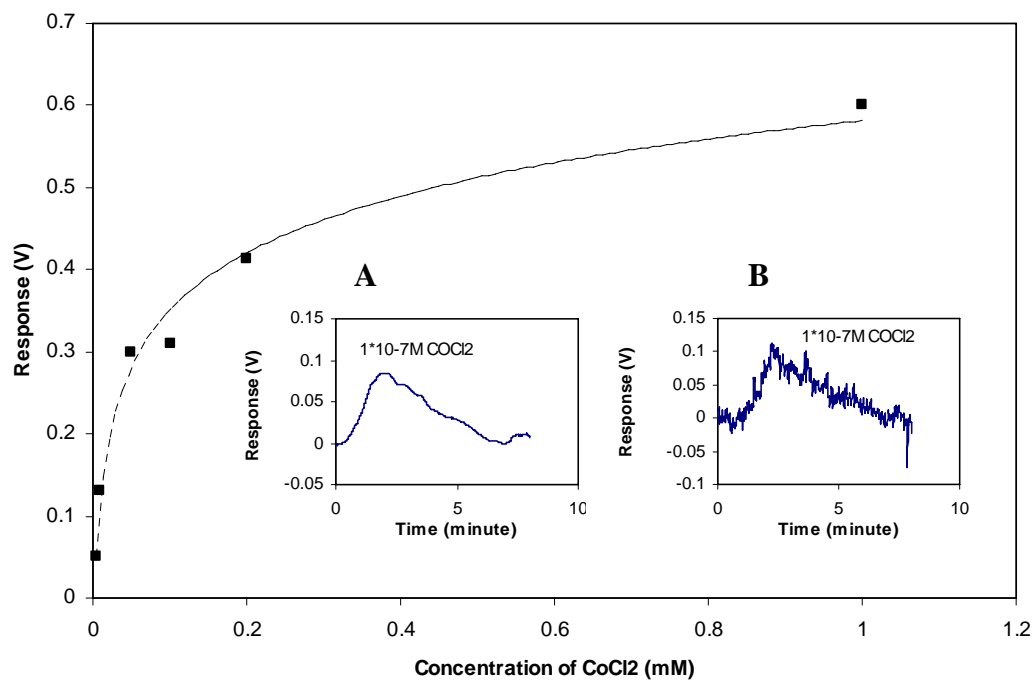


**Figure 12** Concentration-based response curve of AET functionalized (18 hrs immersion time) MC. Inset: Real response curve of AET coated (2 hrs. functionalization) MC on exposure to  $1 \times 10^{-7} \text{ M CoCl}_2$  (A) with 32 data point averaging and (B) without smoothing.



smoothing. Optimization of the SAM formation time has resulted in detection limits in the mid-nM range for this metal.

Our studies demonstrate that SAMs of different thiolated ligands on nanostructured MCs can be applied for the detection of a wide variety of metal cations with good sensitivity and reversibility. The former characteristic is partly a result of the unique characteristics of nanostructured MCs while the latter is due to the relatively weak metal ion complexation by SAM of mono-dentated ligands. Moreover, our results indicate the shapes and magnitudes of response profiles are characteristics of metal ions and ligands. Given the large number of possible mono-dentated ligands or combinations thereof, the achieved level of “ionic recognition contrast” (selectivity) bodes well for future efforts to generate spatially dense arrays of MCs with differing SAMs on the MCs and different metal ion response characteristics. We have acquired unique gas phase analyte signatures, and employed pattern recognition techniques to identify analytes based on the signatures in other MC array work[27, 88]. A key future effort will involve developing efficient and reproducible methods to differentially functionalized MC arrays with different thiolated recognition phases.

## **CHAPTER 3: DIFFERENTIALY LIGAND-FUNTIONALIZED MICROCANTILEVER ARRAYS FOR METAL ION IDENTIFICATION AND SENSING**

Chapter 3 sections 3.1-3.3 are an adaptation of a research article *Anal. Chem.* **2007**, 79, 7062-7068. The article demonstrated that arrays of thiolated ligand SAMs could be made and pattern recognition algorithms could be applied to metal ion response signatures to identify metal ions, greatly enhancing the selectivity of the system.

### **3.1 INRODUCTION**

With ever-increasing industrial sprawl, the likelihood of release of pollutants into the environment increases. Technologies for environmental monitoring must keep pace with expanding industrial demands. One class of environmental pollutants that has garnered much attention recently is that of heavy metals. Heavy metals are particularly dangerous to the entire ecosystem because not only are they toxic, but they possess the ability to bioaccumulate in organisms[89]. Bioaccumulation increases the heavy metal concentration present in an organism and therefore increases toxic effects. Heavy metal poisoning has shown to cause medical difficulties with, but not limited to, nervous, gastrointestinal, and cardiovascular systems[89]. The health threat that heavy metal contamination can pose necessitates a technology able to detect and identify metal ions present in our environment.

Currently, methods used to detect metal cations include liquid or gas phase chromatography[90-92], flow injection systems[93], electrochemistry[94, 95],

atomic absorption[96], solid-phase extraction[97], fluorescent sensors[98], inhibition-based enzymatic assays[99], and immunoassay[100]. However, many of the techniques are not amenable to environmental sensing because they are expensive and/or time consuming. Newer, more adept technologies must be produced to confront the shortcomings of older technologies.

MC sensors have emerged recently as sensing transducers that offer greater mass sensitivity than comparable sensors such as QCMs, FPW oscillators, and SAW devices[101] due in large part to their very small dimensions. MCs have been utilized in many chemical and biochemical sensing applications[24, 31, 32, 36, 102-111]. Not only do MCs demonstrate greater sensitivity, but they also are relatively low in cost, they can be used in an array format, and they can be integrated into on-chip electronic circuitry.

When a target analyte interacts with an immobilized RP on one side of the MC, the interaction causes surface stress on that particular side of the MC[101]. However, the opposite (blank) side of the MC is largely passive to the target analyte. The interaction of the analyte with only one side of the MC creates a differential surface stress, which is relieved by the MC bending. As stated previously, the bending of the MC (tip deflection,  $z_{\max}$ ) can be characterized and approximated by Stoney's equation[29]

$$z_{\max} = \frac{3l^2(1-\nu)}{Et^2} \Delta\sigma \quad (5)$$

where  $\nu$  and  $E$  are, respectively, the Poisson ratio and Young's modulus for the cantilever,  $t$  is the thickness of the MC,  $l$  is the cantilever effective length, and  $\Delta\sigma$  is analyte-induced differential surface stress ( $\Delta\sigma_{\text{active (i.e., RP) side}} - \Delta\sigma_{\text{passive side}}$ ).

Recently, MCs have shown promise in the area of metal cation detection[112]. We demonstrated that by functionalizing gold nanostructured MCs with thiolated ligand SAMs, the MCs would respond to different metal cations present in a sample. The ligand functionality interacted with the metal cations satisfying only a portion of the metal's coordination sphere; this allows for reversible interactions. The procedure used to nanostructure the surface prior to ligand functionalization results in good sensitivity despite the modest binding constants between the mono-dentated ligands and metal ions.

In this chapter, prior work is expanded upon by using MCAs with multiple MCs differentially functionalizing with thiolated ligand SAMs, thereby creating for the first time a true MCA with ionic discrimination capabilities. The underlying dealloyed nanostructured surface was created by codepositing Ag and Au and then etching the Ag from the composite layer[113]. Properties of this nanostructured dealloyed surface such as, thickness, gold to silver deposition ratio, and etching time were more thoroughly studied and optimized. Electrochemical and in-situ derivitization experiments were performed to demonstrate the impact that dealloyed layer changes would have on the thiolation of the surface. Surface enhanced Raman spectroscopy (SERS) experiments were performed directly on MC surfaces to demonstrate that a capillary coating procedure could be used to successfully differentially functionalize each of the

diminutive cantilevers in an array with a different thiolated ligand. Sensor performance experiments were then performed to demonstrate the sensitivity and selectivity (differentiating capabilities) of the MCA sensor. Finally, pattern recognition algorithms were applied to the selectivity studies to classify metal ions in unknown samples.

### **3.2 EXPERIMENTAL**

Silicon MCs with dimensions 400  $\mu\text{m}$  length, 100  $\mu\text{m}$  width and 1  $\mu\text{m}$  thickness were commercially available (Mikro Masch Co., Sunnyvale, CA). The chromium, gold and silver metals (99.9% in purity) used in vapor deposition were obtained from Kurt J. Lesker, Gatewest, and Alfa Aesar Co., respectively. The flexible fused silica capillary was purchased from Polymicron Co. with 350  $\mu\text{m}$  outer and 250  $\mu\text{m}$  inner diameters. All the metal chloride analytes, salts for preparation of buffer solution, thiolated ligands (List below in Table 2), and the 4-aminothiophenol (ATP) and o-Mercaptobenzoic acid (MBA) used in SERS experiments were obtained from either Sigma or Fisher at highest purity and used as received. HF buffer containing ammonium fluoride and HF used for the capillary etching was purchased from Transene Company. Water used for preparation of solutions was obtained from a Barnstead E-Pure water filtration system.

The creation of MCs having a silver, smooth gold or dealloyed surface was achieved by using a PVD approach. More details about the vapor deposition instrumentation and approach can be found elsewhere[112, 113].

**Table 2** List of Thiolated Ligands

<b>Acronyms</b>	<b>Name of Thiolated Ligand</b>
AET	2-aminoethanethiol
MP	3-mercaptopropanol
Cysteine	Cysteine
MPA	3-mercaptopropanoic acid
MUA	11-mercaptoundecanoic acid

Dealloyed nanostructured surfaces with a composite 50/50 Au/Ag film with different thickness of 50 nm, 75 nm, 100 nm, 150 nm and 200 nm were deposited using the vapor deposition approach. 3-5 nm of Cr was deposited first then 15 nm of Au was deposited subsequent to the Cr. Finally, the Ag/Au composite film was created by co-deposition of Ag and Au. During the deposition, both the deposition rate and resulting coating thickness were monitored using a QCM. To create nanostructured dealloyed surfaces from the Au/Ag film, the silver was etched out of the composite film by placing the cantilevers in an aqueous solution of 0.2% w/v H<sub>2</sub>AuCl<sub>4</sub> for about 2.5 min. Cantilevers were then rinsed with copious amounts of water after etching. The Ag coated cantilevers for SERS experiments were also created through the vapor deposition approach by depositing 10 - 15 nm of Ag to create a SERS-active Ag-island film on the MC. All Ag/Au, smooth Au or Ag-coated cantilevers used in our studies were chemically modified with SAMs of *n*-alkyl compounds with a thiol group for immobilization of the ligand to the metallic MC surface on one end and a mono-dentated ligand functionality for the complexation of sample metal ions on the opposing end.

To differentially functionalize each cantilever with different thiolated ligands (Table 3), a capillary coating apparatus was designed. The flexible capillaries were aligned and mounted horizontally in sequentially parallel channels with 500  $\mu$ m spacing between them using a V-groove holder machined in-house (note: the MC pitch is 250  $\mu$ m so alternate MCs are aligned with the

**Table 3** Optimized concentrations of ligand solutions

<b>Thiol Ligand Solution</b>	<b>Concentration (mM)</b>
AET	25
MP	25
Cysteine	10
MPA	5
MUA	1
ATP	0.01
MBA	0.01



capillaries). To allow the MCs to be inserted into the capillaries, some pretreatment of the capillaries was carried out. First the polyimide coating on one end of the capillaries was burned off, and the other end was sealed with soft playdough®. The burned end was then dipped in HF buffer [Caution: HF is very corrosive to skin] and etched for 100 minutes to reduce the outer diameter. The sealed end was then cut off. Deionized water was allowed to fully fill the etched capillaries several times until the etched end appeared to be clean. Meanwhile, the nanostructured MCAs were fixed on an x-y-z stage, with all the levers in the direction parallel to the capillaries. The x-y-z stage was then manipulated, using a charge coupled device camera for visualization, to allow for insertion of the MCs into the capillaries. Once the capillaries were inserted into the capillary ends for functionalization, the opposite end of the capillaries were inserted into the appropriate thiol solutions and filled by simple capillary action. During MCA functionalization, MCs and etched capillary ends were visualized with a WAT-902C camera connected to a Sony Trinitron Video Monitor, which provided a 20x magnification. All SERS spectra were collected by using a modified version of a LabRam Spectrograph from JY-Horiba[114]. The instrument used an Olympus BX-40 microscope with a 10x (0.25 NA, 1) objective that delivers up to 8.9 mW of the 632.8 nm radiation from a He-Ne laser. The scattered light was dispersed with a 600 grooves mm<sup>-1</sup> grating, imaged with a 1024 x 256 thermoelectrically cooled charge-coupled device (CCD) camera, and processed with Labspec 4.03 software. An x-y-z stage was used to adjust the focusing of the microscope

objective and the positioning of the laser spot under stationary and translating conditions.

MCAs were mounted in a brass flow cell in an optical system[115]. The cell had one inlet port for background/analyte delivery, one outlet port, and a glass window to facilitate the observation of cantilever deflection. A beam of laser light from an array of vertical cavity surface emitting lasers (VCSELs) (Avalon Photonics, 850 nm, 5 mW) was focused onto the tip of each MC, and the reflected beam was captured and monitored by a single position-sensitive detector.

A single lens was used to focus the VCSELs so that the beam from each VCSEL was focused onto a single corresponding cantilever (12 VCSELs onto 12 cantilevers). The deflection of the cantilever resulted in a corresponding motion of the reflected beam as monitored by the PSD. An in-house-created LabView program controlled a multiplexing scheme that allowed the VCSELs to be activated individually so that one MC was illuminated at a time and the motion of all MCs was monitored by the single PSD. Analyte solutions were delivered to the flow cell via a system of vessels connected to three-way valves allowing for switching between different solutions (buffer and samples) with minimal disturbances of the flow. Each measurement in the study represents a 60 second injection of a metal chloride solution. All metal chloride solutions were prepared in pH 5 AB, which was also used as a background buffer solution. Chemically modified cantilevers were allowed to equilibrate in the background solution until stable baseline was achieved before any measurements.

In the SERS experiment, the focusing laser scanned in a perpendicular direction across 4 adjacent cantilevers functionalized alternately with ATP and MBA. SERS spectra were recorded while the area interrogated moved laterally over a total 1 mm distance. For each cantilever 50 spectra were recorded (one every 2  $\mu\text{m}$  translational step). For each spectra the peak height of the characteristic Raman band of ATP (1010-1050  $\text{cm}^{-1}$ ) and MBA (1055-1095  $\text{cm}^{-1}$ ) was recorded and plotted.

For MCA measurements, an in-house-created LabView program was used to control each VCSEL to be activated individually so that one cantilever was illuminated by only one VCSEL at a time. At the beginning of each cycle, the first VCSEL was activated, illuminating the corresponding cantilever 1. The motion of the reflected beam was monitored by the PSD, and output signal from the detector was sampled by a 16-bit A/D converter at a rate of 1 kHz. 50 samples by the A/D converter were averaged to comprise one point. The sequence was then repeated for VCSEL/cantilevers from 2<sup>nd</sup> to 12<sup>th</sup> (the last). The entire cycle of measuring and recording all 12 MCs takes less than 1 s; therefore, a delay was added so that the cycles begin at 1-s intervals. VCSEL control and data acquisition I/O were performed using a National Instruments NI-6014 DAQ card in an 800-MHz Pentium III PC[116]. Although the MCA and VCSEL arrangement allows for the monitoring of all 12 cantilevers, in the selectivity studies only 5 cantilevers responses (see below), one for each phase, are represented. However, the data used by the pattern recognition algorithm included responses from all 12

cantilevers comprising the array with each of the 5 phases represented multiple times.

Analysis of the entire response profile (responses recorded once per second for each MC during the entire 60 second analyte injection period) for the array for each metal ion was used in an attempt to classify the metal ions. Prior to classification, the information contained within the analyte-induced bending dynamics of the MCAs must be distilled into a form that can be used with existing classification methods. Since inputs for general classification method are N-dimensional vectors, it is necessary to transform the information contained within the time series response of each cantilever into a single vector. It was demonstrated in Archibald et al[115] that independent component analysis can be used to compress the movement of an array of micro-cantilever over a period of time, into a single feature, which is a N-dimensional vector, that was used by neural networks to accurately classified both the type and concentration of the tested analyte. Below the method of transforming MCA signals into features[115] is briefly introduced.

Given an array of N cantilevers, suppose that  $x(t)$  represents the N-dimensional time signal for the entire MCA, and this signal can be representing by a linear mixing of independent sources, or

$$x(t) = As(t) \quad (8)$$

for  $s(t)$  the M-dimensional time series vector of independent sources and  $A$  the  $N \times M$  mixing matrix. If the mixing matrix has full rank and the number of sources is less than or equal to the number of cantilevers, then independent

component analysis will recover  $W$ , the mixing matrix given only the signal  $x(t)$ , such that

$$W^{-1} = SPA \quad (9)$$

Here,  $S$  and  $P$  are arbitrary scaling and permutation matrices respectively. Stated simply, given only the measured motion of the MCA data, the independent component analysis method produces the independent sources of this signal and the mixing matrix, up to arbitrary scaling and permutation of the sources. The benefit of determining this transformation is that the columns of the mixing matrix provide distinct features that can be used for accurate classification. In this study, only the most dominant feature (the column in the mixing matrix with the greatest magnitude) is used in classification[115].

Support vector machines (SVM), a classification paradigm developed over the last decade in the field of machine learning theory[117], have proven to be an effective tool across many scientific disciplines. In order to describe the core ideas of SVM we must consider the features described above or N-dimensional vectors, which can equally be consider as hyper-dimensional points. SVM is a binary classifier, meaning it is designed to identify only two different groups. SVM classification of two groups of features occurs by finding a surface that optimally separates these groups. Once this surface is determined, classification occurs for any new feature presented to SVM by calculating which side of the surface this point lies. The surface that optimally separates the two groups of features is termed the decision surface. Strength of SVM is that complex decision surfaces can be generated at low computational cost through the use of kernel

functions, which have the effect of transposing features into spaces that increase the linear separability of the two groups of features. The geometric nature of the SVM classifier makes it possible to train adequately on reduced sets. One major drawback of SVM is that classification is binary. However, this issue is overcome in a simple and robust procedure that consists of training several SVM's simultaneously in a one-against-one scheme[118], and this is the procedure used in this chapter (see below).

### **3.3 RESULTS AND DISCUSSION**

In our previous studies using SAMs as RPs for metal ion detection[112], optimization of the sensor response focused on parameters concerning the SAMs. Studies involving parameters such as functionalization time, thiol concentration, thiol chain length and functionality were performed. In this present work, much attention was paid to optimization of the underlying dealloyed nanostructured layer. The first parameter studied concerning the dealloyed layer was that of metal layer thickness. Experiments were carried out measuring responses of SAM functionalized dealloyed layers to metal ions for metal layers ranging from 25 – 200 nm. Figure 13 demonstrates that as the dealloyed thickness of the mercaptopropanol coated cantilever was increased up to 150 nm, the response to 0.1 mmol/L of  $\text{Cu}^{2+}$  also increased. However, as the dealloyed layer thickness was further increased to 200 nm, the response decreased slightly. According to the Stoney Equation (Eq. 5), as the cantilever stiffness increases the response decreases (note  $E t^2$  in denominator). The increase in dealloyed thickness results in an increase in surface area (see below) and the  $\Delta\sigma$  term in Eq. 5 that resulting

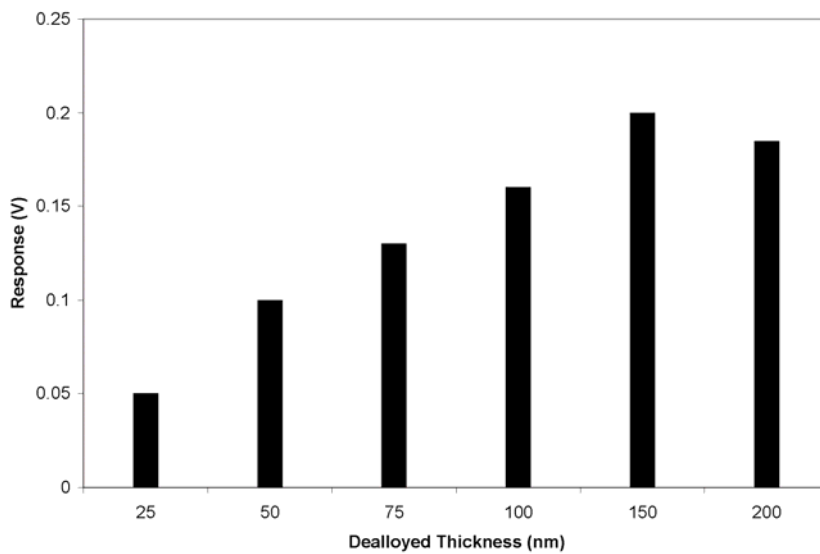


**Figure 13** The effect of dealloyed thickness was studied by monitoring the response to a 0.1 mmol/L  $\text{Cu}^{2+}$  solution for MCs with different thicknesses of the dealloyed layer and functionalized with MP.

from coulombic forces associated with metal-metal repulsion can be expected to increase as well[112]. However, at some point the effect of increasing stiffness (note both terms in the denominator change with dealloyed thickness) appears to reverse (dominate) the trend due to increasing  $\Delta\sigma$ . Experiments involving varying the Ag/Au ratio from the normal 50/50 to 40/60 and to 60/40, along with experiments varying the dealloying etching time from 2.5 min. to 5 and 10 min., did not yield any improvements.

Further experiments were performed to try to better understand why the increased thickness of the underlying dealloyed layer demonstrated an enhancement in response of the MC to metal ions. Figure 14 shows the response of three different cantilevers coated with 35 nm of smooth gold and 50 nm and 150 nm dealloyed layers to an in-situ functionalization with a SAM of propane thiol. The 35 nm smooth gold surface shows the smallest response to the formation of a monolayer of propane thiol, with the 50 and 150 nm dealloyed responses considerably larger. A larger thickness gives a larger response to the formation of propane thiol monolayer suggesting a larger amount of thiol immobilized, but as stated above a larger dealloyed thickness may decrease the ability of the cantilever to respond due to increased stiffness.

To quantify the amount of thiol on the each surface, cyclic voltammetry experiments, using the strategy of Widrig et al[119], were performed with silicon wafers, which were vapor deposited and functionalized at the same time as the three cantilever types in the thickness study. The cyclic voltammetry experiments demonstrated that the 35 nm smooth gold coated silicon wafer was coated with



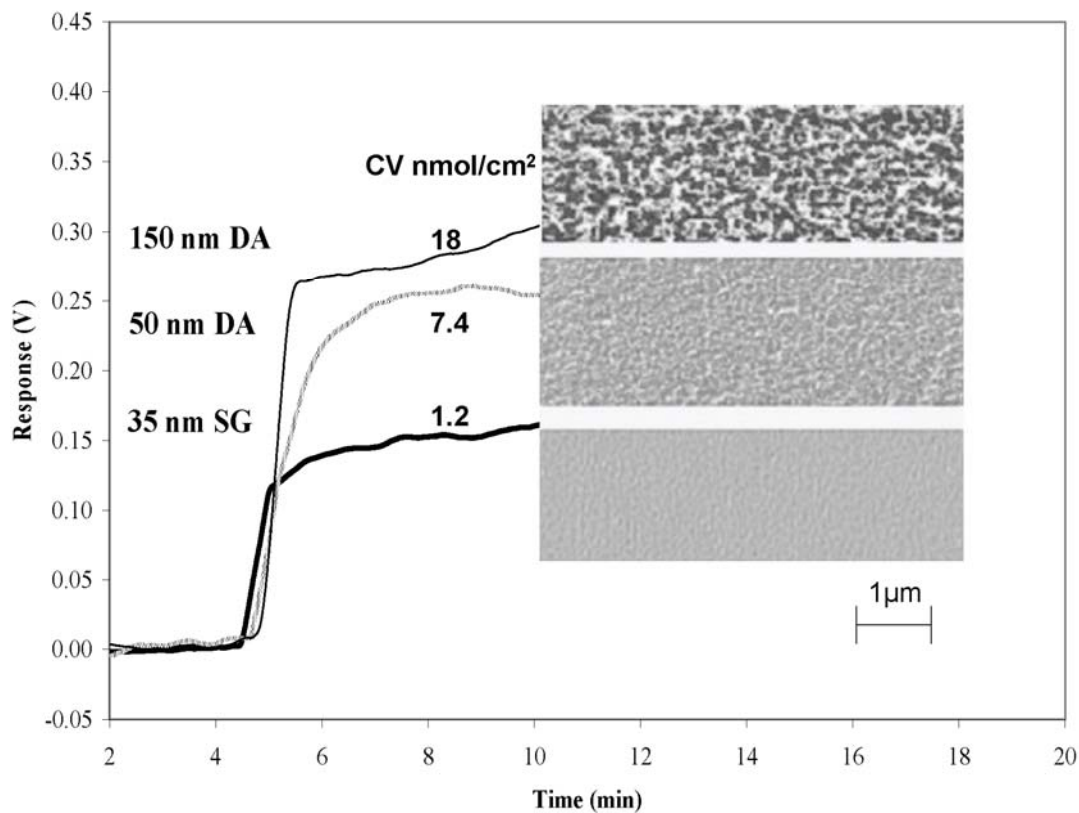


**Figure 14** Surface thiolation studies were carried out by measuring the response of each cantilever (35 nm smooth gold, SG, 50 and 150 nm dealloyed, DA) to an in-situ functionalization with 1 mmol/L propane thiol. Oxidative desorption of the propane thiol from the gold surface through cyclic voltammetry made it possible to quantify the amount of thiol on each surface. SEMs of each surface were taken at 8000x magnification.

1.2 nmol/cm<sup>2</sup> of propane thiol, while 50 and 150 nm dealloyed surfaces were coated with 7.4 nmol/cm<sup>2</sup> and 18 nmol/cm<sup>2</sup> respectively. The larger trend in the cyclic voltammetry values versus actual responses during functionalization with propane thiol underscores the interplay between increases in surface stress with greater surface area and the changes in stiffness. The SEM images, seen in Figure 14, indicate the potential importance of surface morphology on determining response characteristics of the MCs. The greater the degree of roughness and surface crevices, the greater the available surface for thiol immobilized. It can be seen that the 50 nm dealloyed has greater roughness than the smooth gold. The thicker 150 nm dealloyed seems to have transitioned from a roughened surface to a more porous one. Surface area may not be the only factor in determining  $\Delta\sigma$  associated with functionalization and/or binding of metal as the effectiveness of translating the energies associated with those processes into potential energy stored in the bent cantilever can reasonably be expected to be morphology dependent[31].

The first step in creating a differential responding MCA involves developing a method that allows differential coating of the cantilevers in an array. In our prior gas phase sensing work, differential coating was accomplished by singularly vapor depositing a RP through a slit mask onto one cantilever[115]. While this practice of sequentially depositing phases onto each cantilever does allow for creation of arrays, the process is time consuming, tedious, and the RP are not covalently anchored to the cantilever surface to enhance stability. In this work, MCAs are prepared in a liquid phase reaction process via capillary coating

individual cantilevers with thiolated reagents. Figure 15 demonstrates how the capillary coating process is accomplished. The top photograph displays several cantilevers of the MCA inserted into different capillaries by way of a micrometer controlled stage. Then, in the bottom photograph, the functionalization solution fills the capillary through capillary action. The picture demonstrates that the functionalization solution was contained in the capillary and no solution leaks out on the base of the MCA chip. If solution were to leak out of the tip of the capillary, cross-contamination problems could arise and the cantilevers could be coated with more than one type of thiolated ligand. The SERS experiment in Figure 15B demonstrates that the thiolated ligand RP were in fact immobilized on the surface. In this experiment, silver coated MCs were inserted into capillaries that were subsequently filled with either ATP or MBA and allowed to react for 2 hours. After functionalization, the MCs were removed from the capillaries and SERS spectra were collected from each MC surface in a dry state by the spatial translation method described above. Figure 15B shows the intensity of two different Raman bands specific for ATP ( $1010\text{-}1050\text{ cm}^{-1}$ ) and MBA ( $1055\text{-}1095\text{ cm}^{-1}$ ) as the instrument scanned laterally across four cantilevers in the array. The experiment not only confirms that the cantilevers are differentially coated with ATP and MBA, but that the coating is fairly uniform across the width of the cantilever surface and there is no cross-contamination. While MCA sensing and this SERS experiment were performed with distinctly different instrumental arrangements and different cantilever metallic coatings, in principle it should be possible to add the SERS component to MCA measurements directly, perhaps

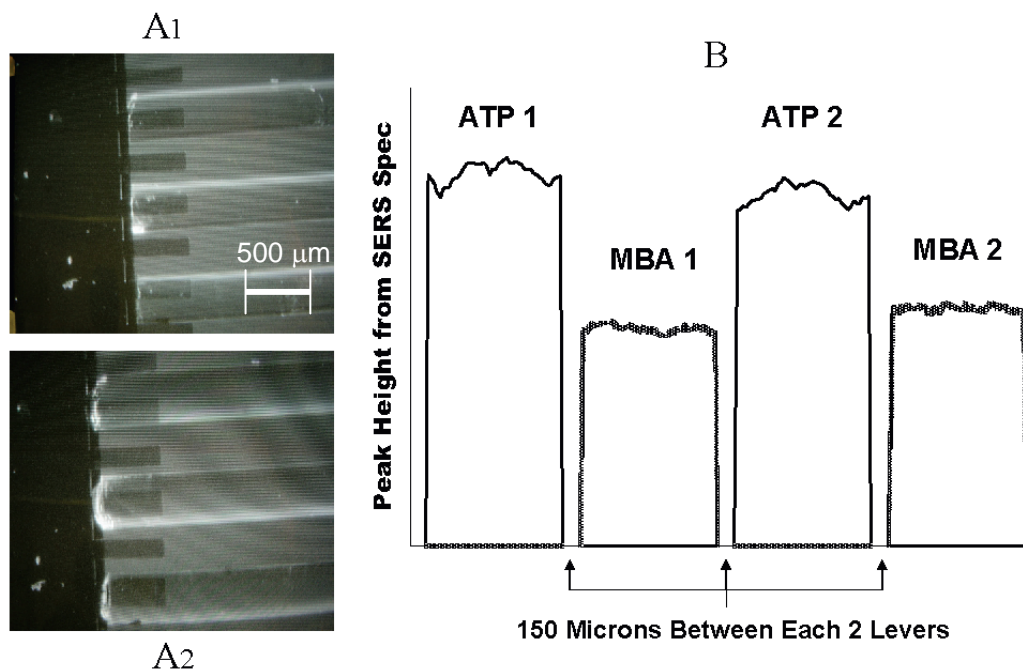


**Figure 15** The ability to differentially functionalize adjacent cantilevers in a MCA is demonstrated using a SERS approach. Differential functionalization is accomplished by a capillary coating process pictured in **A1** dry insertion of the cantilevers into the capillaries and **A2** with the functionalization solution reaching the cantilevers via capillary action. **B** spatially displays the peak height of characteristic Raman bands for two thiolated compounds (ATP 1010-1050  $\text{cm}^{-1}$  & MBA 1055-1095  $\text{cm}^{-1}$ ) which were alternately coated on a series of four adjacent cantilevers via capillary coating.

even using the VCSEL radiation for Raman excitation. In fact, in unpublished work, we have observed that dealloyed surfaces exhibit some SERS activity with visible excitation.

To better characterize sensor performance, calibration studies were carried out. The MCA response to calibration experiments was measured for each of the six metal ions included in the study. Table 4 includes the slope of the calibration curve, r-squared value, and relative standard deviation (RSD) for each of the six metal ions. The MCA sensor demonstrated limits of detection as low as  $10^{-8}$  mol/L based on  $3\sigma$  of multiple injections of  $8.0 \times 10^{-7}$  mol/L copper chloride solution divided by the slope of the copper chloride calibration plot.

The purpose of creating a sensor array based on this ligand approach is to impart a greater degree of distributed selectivity to the system. Arrays of RPs can be designed to incorporate a range of analyte-phase interactions (e.g. dipole, van der Waals, hydrogen bonding, electrostatic, coordinate covalent bonding). Each RP in the array may be designed to utilize one interaction more so than the others. The diverse range of analyte-RP interactions in turn provides diversity to the sensor responses. The advanced processing capabilities of pattern recognition algorithms can then be applied to aid in interpretation of the sensor array response. Rather than a high degree of selectivity between a very specific analyte-RP interaction (e.g., Bioaffinity or chelate metal interactions), that generally involves large binding constants and a lack of reversibility, differential selectivity has been imparted to the system through the approach applied herein.

**Table 4** The slope, r-squared value, and RSDs for the response to the MCA to three injections of each metal ion at five different concentrations including ( $1.6 \times 10^{-7}$ ,  $8.0 \times 10^{-7}$ ,  $8.0 \times 10^{-6}$ ,  $2.0 \times 10^{-5}$ , and  $1.0 \times 10^{-4}$  mol/L)

Phase	MP			AET			MPA			Cyst		
	Metal	Slope	R Squared	RSD	Slope	R Squared	RSD	Slope	R Squared	RSD	Slope	R Squared
CuCl <sub>2</sub>	748	0.9578	9.02	769	0.9343	11.24	1065	0.9979	9.92	739	0.9373	12.35
CoCl <sub>2</sub>	578	0.9698	8.94	597	0.9577	9.97	635	0.9039	10.42	NA	NA	11.64
CsCl	780	0.6635	11.1	753	0.9236	12.48	1127	0.8797	10.89	NA	NA	9.95
LiCl	547	0.9255	10.7	598	0.9333	12.32	1042	0.9736	12.63	529	0.9114	9.02
FeCl <sub>3</sub>	528	0.9712	4.3	NA	NA	5.67	NA	NA	4.71	510	0.9607	4.29
AlCl <sub>3</sub>	956	0.8878	10.2	832	0.9997	10.13	NA	NA	10.78	852	0.7668	9.58

In this chapter, electrostatic and coordination analyte-phase interactions were taken advantage of by each mono-dentated RP. However, the ligand functionality for each RP was altered (distributed among the various MCs in the array), effectively changing the interaction of the RP with each metal ion. Selectivity studies were carried out to determine the diversity of response signature of each analyte. Responses to different concentrations of each analyte were measured for all the RPs in the array. Figure 16 demonstrates the diversity of response from metal ion to metal ion. No two response patterns are extremely similar to each other. This apparent response diversity bodes well for metal ion classification via pattern recognition algorithms.

The classification (metal ion identification) accuracy of the MCA sensor was determined using a leave-one-out cross-validation scheme on the independent component analysis generated features. For each trial, a one-against-one SVM multi-classifier was trained using all the remaining trials. The experimental trials consisted of triplicate injections of five concentrations (range of  $10^{-4}$  –  $10^{-7}$  mol/L) of each analyte. One of the concentrations in the middle of the range was repeated in triplicate for a total of 18 trials for each metal ion analyte. Each trial contained 12 data sets, one for each cantilever (even though some of the cantilevers were redundant or dealloyed blanks). Thus for each trial, the SVM is trained blind to that particular one-out-of-eighteen trial. Once the SVM is completely trained the trial that was removed from the training can be tested and classified. The generalized prediction rate for each analyte is the fraction of times each trial was classified correctly from a blindly trained SVM.

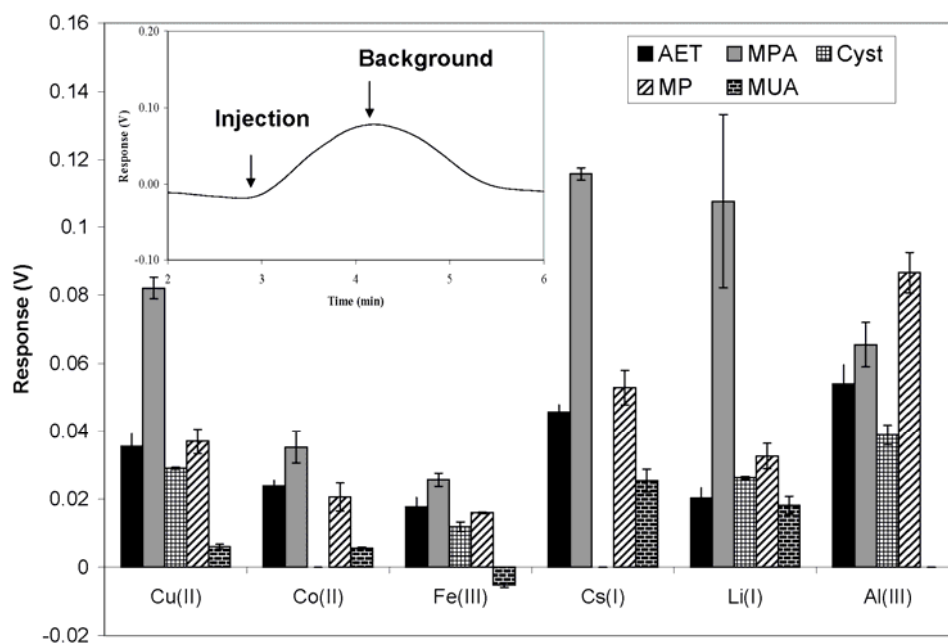


**Figure 16** The response diversity to each metal ion is demonstrated in the selectivity plot. In these experiments, 0.01 mmol/L solutions of each metal ion were injected for 60 sec. and the peak signals are plotted. The insert shows a representative entire response profile of a mercaptopropanol coated cantilever to 0.01 mmol/L Cu<sup>2+</sup>. In this work a 1 mV response corresponds to roughly a 1 nm MC tip deflection.



**Table 5** Generalized prediction rates for each analyte using leave one out cross-validation of one-against-one SVM multi-classification with independent component analysis feature extraction.

Predicted fraction for each analyte						
Tested Analyte	AlCl <sub>3</sub>	CoCl <sub>2</sub>	CsCl	CuCl <sub>2</sub>	FeCl <sub>3</sub>	LiCl
AlCl <sub>3</sub>	0.8889	0	0	0.1111	0	0
CoCl <sub>2</sub>	0	0.7222	0.0556	0.1111	0.1111	0
CsCl	0	0	0.8333	0.0556	0	0.1111
CuCl <sub>2</sub>	0	0.1667	0.0556	0.7778	0	0
FeCl <sub>3</sub>	0	0.1111	0.1111	0.0556	0.7222	0
LiCl	0	0	0.1111	0	0.0556	0.8333

The generalized prediction rate is a powerful measurement of how much informational content is generated from the sensor array for each analyte, and these generalized prediction rates are given in Table 5. It can be seen in this table that the sensor array is responsive to  $\text{Al}^{3+}$ ,  $\text{Cs}^+$ ,  $\text{Fe}^{2+}$ , and  $\text{Li}^+$ ; producing enough information that these metal ions can successfully be identified at rates approaching 90%. However, this is not the case for the doubly charged cations  $\text{Co}^{2+}$  and  $\text{Cu}^{2+}$  where the generalized prediction rates are considerably less significant. For example, the  $\text{Cu}^{2+}$  was misclassified half the trials. Improvements in classification may be realized with improved feature extraction methods and as the library of experimental results for this sensor array builds, providing increased information about the dynamical range and details for each analyte. The fact that the pattern recognition incorporated the entire concentration range, including the concentrations close to the limit of detection where responses were less reproducible, underscores the power of this approach to accurately classify unknown analyte injections.

In summary, the advantages afforded by configuring MCs in an array format functionalized for differential selectivity is demonstrated for the first time. An ability to uniquely functionalize the individual cantilevers in arrays is verified by a spectroscopic approach. Sensor performance is optimized through altering parameters related to the underlying nanostructured dealloyed layer. The optimal dealloyed layer for sensing was shown by various surface characterization methods to be related to increasing amount of thiol ligand bound to the sensing surface, while also limiting overall cantilever thickness. At optimal conditions

the MCA demonstrated limits of detection as low as  $1 \times 10^{-8}$  M. Selectivity experiments yield response signatures that appear unique to the metal ions tested and, when used in conjunction with pattern recognition algorithms, provide a good ability to classify each metal ion even with limited training sets.

### **3.4 FURTHER WORK: MICROCANTILEVER LC HYPHENATION**

#### **3.4.1 Introduction**

Pattern recognition algorithms demonstrated that adequate metal ion selectivity could be generated when applied to thiolated-ligand MCA responses. However, when pattern recognition algorithms are applied to the MCA responses of metal ion mixtures they demonstrate an inability to distinguish each metal present in the mixture. Therefore, new attempts must be made to devise solutions that allow MCAs to detect each component in metal ion mixtures.

Ion-exchange chromatography (IEC) has been used for years to separate metal ions in a mixture[120-135]. Several researchers have incorporated unconventional detectors for detection of metal ions separated by IEC[136, 137]. Thiolated SAM coated MCAs have been demonstrated for detection of metal ions (see above) and may be readily coupled to IEC for separation and detection of metal ions in a mixture. Current detectors for IEC demonstrate no ability to distinguish between the components of different chromatographic peaks apart from retention times. Additionally, current detectors possess no ability to identify the analyte present in the chromatographic peak. The combination of pattern recognition algorithms, a MCA sensor, and IEC might allow for not only

measurement of a chromatographic peak, but identification of that peak greatly enhancing the selectivity of the system.

In this further study, a standard IEC separation of a metal ion mixture was established to test the feasibility of using a thiolated SAM coated MCA as a detector for IEC of metal ions. Experiments were conducted to determine methods to improve the sensitivity and to minimize the noise of the MCA to metal ions. Additionally, flow cell designs were also studied to determine the optimal flow cell volume for adequate detection of metal ion chromatographic peaks.

### **3.4.2 Experimental**

Silicon MCs the same as detailed previously in this chapter were commercially available (Mikro Masch Co., Sunnyvale, CA). The metals used in vapor deposition were obtained from Kurt J. Lesker, Gatewest, and Alfa Aesar Co., respectively. The flexible fused silica capillary detailed previously was purchased from Polymicron Co. All the metal chloride analytes, salts for preparation of buffer solution, and thiolated ligands were obtained from either Sigma or Fisher at highest purity and used as received. HF buffer containing ammonium fluoride and hydrofluoric acid (HF) used for the capillary etching was purchased from Transene Company. Water used for preparation of solutions was obtained from a Barnstead E-Pure water filtration system.

The creation of MCs having a smooth gold or dealloyed surface was achieved by using a PVD approach. More details about the vapor deposition instrumentation and approach can be found elsewhere[112, 113]. Dealloyed nanostructured surfaces with a composite 50/50 Au/Ag film with a thickness of

150 nm were deposited using the vapor deposition approach. All Ag/Au, smooth Au coated cantilevers used in our studies were chemically modified with SAMs of *n*-alkyl compounds with a thiol group for immobilization of the ligand to the metallic MC surface on one end and mono-dentated and bi-dentated ligand functionalities for the complexation of sample metal ions on the opposing end.

To differentially functionalize each cantilever with different thiolated ligands, a capillary coating apparatus was designed. This apparatus was described in detail previously in this chapter in section 3.2.

MCAs were mounted in a variety of flow cells (see below) in an optical system[115]. The largest volume flow cell (D) was made of brass, was sealed with an o-ring and had a volume of approximately 150  $\mu$ L. The intermediate flow cell (C) was also made of brass, was sealed with an o-ring and the volume of the flow cell was 75  $\mu$ L. The small volume flow cell (B) was made of delron, was sealed with a gasket and had a volume of 5-10  $\mu$ L. These cells had one inlet port for background/analyte delivery, one outlet port, and a glass window to facilitate the observation of cantilever deflection. A beam of laser light from an array of vertical cavity surface emitting lasers (VCSELs) (Avalon Photonics, 850 nm, 5 mW) was focused onto the tip of each MC, and the reflected beam was captured and monitored by a single position-sensitive detector.

A single lens was used to focus the VCSELs so that the beam from each VCSEL was focused onto a single corresponding cantilever (12 VCSELs onto 12 cantilevers). The deflection of the cantilever resulted in a corresponding motion of the reflected beam as monitored by the PSD. An in-house-created LabView

program controlled a multiplexing scheme that allowed the VCSELs to be activated individually so that one MC was illuminated at a time and the motion of all MCs was monitored by the single PSD. Analyte solutions were delivered to the flow cell via a system of vessels connected to three-way valves allowing for switching between different solutions (buffer and samples) with minimal disturbances of the flow. Each measurement in the study represents a 60 second injection of a metal chloride solution. All metal chloride solutions were prepared in pH 5 AB. Several background solutions/mobile phases were used in the experiments they consisted of mobile phase 1: 1.0 mmol/L of  $\text{Ce}(\text{NO}_3)_3$  and 0.01 mmol/L of sodium dodecyl sulfate (SDS), mobile phase 2: 3.0 mM  $\text{HNO}_3$  and 1.0 mmol/L of  $\text{Ce}(\text{NO}_3)_3$ , and mobile phase 3: AB pH 5 and 1.0 mmol/L of  $\text{Ce}(\text{NO}_3)_3$ . Chemically modified cantilevers were allowed to equilibrate in the mobile phase solution until stable baselines were achieved before any measurements were made. For MCA measurements the method was described previously in section 3.2.

The high performance liquid chromatography (HPLC) system used in these experiments was a Hewlett Packard Model 1100. The UV detector wavelength for indirect UV detection experiments was set at a fixed wavelength of 254 nm.

### **3.4.3 Results and Discussion**

The first step in the study was to establish a standard separation procedure for several metal ions and then validate that procedure through an established detection scheme. The validated standard separation results could

then be used to compare to the MCA sensor response when used as a detector for metal ions separated by IEC. The standard separation procedure developed involved the separation of  $\text{Cs}^{+1}$ ,  $\text{Co}^{+2}$ ,  $\text{Sr}^{+2}$ ,  $\text{Ba}^{+2}$ , and  $\text{Pb}^{+2}$  ions in a mobile phase consisting of an aqueous solution of 1.0 mmol/L  $\text{Ce}(\text{NO}_3)_3$  and 0.01 mmol/L SDS. The column used to separate the metal ions was prepared in-house by dynamically functionalizing a standard commercially available C-18 column with SDS. The sulfate group of the SDS then acts as the ion exchanger in the column. The dynamic coating of the column with SDS is accomplished by flowing a solution of 0.01 mmol/L SDS through a standard C-18 column for 1 hr at a rate of 1.0 mL/min. The hydrophobic end of the SDS interacts with the hydrophobic C-18 and a quasi-ion exchange column is created. The SDS functionalization has a life-time of up to 4 months. The  $\text{Ce}(\text{NO}_3)_3$  is added to the mobile phase to accomplish indirect UV detection. Cerium(III) absorbs UV light at 254 nm, as an analyte metal ion is confined to a discrete band by the chromatographic column, the concentration of cerium(III) in that band is very low. As the analyte metal ion band passes by the detector more UV light passes through the sample and a negative peak in the chromatogram results. The indirect UV detection scheme was the standard detection method used in the experiments to establish a standard metal ion IEC separation. The experimental elution order of the metal ions in the devised standard separation procedure (Figure 17) was consistent with the expected elution order from the literature[138]. With an established separation procedure and experimental elution times, the MCA sensor could be incorporated into the IEC system to be used as a detector for metal ions.

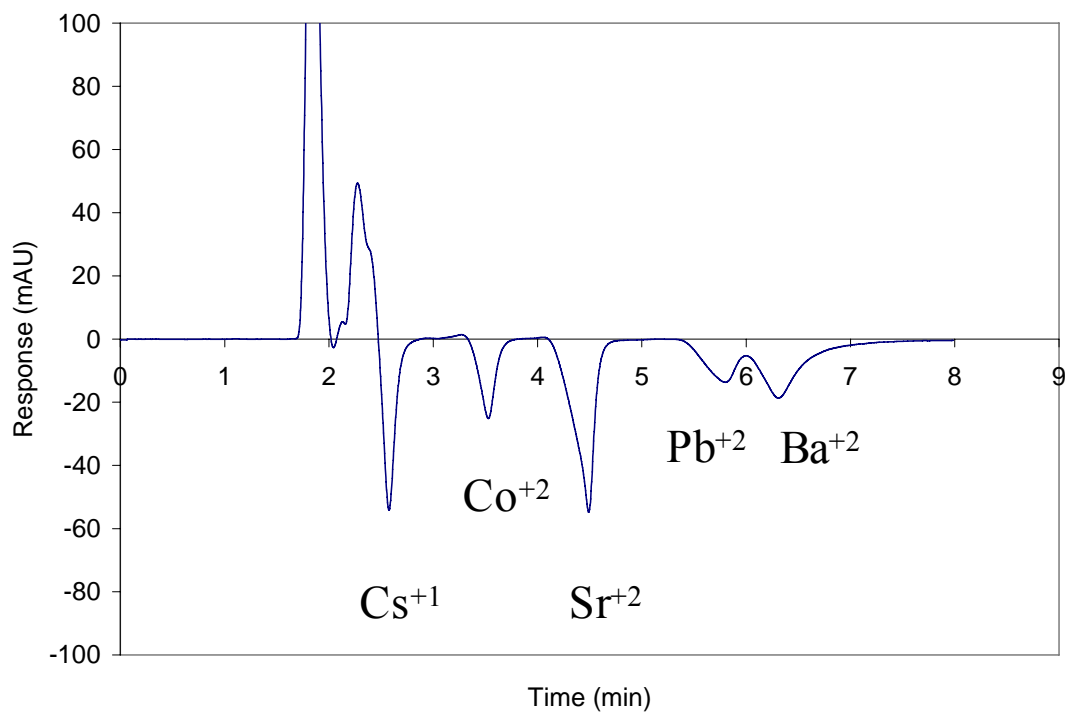


**Figure 17** Cation Exchange Separation of metal ions and indirect UV detection



Before the MCA was incorporated into the IEC system, experiments were first conducted to demonstrate that the procedural mobile phase containing cerium nitrate and SDS would not interfere with the interaction of the ligand functionalized SAM coated MCs with metal ions. Injections of  $1.0 \times 10^{-4}$  mol/L copper chloride were made in triplicate into the flow cell housing the MCA using a traditional gravity flow scheme detailed in chapter 2. Figure 18 shows the response of one cantilever in the MCA sensor to triplicate injections of the copper chloride solution. The responses being on the same order of magnitude (50-100 mV) as previous experiments in this chapter demonstrate that the procedural mobile phase does not interfere with the sensor ligand-metal ion interaction. The responses also demonstrate that the MCA is reversible in this particular mobile phase.

Even though the SDS dynamically coated C-18 column provided sufficient separation, in an effort to make the separation procedure more standardized and reproducible a commercially available strong cation exchange column was purchased and incorporated into the experiments. Incorporation of a new column into the system necessitated the use of a new stronger mobile phase containing nitric acid with a higher ionic strength. Several different metal ions of interest,  $\text{Li}^{+1}$  and  $\text{Cd}^{+2}$ , were taken into consideration at this point of the study and were separated using the new strong cation exchange column (Figure 19). Barium and lead were left out of the metal ion mixture because with the strong cation exchange column the elution times were too large. The strong ion exchange demonstrated better performance according to chromatographic peak shapes than

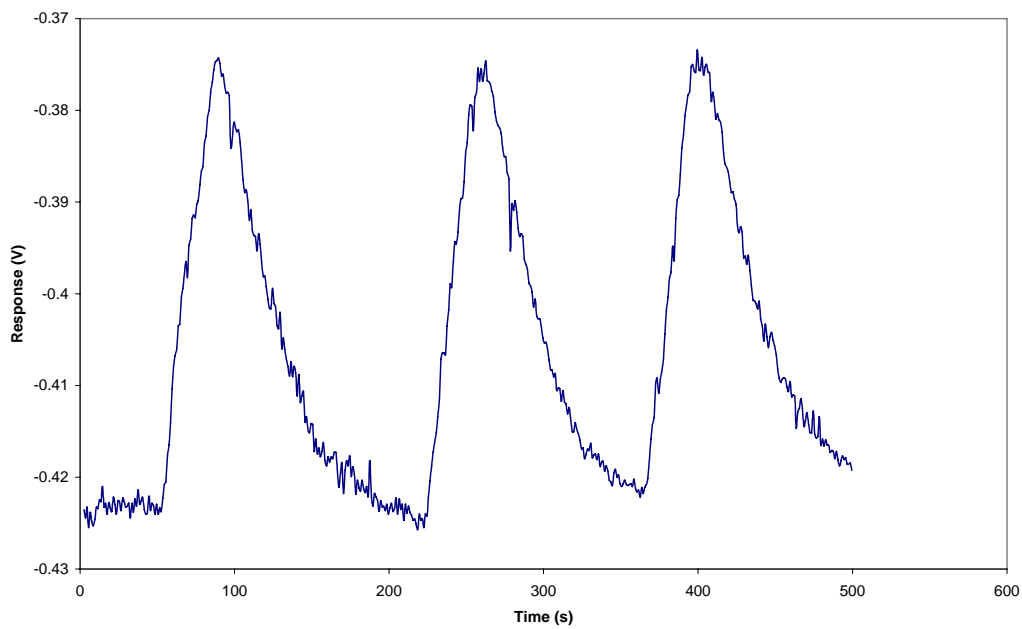


**Figure 18** Triplicate measurements of 0.1 mmol/L CoCl<sub>2</sub> in mobile phase 1 using the traditional injection technique.

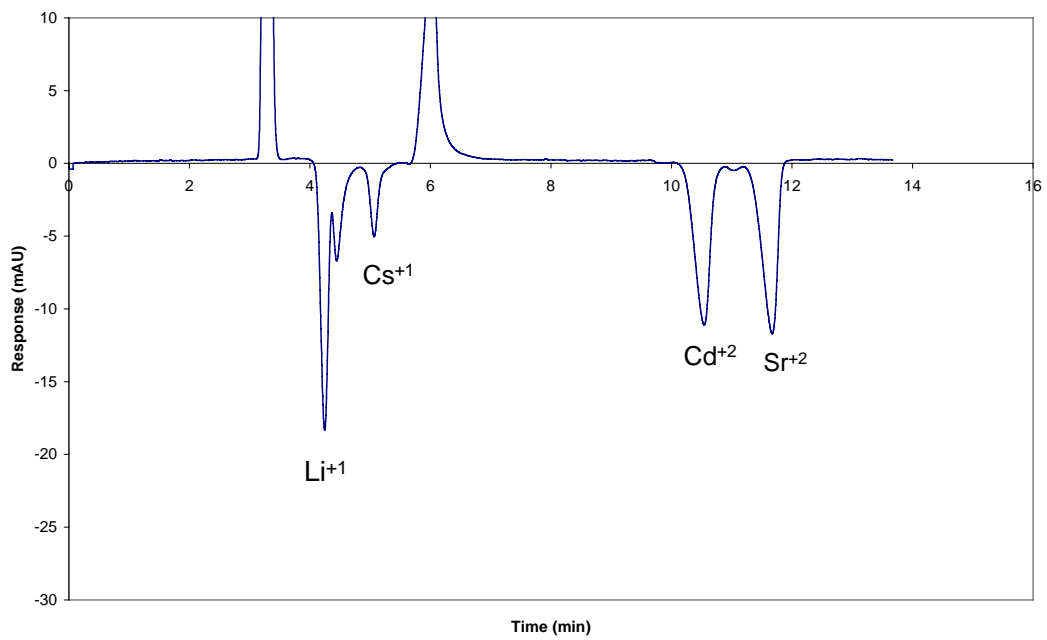


**Figure 19** The separation of metal ions using a commercially available strong cation exchange column.

the previously used SDS C-18 column. This may be due to the fact that the ion exchanger was more evenly distributed through the commercially available column than through the dynamically coated SDS column. The MCA sensor was used as a post ion exchange column detector for detection of separated metal ions. The first experiments conducted after the coupling of the MCA sensor and IEC had a very noisy baseline and no response to metal ions was detected with the MCA. The new mobile phase used in the experiments was thought to interact with the metal ions causing a decrease in sensitivity and emergence of the baseline noise problem.

In an effort to overcome the issues introduced by the strong cation exchange column's incorporation into the experiments, a two pronged approach focused on identifying/eliminating baseline noise and increasing sensitivity of the MCA was undertaken. The first attempt at eliminating the source of the baseline noise was a simple normalization of the data. This was done by making measurements with cantilevers coated with thiolated ligand SAMs and cantilevers coated on with a dealloyed layer. SAM coated cantilever responses were divided by dealloyed cantilever responses to determine if the low frequency baseline noise could be eliminated and the metal ion peaks isolated. The noise was evaluated based on the standard deviation of the data set. The normalization had no impact on the low frequency noise and provided no improvement of the noise.

As a result of the ineffectiveness of the normalization further attempts at identifying the source of the low frequency noise were made. The flow rates used in the MCAD-IEC experiments were higher than the flow rates used in traditional

MC sensing experiments. Therefore, one possible source of the noise was thought to be flow rate related. To test this source of noise, the mobile phase was flowed through the flow cell (D) at different rates ranging from 0.1 to 3.0 mL/min. At each flow rate, the standard deviation of the data set was computed and compared. There was no significant improvement in the baseline noise at lower or higher flow rates. As the flow rates were changed, the low frequency baseline noise was present in each measurement suggesting that the noise was not flow rate related.

Another potential source of the noise was thought to be the pulsations of the HPLC pump itself. Therefore, experiments were conducted in which the mobile phase was flowed through the flow cell (D) by gravity flow and by the HPLC pump. The standard deviations of the baseline in each of these experiments were then compared. It was expected that the noise would be larger when the HPLC pump was used to push mobile phase through the flow cell. However, this was not the case; the noise was the same in both flow methods. Therefore, the possibility of the HPLC pump causing noise in the system was eliminated.

During these experiments, it was noted that the longer the experiment lasted, the more improvement could be seen in the baseline noise. Based on this fact, it was thought that the solid state VCSELs used to track cantilever movement may need a small amount of warm-up time before becoming stable. To test this hypothesis, baseline measurements were recorded over 2000 seconds. The 2000 second measurement was then broken down into two halves. The standard deviation of the baseline noise was then calculated separately for 0 to 1000

seconds and 1001 to 2000 seconds. The standard deviations were compared for the two sections and it was revealed that the noise of 1001 to 2000 seconds was reduced for 11 of the 12 cantilevers in the array (Figure 20). The laser warm-up time appeared to lend some improvement to the baseline noise. For all future experiments, the lasers were warmed up by allowing them to run for 10 minutes before an experiment was started. The lack of response of the metal ion in the new flow cell to the MCA was thought to be a sensitivity issue, so different approaches to enhancing the sensitivity of the MCA were devised and tested. The first attempt at enhancing the sensitivity of the MCA was to thin the silicon cantilevers before deposition or coating by placing the silicon chip in a solution of KOH. The thinning however only increased the noise of the thiolated ligand coated MCA and did not enhance the response of the MCA to a lithium chloride solution. The next attempt at enhancing the sensitivity of the MCA was made by functionalizing the dealloyed surface of the MC with bi-dentate thiolated ligands rather than mono-dentated thiolated ligands. A  $1.0 \times 10^{-4}$  mol/L solution of lithium chloride was injected into a flow cell housing an MC functionalized with a thiol with amine and carboxylic acid functionalities. The response was lower (0.02 V) than the (0.1 V) response of the mono-dentated thiolated SAM with either amine or carboxylic acid functionalities. A third approach at enhancing the MCA response to metal ions was to imprint a specific metal ion during the SAM formation time. As the SAM formed in the presence of a specific metal ion, then the SAM would be imprinted to preferentially interact with that particular metal

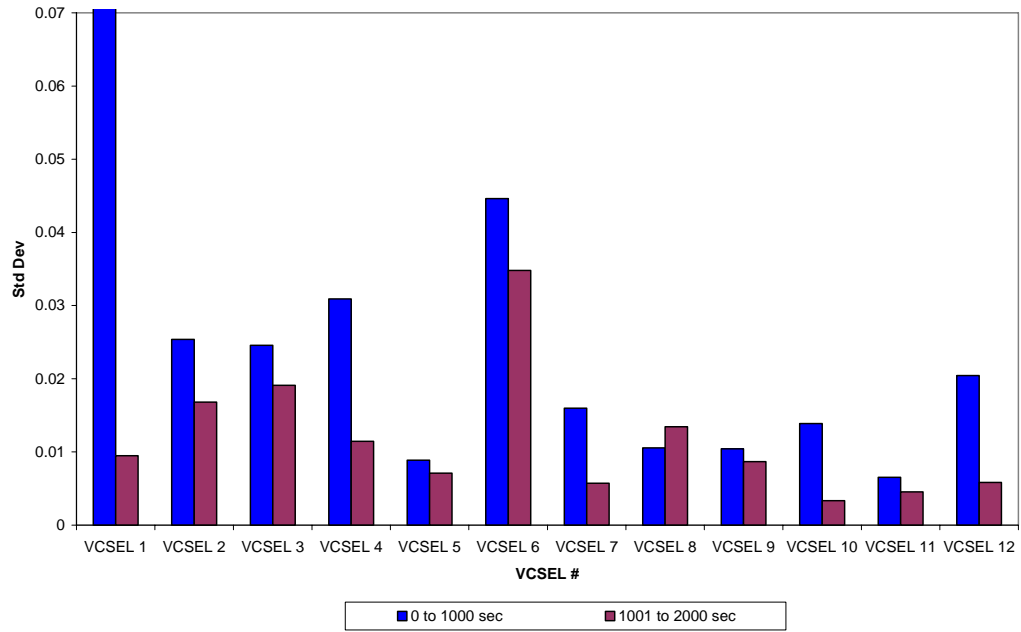


**Figure 20** Effects of laser warm-up time on noise levels.

ion. However, after SAM formation was complete, the MC imprinted for a specific metal ion showed no preference for that metal ion when exposed to it. However, it is anticipated that the imprinting approach might prove more fruitful with more experimental work.

Chromatographic changes were made also in an attempt to enhance the sensitivity of the MCA. A sample background weaker than the mobile phase was injected with a single metal ion sample to cause the metal to stack in the region at the end of the sample plug. Even when performing the stacking experiment, a signal from the metal ion could not be measured with the MCA. A weak ion exchange column was incorporated into the system rather than the strong ion exchange column. The weak ion exchange column was used because it was a concern that the strong mobile phases needed in strong cation exchange chromatography were degrading the MCA sensing phase over time. Also, weaker mobile phases could be used in the experiments without a significant increase in retention time of the metal ions. It was thought that the strong mobile phases could have been hindering the interaction of the metal ion with the MCA. When the weak ion exchange column and the weak mobile phases were incorporated into the system, a response to any metal ion was still not measure with the MCA. Therefore, other factors that could be impacting the response were studied.

With some of the noise issues solved, further MCAD-IEC experiments were performed. Single component metal ion solutions were tested in an effort to obtain a MCA response to a chromatographic metal ion peak. Figure 21 demonstrates that a copper peak could be detected with a MCA sensor after



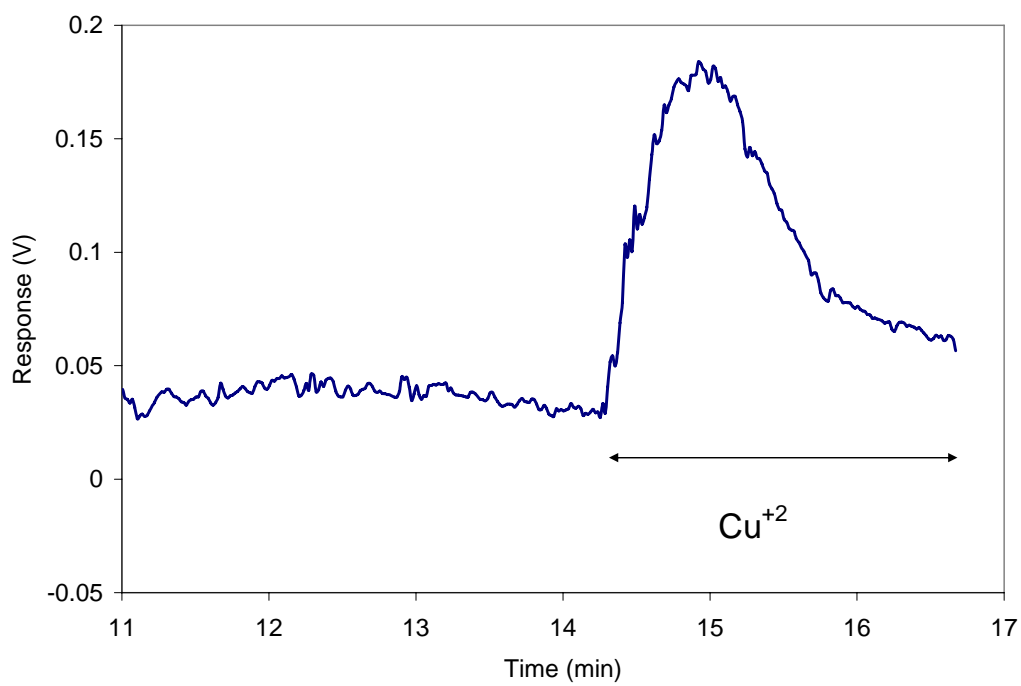


**Figure 21** Peak tailing demonstrated by a MPA coated cantilever's response to copper chloride after eluting from the ion exchange column.

separation with the ion exchange column. However, as is evident in Figure 21, while sufficient sensitivity could be achieved with this design significant tailing was present in the chromatographic peaks. The tailing was believed to be caused by the poor washout of the current flow cell (D) design which housed the MCA sensor. The flow cell's volume (150  $\mu\text{L}$ ) was believed to be too large for adequate washout. The asymmetrically broad peak demonstrates excessive volume and poor washout related to stagnant areas within the flow cell. Trapped analyte slowly leaves the stagnant areas of entrapment and interacts with the MCA causing the back half of the chromatographic peak to exhibit a large amount of tailing (Figure 21).

Therefore, a new flow cell designs (B and C) were devised and incorporated into the MCAD-IEC experiments. The new designs were based on the fact that a smaller internal volume would minimize the contributions of washout problems to peak tailing. The new flow cell designs had internal volumes of 5-10  $\mu\text{L}$  (B) and 75  $\mu\text{L}$  (C). The washout profiles of each flow cell was tested by injecting a plug of material that had no absorbance in a mobile phase containing cerium nitrate which has a high absorbance at the wavelength used for the experiment (254 nm). The rate at which the non-absorbing species is washed out of the flow cell can be seen in Figure 22. The ideal situation for minimizing a flow cell's impact on the washout of the system was measured by simply replacing the flow cell in the system with a union (blue trace A). A union is designed to have negligible washout volume; therefore a flow cell with a washout profile similar to that of the union would be ideal for our purposes. In

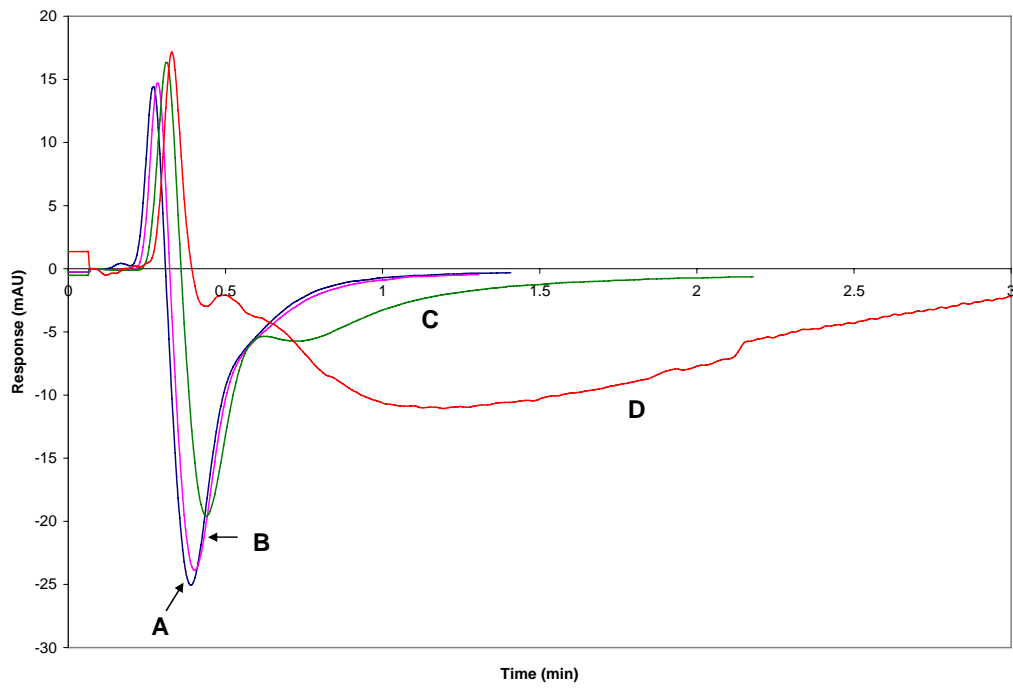


**Figure 22** Flow profiles in several different flow cell geometries are depicted.

these experiments, the new flow cell design (pink trace, B) performed almost just as well as the union. However, the original flow cell design demonstrates the presence of significant washout volume (red trace, D). The flow cell design (C) with an intermediate volume of 75  $\mu\text{L}$  showed an improved, but not ideal washout profile (green trace, C). The sample plug clears the union and the small volume flow cell (B) design in 45 seconds, but in the large volume flow cell (D) design, it takes the sample plug more than 3 minutes to completely washout of the flow cell.

The small volume flow cell (B) design appeared enable the reduction of peak tailing according to the washout profiles. However, when simple MCAD-IEC experiments were performed with a single component metal ion, no MCA response to the metal ion could be obtained.

The decrease in the flow cell volume caused a large increase, thirty times larger, in the linear flow velocity of mobile phase in the flow cell. The kinetics of the sensor ligand-metal ion interaction may not be fast enough to allow for sufficient sensing of the metal by the MCA with the increased linear flow velocity. To determine if the increased linear flow velocity was causing sensing problems experiments were conducted with a sample plug of  $1 \times 10^{-4}$  mol/L copper chloride injected directly into the MCA flow cell at different flow rates. Experiments were carried out at flow rates of 1.0 mL/min (blue trace), 0.1 mL/min (pink trace) and 0.03 mL/min (green trace). Response of a MP coated cantilever is shown in Figure 23. It is evident by these results that the response of the MCA is dependent on the flow rate the small flow cell is used. The highest flow rate appears to not allow the metal ion sufficient time to interact with the

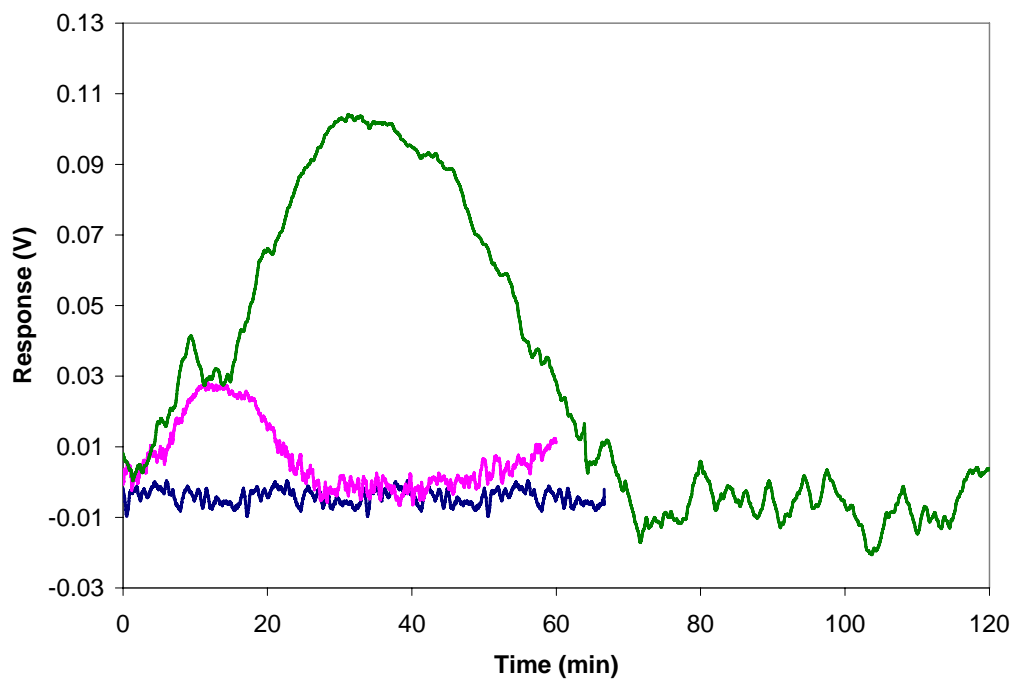


**Figure 23** Flow rate study with new flow cell design.

MCA and no response is measured. The 0.1 mL/min flow rate allows for some of the metal to interact with the MCA, but a small response measured. The lowest flow rate, 0.03 mL/min, allows for good interaction of the metal ion with the MCA. However, this flow rate is so small that it is not appropriate for IEC. The time needed to separate a series of metals at this flow rate would be 6-7 hours. Not only would the experimental time be unreasonable, but axial diffusion may excessively broaden peaks.

After the design and testing of the low volume flow cell, a discussion about flow cell volumes in a handbook of radioactivity was found. In this piece of literature it is shown that the optimal flow cell volume for a chromatographic detector is 0.1 to 0.2 times the volume of the smallest chromatographic peak[139]. For the experiments detailed in this chapter the optimal flow cell volume would be between 30 and 60  $\mu\text{L}$ . Therefore the large volume (150  $\mu\text{L}$ ) flow cell (D) and the intermediate volume (75  $\mu\text{L}$ ) flow cell design (C) were above an optimal volume and significant tailing was present in the chromatographic peaks. The new 10 – 5  $\mu\text{L}$  flow cell, while eliminating washout problems, is smaller than an optimal volume. Additionally, the reference states that sensitivity can be increased by decreasing flow rate which was demonstrated by Figure 23 and that increasing the size of the flow cell will increase sensitivity.

The experiments detailed in the final section of this chapter concluded with the flow cell problem. Flow cells with volumes of 150-75  $\mu\text{L}$  for MCA chromatographic detectors provided good sensitivity, but the chromatographic peaks showed a large amount of tailing. A smaller volume flow cell (10-5  $\mu\text{L}$ )

designed to eliminate peak tailing decreased the sensitivity of the system so much so that it could only be recovered by decreasing the flow rate. Additionally, at the decreased flow rate, needed to regain sensitivity, the experimental time is too long and the separation may not even be maintained due to diffusion. Future work will involve new flow cell designs and the testing of the new designs.

## **CHAPTER 4: DIFFERENTIALLY POLYMER COATED MICROCANTILEVER ARRAYS FOR GAS PHASE SENSING AND IDENTIFICATION**

### **4.1 INTRODUCTION**

For years sensitive chemical waste has been stored in barrels either buried in the earth or stored in warehouses. These barrels however have presented several environmental problems because of leaching of the chemicals inside of the barrels into the environment. The chemicals stored in the barrels can react with each other, creating byproducts that are even more dangerous than the original materials stored. Many of these chemicals are somewhat volatile and therefore present in detectable levels in the gas phase. The need for innovative sensors to allow for detection of chemicals and byproducts present in the barrels and to selectively detect each component present in the barrel mixture is increasing. The broad range of chemicals possibly present in these barrels necessitates that the chemical sensor be selective in its detection.

Not only have MCs been used for metal ion detection in the liquid phase, but, MCs coated with polymers have proven to be adequate sensors for gas phase applications[103, 140-143]. The small size of MCs offers sensitivity generally a couple orders of magnitude higher than other analyte responsive sensors, including QCM, FPW oscillators, and SAW sensors[101]. Other advantages have been mentioned in previous chapters.

As analyte diffuses into the polymer RPs coated on one of the MC surface, intermolecular forces change causing differential surface stress in the MC. Differential stress induced by analyte interaction on one side of the MC causes the



cantilever to bend. Bending of the MC (tip deflection,  $z_{\max}$ ) is governed by Stoney's equation[29] previously described.

In this study, a large number of gas phase components (hydrogen, carbon dioxide, ethanol, methane, methylene chloride, trichloroethylene, acetone and methanol) possibly present in these storage barrels were introduced to a MC sensor array. The MCA consisted of several vapor deposited polymeric RPs with thicknesses between 150 and 650 nm. In this chapter, the chemical selectivity by virtue of the large number of RPs coated on the array was evaluated using pattern recognition algorithms. The ability of the pattern recognition algorithm to identify and quantify the analytes injected into the system was examined. Various environmental parameters were also altered to determine if the change would impart some additional environmental selectivity to the system. Parameters of the flow cell environment such as temperature and humidity were altered to determine if they would enhance the selectivity of the MCA toward the gas phase analytes. Additionally, a diffusion controlled analyte introduction technique was studied to determine if it would enhance the selectivity of the system.

## **4.2 EXPERIMENTAL**

Experiments were performed using commercially available silicon arrays (sixteen cantilevers per array) of MCs having dimensions of the MCs used previously. The metals deposited on the MCs were obtained from Kurt J. Lesker, Gatewest, and Alfa Aesar Co., respectively, at 99.9% purity. Chemicals used as RPs for each cantilever were all purchased from Aldrich. Analyte gases were either purchased in tanks from Airgas or the headspace was drawn through a vial

with a septum from the chemical in liquid form purchased from Aldrich. The cantilevers were coated as is depicted in Table 6.

For measurements, the cantilevers were first cleaned as described previously. The process of creating the nanostructured MCs having a dealloyed surface is described in detail elsewhere[77]. In order to create gold nanostructured surface on one side of the cantilevers, a composite metal coating was created using PVD in vacuum from tungsten boats (Cooke Vacuum Products, model CE 301, South Norwalk, CT). Cantilevers that are nanostructured by this dealloying process have been shown to provide substantially larger responses than simple smooth surface cantilevers<sup>9,29</sup>.

Different chemical coatings RPs were thermally evaporated correspondingly on different cantilevers (one coating per cantilever) using the PVD approach<sup>2,18</sup>. The PVD procedures were carried out in a vacuum chamber with resistively heated sources at a pressure of approximately  $1 \times 10^{-6}$  torr. Alumina crucibles with tungsten heaters were used for evaporation of the RPs. A 150 $\mu$ m wide slit was used to selectively expose a single 100 $\mu$ m wide cantilever to accomplish our goal of depositing different RPs on each single cantilever. FT-IR studies were carried out on a Bomem FT-IR by collecting spectra from silicon wafers which were coated by PVD with RPs used in the study. Gel permeation chromatography (GPC) experiments were also carried out to determine the molecular weight distribution of the vapor deposited polymer. The GPC system consisted of a Knauer K-501 pump with a Knauer K-2501 UV detector and a Knauer K-2301 RI detector. The column was a 60 cm long stainless steel column

**Table 6** RPs used for gas phase sensing array

<b>Name</b>	<b>Abbreviation</b>	<b>Thickness (nm)</b>
Poly(diphenoxyphosphazene)	PDPP	300
Dealloyed	DA	50
Nafion	Nafion	400
4-tert-Butylcalix[6]arene	Cal-6	400
3-Amino propyl triethoxy silane	APTES	400
4-tert-Butylcalix[4]arene	Cal-4	400
Heptakis(6-O-tert-butyl dimethylsilyl-2,3-di-O-acetyl)- $\beta$ -cyclodextrin	Ac $\beta$ CD	300
Heptakis(6-O-tert-butyl dimethylsilyl-2,3-di-O-acetyl)- $\beta$ -cyclodextrin	Ac $\beta$ CD	300
Tetrabutylammonium p-toluenesulfonate	TBATS	400
Tetrabutylammonium p-toluenesulfonate	TBATS	150
Copper phthalocyanine	CuPC	400
Poly(ethyleneimine)	PEI	600
N,N,N',N'-Tetrakis(2-hydroxypropyl)ethylenediamine	THPED	400
N,N,N',N'-Tetrakis(2-hydroxypropyl)ethylenediamine	THPED	650
Poly(isobutylene)	PIB	300
Poly(epichlorohydrin)	PECH	300

with a  $10^5 \text{ \AA}$  linear and a  $100 \text{ \AA}$  PS-SDVB crosslinked packing. The deposition rate and the thickness of the resulting films were measured using the PVD system's QCM. The rate was varied from  $0.05$  to  $0.1 \text{ nm s}^{-1}$  for different phases. RP coatings of approximately  $150\text{--}650 \text{ nm}$  thickness were deposited.

MCAAs were mounted in a brass flow cell in an optical system<sup>18</sup> that has the physical arrangement described previously in chapter 3. The brass flow cell has a total volume of  $150 \text{ }\mu\text{l}$ . The cell has one port for carrier gas/analyte delivery, one outlet port, and a glass window to facilitate the observation of cantilever deflection. Modifications were made to the original brass flow cell by extending the back of the flow cell. The extended portion of the flow cell allowed for the incorporation of tubing used for temperature control. A hole was drilled in the extended portion of the flow cell to allow insertion of a J type thermocouple to monitor the temperature of the array flow cell used in these experiments. Also, the temperature of the brass flow cell was controlled by flowing cooled or heated water through stainless steel tubes that were connected to the flow chamber in the extended portion of the cell. The water flow was controlled by a simple peristaltic pump.

Diffusion controlled injection experiments were conducted by attaching the inlet and outlet of the flow cell to bags containing gases. The bag attached to the inlet contained background helium, while the bag attached to the outlet contained the analyte of interest. The analyte bag was isolated from the MCA flow cell by a valve. At the desired point in an experiment the valve could be

opened to allow for diffusion controlled transport of the analyte from the bag to the flow cell.

Cantilever deflections were monitored using a beam bending technique similar to that used in AFM. A beam of laser light from an array of vertical cavity surface emitting lasers (VCSELs) was focused onto the tip of each MC and the reflected beam was captured and monitored by a single PSD (PSD)<sup>18</sup>. A single lens was used to focus an array of VCSELs (Avalon Photonics, 850nm, 5mW) such that the beam from each VCSEL was focused onto a single corresponding cantilever (12 VCSELs onto 12 cantilevers). The deflection of the cantilever resulted in a corresponding motion of the reflected beam as monitored by the PSD. An in-house created LabView described previously controlled the system.

#### **4.3 RESULTS AND DISCUSSION**

The response of an MC to an analyte cannot be said to be an information rich response like that of a vibrational spectrum. For MCs to become more widely used methods must be developed to increase the selectivity of the MC sensor system. Enhancement of selectivity of the system can be accomplished by using the MCs in an array format. A PVD approach was used to coat each cantilever in the array with a different polymer. A 150  $\mu\text{m}$  slit was used to expose one 150  $\mu\text{m}$  cantilever to the vapor deposition at a time. In an effort to demonstrate that this could be accomplished FT-IR spectra were collected from silicon wafers that were exposed to a deposition of the polymers used as RPs in this study. Figure 24 shows the FT-IR spectra of PDPP with a reference PDPP sample and with a vapor deposited PDPP onto a silicon wafer. In addition to FT-

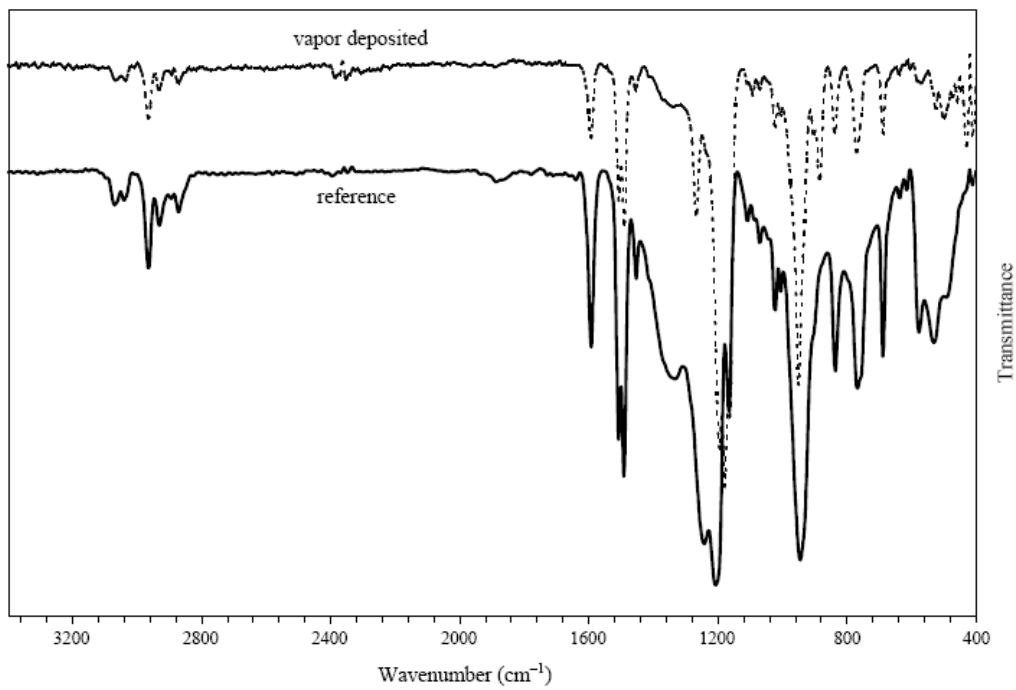


**Figure 24** FT-IR spectra of polymer PDPP before and after vapor deposition on a silicon wafer.

IR spectra, GPC measurements were made on the vapor deposited polymers to determine their average molecular weights. The GPC measurements showed that as the RPs underwent vapor deposition, they were deposited as small molecular weight oligomers rather than as the bulk polymer.

After characterization of the vapor deposited RPs, responses of the MCA to injections of different gas analytes were measured. Each RP has different chemical properties and will therefore interact differently with each gas phase analyte. A MCA with a large number of RPs has a large number of unique interactions. Each of these interactions can be combined to give an analyte specific signature. Figure 25 shows the analyte signature of trichloroethylene (TCE) over ten different RPs initially and 5 weeks after the initial measurement. The more diverse the analyte-RP interactions and the more RPs comprising the array, the more distinct the analyte signature will be and larger the degree of chemical selectivity. The technique is not as inherently selective as a technique like vibration spectroscopy or chromatography. Therefore, the high degree of chemical selectivity provided by the use of arrays must be taken advantage of in MC sensors. The chemical selectivity supplied by using the sensors in the array format in combination with pattern recognition algorithms represents a pathway to enhancing the selectivity of the system. The pattern recognition algorithms provide the experimentalist with the ability to analyze the responses of each RP of the MCA and combine all of the information for identification of the analyte.

The system studied to determine the power of MCAs combined with pattern recognition algorithms was the carbon dioxide/hydrogen system. Instead

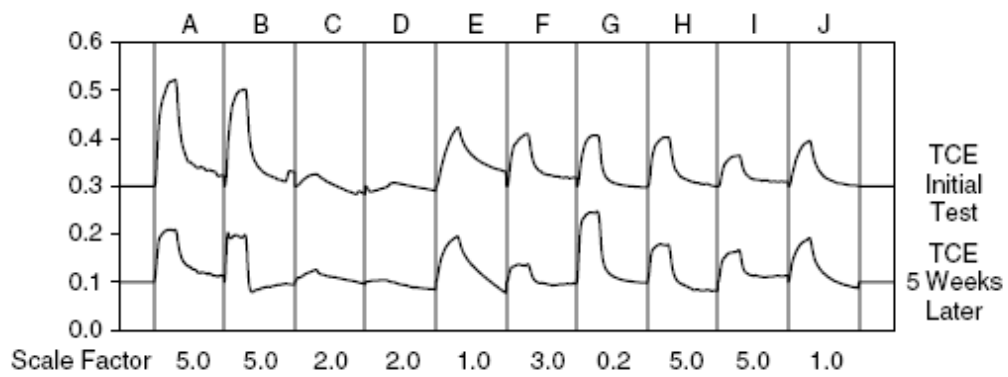


**Figure 25** Response of 10 RP coated MCs to 10% TCE in a He background gas (initially and at 5 weeks).



of injecting the gas analyte into the flow cell using a syringe pump or by diffusion, gas was injected with a fixed loop injector. The fixed loop injector enabled injection of a fixed amount of sample in a confined sample plug. The use of the fixed loop injector increased the reproducibility of sample injections leading to more reproducible results. Samples composed of 50-50 mixtures of hydrogen and helium and carbon dioxide and helium were injected into the flow cell housing the MCA. The two starting samples were then mixed to create samples having a range of hydrogen and carbon dioxide concentrations. The data collected from these experiments was given to a collaborating researcher Dr. Richard Archibald, who combined the data with pattern recognition algorithms. In the pattern recognition algorithm a leave-one-out cross validation test was performed on ICA features using a radial basis function SVM. Table 7 displays the results of the pattern recognition algorithm as it was presented with data from array responses for mixtures of hydrogen and carbon dioxide. The pattern recognition algorithm performs very well when the amounts of each gas in the mixture are very different (i.e. 9:1). However, when the amounts of gases in the mixture are similar, the pattern recognition algorithm does not perform as well. The pattern recognition algorithms developed by Dr. Archibald[115] when presented with single component analyte gases were able to not only identify the analyte gas, but were also able to identify the concentration of each gas phase analyte with an error of 8%.

In addition to the chemical selectivity imparted by the use of MCAs, it was thought that adjustment of environmental parameters may offer another

**Table 7** Predicted vs. actual concentration for gas mixture.

Predicted vs. actual concentration in the mixture of CO <sub>2</sub> and H <sub>2</sub>	
Actual Mixture of CO <sub>2</sub> and H <sub>2</sub>	Predicted mixture of CO <sub>2</sub> and H <sub>2</sub> (mL/min)
0.9:0.1	0.8947:0.0843
0.8:0.2	0.8548:0.1000
0.7:0.3	0.6279:0.3202
0.6:0.4	0.4946:0.4469
0.5:0.5	0.2603:0.5902
0.4:0.6	0.4369:0.5336
0.3:0.7	0.2603:0.5902
0.2:0.8	0.3017:0.7628

method of enhancing selectivity of the system. Therefore, experiments were conducted to determine if some additional environmental selectivity could be imparted to the system. The first experiments conducted aimed at imparting environmental selectivity to the system involved alteration of the environmental (flow cell) temperature. In the case of a two gas analyte system it was anticipated that a reduction in environmental temperature (-20° C) would cause the analyte gas with the lower vapor pressure to condense to a more liquid like analyte while permitting the gas with the higher vapor pressure to remain in the gas phase. Thus, the response of the polymer coated cantilevers to the lower vapor pressure gas at lower temperatures would decrease and the response to the higher vapor pressure gas would remain the same. The controlled manipulation of the analyte vapor pressure through environmental temperature change was thought to be a pathway to generate selectivity in the responses of the MCA. This temperature generated selectivity could then be extrapolated to each of the gas phase analytes comprising the study. To test the temperature controlled selectivity concept 10% carbon dioxide and hydrogen gas in a helium background gas were injected separately into the flow cell housing the MCA. MCA responses were measured for carbon dioxide and hydrogen at room (25 °C), heated (45 °C), and cooled (5 °C) temperatures. Each gas showed an increase in the response as the environmental temperature was decreased. The difference in the room temperature and cooled responses for hydrogen and carbon dioxide were both calculated. The calculated differences were then plotted and the ratio of the hydrogen response change to the carbon dioxide response change was calculated

(Figure 26). The increase in response of both gases suggested that as the environmental temperature decreased the gases began to condense onto the RPs of the MCA giving a larger response for each gas. For the same reason, as the temperature of the flow cell environment was increased to 45 °C the magnitude of response to carbon dioxide and hydrogen decreased for each RP. Of course temperature may also affect the response characteristics of the system aside from a partitioning effect.

The response ratios were almost constant across each phase comprising the array. The constant response ratio demonstrated that the added selectivity to the system is environmentally related and not related to RP. Therefore, environmental temperature changes do impart some additional selectivity to the array.

Environmental temperature changes did impart some additional selectivity to the system. Therefore, another environmental parameter was studied to determine if it would influence the selectivity of the MCA. It was thought that by increasing the humidity, as difficult as it is to control, of the system the polarity of the background gas would increase, thereby enhancing the selectivity of the system. Once again the MCA responses to 10% carbon dioxide and hydrogen gases in helium were studied to understand the effect of humidity on the system. Humidity was added to the system by spiking each gas phase analyte with 20% by volume water vapor. Figure 27 demonstrates the impact that humidity has on the response of a THPED coated cantilever to hydrogen and carbon dioxide. In the humidity experiments the direction of bending of the cantilever changed from a

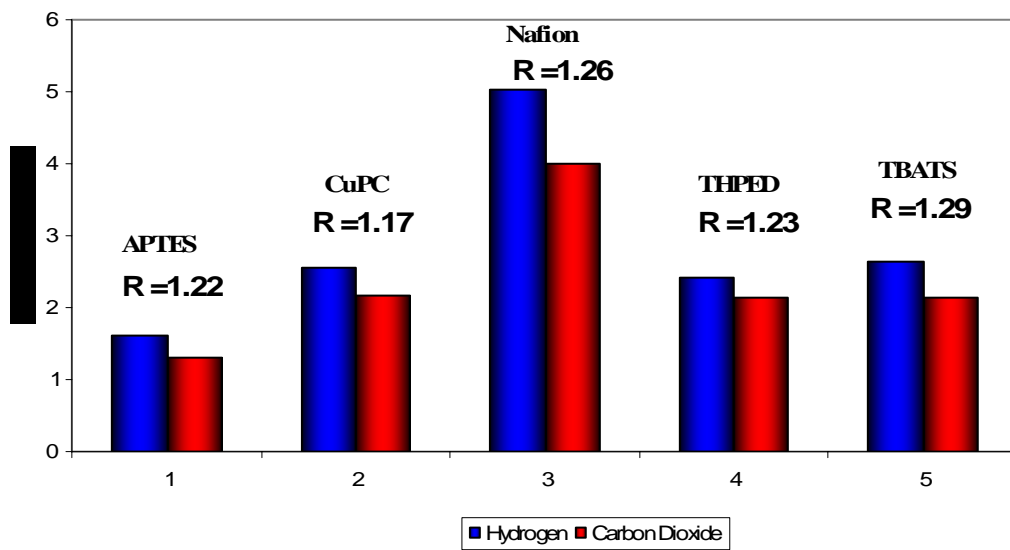


**Figure 26** Temperature effects on response of THPED coated cantilever to hydrogen and carbon dioxide.

compressive response under normal conditions to a tensile response. The tensile response occurs when the sensing phase contracts rather than expands. The tensile response magnitude for carbon dioxide was 7 times larger than that of hydrogen when humidity was added to the system. However, the response appears to be due to some polar gas phase components (possibly water) leaving the polymer sensing layer and partitioning into the now more polar gas phase. The exiting gas causes the polymer to shrink rather than swell and a tensile response results. The changes in MCA response resulting from humidity fluctuations appear not to be related to the analyte gases, but to some other gas phase component (possibly water vapor). Therefore, a humidity change as a means of imparting selectivity to the system is not a promising pathway. In fact, the lack of control of humidity becomes a complication rather than a benefit.

Another approach to imparting selectivity to the MCA was by using diffusion controlled transport of the analyte gases of interest. Each gas phase analyte has a different diffusion coefficient and therefore will be transported at a different rate across a given distance. It was thought that each gas would have a characteristic transport time, based on equation 10 relating molecular weight of the analyte to its diffusion coefficient.

$$D_{air} = \frac{0.001T^{1.75}M_r^{1/2}}{(P(V_A^{1/3} + V_B^{1/3}))^2} \quad (10)$$

Where  $D_{air}$  is the diffusion coefficient in air,  $T$  is the temperature in Kelvin,  $M_r$  is a function of the molecular weight of the analyte,  $P$  is the pressure in atmospheres,  $V_a$  is the volume of the air, and  $V_b$  is the volume

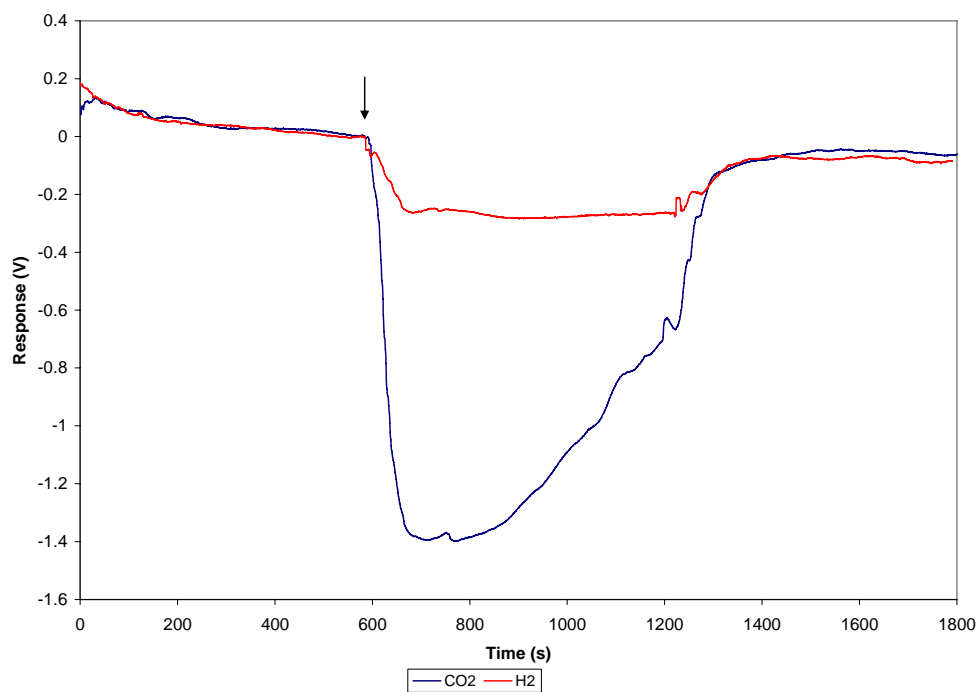


**Figure 27** Humidity effects on the response of a polymer coated MC to gas phase analytes.

of the analyte of interest. The flow cell housing the MCA sensor was put in an isolated system with a bag filled with an analyte gas and a valve separating the bag and a transfer line to the flow cell. At the beginning of the experiment the valve was opened to allow for diffusion controlled transport of the analyte gas into the flow cell. In preliminary experiments the hydrogen gas reached the MCA much faster than the carbon dioxide, which was expected. According to preliminary experiments, the diffusion controlled transport appeared to offer good pathway toward enhancing the selectivity between the gas analytes comprising the study. However, after further experiments it was evident that pressure problems existed in the system. The diffusion controlled transport times over a given distance for repeated experiments changed significantly for both hydrogen and carbon dioxide. The large discrepancies in transport times were thought to be caused by pressure fluctuations in the system. The system was believed to be isolated and the transport of analyte gases totally controlled by diffusion. However, the system was in fact not isolated and other factors were affecting gas transport. The vulnerability of the experimental setup to external interference discouraged further experiments involving diffusion controlled transport. However, in a more controlled isolated system diffusion controlled transport of analytes as a pathway to increase the selectivity of the system would be viable.

In conclusion, MCA responses combined with pattern recognition algorithms proved to be an excellent method of generating selectivity to the system. Not only was analyte identification a possibility with pattern recognition algorithms, but analyte concentration could also be distinguished. Environmental



changes such as temperature and humidity in the carbon dioxide/hydrogen system demonstrated the ability to impart some additional selectivity to the system in the case of temperature changes. However, humidity changes were hard to control and a change in humidity appeared to impact other gases phase components masking the analyte response. The diffusion controlled transport system was very susceptible to external interferences. The external interferences, such as pressure changes, did not allow diffusion controlled transport to be used as a means of generating selectivity in regard to gas phase MCA experiments. However, with a more isolated system, diffusion controlled transport could represent an additional pathway to increasing the selectivity of the system.

## **CHAPTER 5: FACILE HYPHENATION OF GAS CHROMATOGRAPHY AND A MICROCANTILEVER ARRAY SENSOR FOR ENHANCED SELECTIVITY**

Chapter 5 is an adaptation of a research article *Anal. Chem.* **2007**, *79*, 364-370. The article demonstrated that arrays of polymer coated cantilevers could be made these arrays could be used as detectors for GC. The separation technique before detection greatly enhanced the selectivity of the system.

### **5.1 INTRODUCTION**

Volatile organic compounds (VOCs) may be responsible for the building related illnesses of 30 to 70 million workers in the United States[144]. MC sensors have been applied to the selective detection of individual components of sample VOC mixtures[116]. However, complex mathematical algorithms must be applied to the sensor responses to determine whether or not a component was present and in what amounts. Therefore, a more straightforward method of elucidating single components in a sample mixture would be of interest.

The small size of MC sensors offers sensitivity generally a couple orders of magnitude higher than other analyte responsive sensors, including QCM, FPW oscillators, and SAW sensors[101]. Other advantages include the ability to be integrated with on chip circuitry, an ability to be used as an array, and low cost.

As analyte comes in contact with RPs on one of the MC surfaces, intermolecular forces cause surface stress changes on the coated side of the MC. Differential stress induced by analyte interaction on one side of the MC causes the cantilever to bend. Bending of the MC (tip deflection,  $z_{\max}$ ) is governed by Stoney's equation[29]

$$z_{\max} = \frac{3l^2(1-\nu)}{Et^2} \Delta\sigma \quad (5)$$

where  $\nu$  and  $E$  are, respectively, the Poisson ratio and Young's modulus for the cantilever,  $t$  is the thickness of the MC,  $l$  is the cantilever effective length, and  $\Delta\sigma$  is analyte-induced differential surface stress ( $\Delta\sigma_{\text{active (i.e., MRP) side}} - \Delta\sigma_{\text{passive side}}$ ).

Early MC sensors generally were comprised of one cantilever coated with one RP[24, 32, 102-109, 111, 145]. More recently, MCAs have been developed with many cantilevers in an array coated with different RPs[36, 110, 116, 146, 147]. However, as the number of MCs used in an array increases, the complexity of the array response patterns increases as well. In an effort to deal with increasing complexity, pattern recognition approaches to data mining have been used. Pattern recognition approaches based on linear discriminant analysis[148], principal component analysis (PCA)[149], or artificial neural networks (ANNs) have been applied to sensor responses[149]. Shaffer et al. compared a test of seven different pattern recognition algorithms using responses of SAW sensors[150]. We have employed ANNs to MCA responses to facilitate analyte recognition[116] and, more recently, employed a combination of independent component analysis and ANNs for the same purpose[115]. The complexity of array responses to analyte mixtures has exposed, up to now, the inability of ANNs to elucidate each component of relatively complex mixtures. One such class of mixtures that can cause difficulty for ANNs when attempting multi-component identifications using MCA responses are the VOCs.

Several researchers have utilized pre-sensor separation in detection of complicated mixtures[151-153]. In particular, Zellers et al. performed extensive work in developing a sophisticated yet portable gas chromatograph with tunable retention and detection with surface acoustic array sensors[153]. Tunable retention was accomplished by incorporating two separation columns in tandem with scheduled stop-flow intervals in the first column and independent temperature programming. The portable gas chromatograph surface acoustic array sensor was capable of separating and detecting numerous different components in a mixture.

In this chapter, the straightforward coupling of a standard gas chromatograph to a MCA sensor is demonstrated. To our knowledge this report represents the first report of the GC-microcantilever array detector (MCAD) hyphenation. Calibration studies to determine the performance of the MCA response to VOCs separated by GC were conducted. In addition to calibration studies, a PCA evaluation and operational parameter studies involving column flow rate, column temperature, and array cell temperature were performed. Peak area and peak height reproducibility were determined for one of the VOC mixtures with several different sensing phases in the MCA. A discussion of the influence of MCAD on peak integrity is also presented.

## **5.2 EXPERIMENTAL**

Experiments were performed using commercially available silicon arrays (sixteen cantilevers per array) of MCs having dimensions 400  $\mu\text{m}$  length, 100  $\mu\text{m}$  width, and approximately 1  $\mu\text{m}$  thickness (Mikro Masch Co., Sunnyvale, CA).

Chromium, gold, and silver metals deposited on the MCs were obtained from Kurt J. Lesker, Gatewest, and Alfa Aesar Co., respectively, at 99.9% purity. Chemicals used as RPs for each cantilever were all purchased from Aldrich and are listed in Table 8. VOC analyte mixtures were prepared using acetone, ethanol, TCE, methanol, acetonitrile and pentane as the solvent, purchased from Aldrich each of which were 98.5% pure or greater. Although, 12 cantilevers responses are monitored and 10 different RPs comprise the MCA, the focus of this study included only six good VOC-responding cantilevers. One of these cantilevers is the simple dealloyed surface MC (see below).

For measurements, the cantilevers were first cleaned in a piranha bath (75%  $\text{H}_2\text{SO}_4$ , 25%  $\text{H}_2\text{O}_2$ ) for 30 minutes [Caution: piranha solution reacts violently with organics]. The cantilevers were then thoroughly rinsed in deionized water. The process of creating the nanostructured MCs having a dealloyed surface is described in detail elsewhere[146]. In order to create gold nanostructured surface on one side of the cantilevers, a composite metal coating was created using PVD in vacuum from tungsten boats (Cooke Vacuum Products, model CE 301, South Norwalk, CT). Evaporation of a 5 nm chromium adhesion layer was followed by evaporation of a 15 nm gold layer and, without stopping the evaporation of gold, by co-evaporation of gold and silver until a composite Au/Ag film of ~50 nm thickness was formed. Both the deposition rate and resulting coating thickness were monitored using a QCM. Silver was subsequently etched out of the composite film by placing the MCs in an aqueous solution of 0.2% w/v

**Table 8** List of compounds used as RPs

<b>Phase</b>	<b>Abbreviation</b>
3-Amino propyl triethoxy silane	APTES
Copper phthalocyanine	CuPC
Methyl- $\beta$ -cyclodextrin	Me $\beta$ CD
N,N,N',N'-Tetrakis(2-hydroxypropyl)ethylenediamine	THPED
Tetrabutylammonium p-toluenesulfonate	TBATS
Dealloyed	DA

HAuCl<sub>4</sub> for 2-3 minutes. Subsequently, the MCs were rinsed with copious amounts of water after etching. Cantilevers that are nanostructured by this dealloying process have been shown to provide substantially larger responses than simple smooth surface cantilevers[32, 112].

Different chemical coatings RPs were thermally evaporated correspondingly on different cantilevers (one coating per cantilever) using the PVD approach[116, 146]. The PVD procedures were carried out in a vacuum chamber with resistively heated sources at a pressure of approximately  $1 \times 10^{-6}$  torr. Alumina crucibles with tungsten heaters were used for evaporation of the RPs. A 150 $\mu$ m wide slit was used to selectively expose the single 100 $\mu$ m wide cantilevers to accomplish our goal of depositing different RPs on each single cantilever. The deposition rate and the thickness of the resulting films were measured using the PVD system's QCM. The rate was varied from 0.05 to 0.1 nm s<sup>-1</sup> for different phases. RP coatings of approximately 350–450 nm thickness were deposited.

Figure 28 shows the different components of the instrumentation used in the hyphenated technique as a schematic representation. MCAs were mounted in a brass flow cell in an optical system[146] that has the physical arrangement as shown in Figure 28. The brass flow cell has sufficient thermal mass to permit uniform temperature control and the total volume of the flow path through the cell is approximately 150  $\mu$ l. No attempt to decrease the flow cell volume has been made in this initial proof of concept report of GC-MCAD.

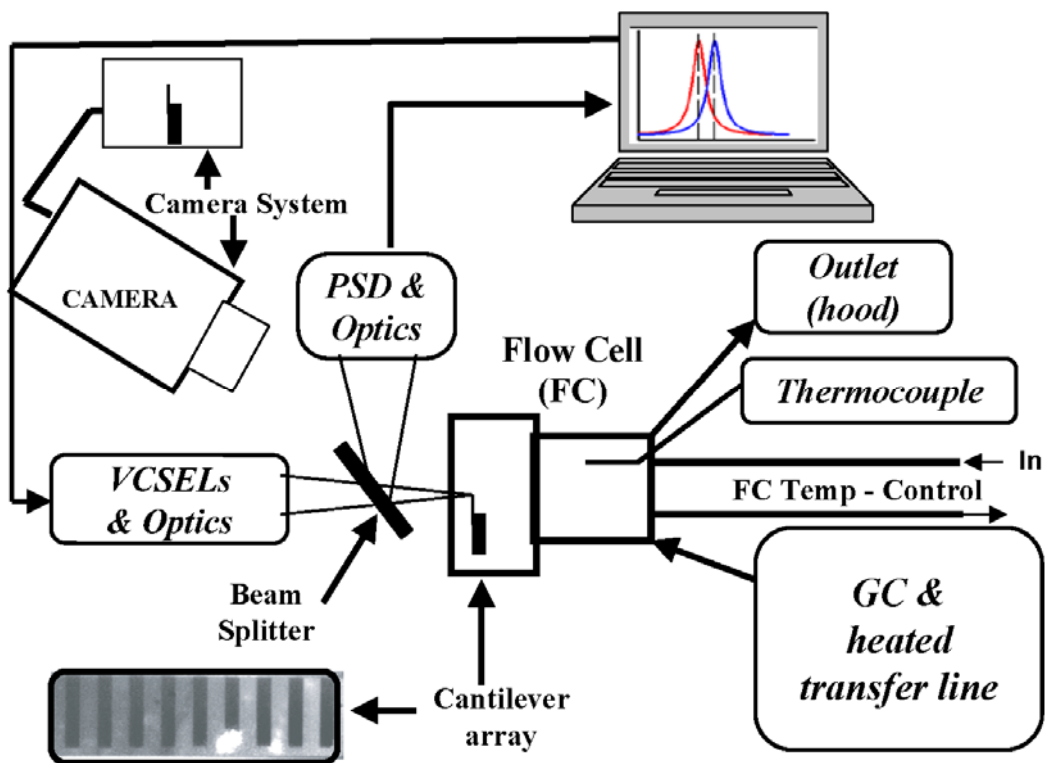


**Figure 28** Illustrations detailing the ease of instrumental hyphenation of a simple gas chromatograph with existing optical detection system used for cantilever measurements. The inset (lower left) is a CCD image of an array of MCs with VCSEL reflection off the fourth cantilever from the right.



Considering the limit of the range of cantilever motion ( $z_{max}$  in Equation 5) of well less than 10  $\mu\text{m}$  and physical size of the MCA, a reduced dimension version of the flow cell could reduce the flow cell volume to 100 nL or less. The cell has one port for carrier gas/analyte delivery, one outlet port, and a glass window to facilitate the observation of cantilever deflection. A J type thermocouple was used to monitor the temperature of the array flow cell used in these experiments. Also, the temperature of the brass flow cell was controlled by flowing cooled or heated water through stainless steel tubes that were connected to the flow chamber in the extended portion of the cell. The water flow was controlled by a simple peristaltic pump. Cantilever deflections were monitored using a beam bending technique similar to that used in AFM. A beam of laser light from an array of vertical cavity surface emitting lasers (VCSELs) was focused onto the tip of each MC and the reflected beam was captured and monitored by a single PSD (PSD)[146]. A single lens was used to focus an array of VCSELs (Avalon Photonics, 850nm, 5mW) such that the beam from each VCSEL was focused onto a single corresponding cantilever (12 VCSELs onto 12 cantilevers). The deflection of the cantilever resulted in a corresponding motion of the reflected beam as monitored by the PSD. An in-house created LabView program controlled a multiplexing scheme that allowed the VCSELs to be activated individually so that one MC was illuminated at a time and the motion of all MCs was monitored by the single PSD.

A GOW-MAC Series 350 gas chromatograph equipped with a 20% carbowax 20 M column was used for separations of VOC mixtures before introduction to the MCAD. This is a very basic GC that is often used in academic

teaching laboratory settings. A thermal conductivity detector (TCD) comprised of 4 Rhenium-tungsten elements served as the integrated GC detector. The injection port and detector temperatures were maintained at 240°C and 145°C respectively. Column temperatures were altered between separations in the range of 90 to 130°C and remained static during each separation.

Coupling of the GC and the MCAD was accomplished by connecting heated tubing from the outlet of the GC to the inlet of the MCAD flow cell. The connecting tubing was 20 cm of narrow-bore 1/16 inch O.D. PTFE with a total volume (including connectors) of less than 50  $\mu$ L. Throughout the experiments, a constant flow of helium carrier gas was maintained through GC and the flow cell, typically at a rate of 35-65 mL/min. Analyte flow was controlled by the gas chromatograph flow rate adjuster.

An in-house created LabView program controlled a multiplexing scheme that allowed the VCSELs to be activated individually so that only one cantilever was illuminated by one VCSEL at a time. At the beginning of each cycle, VCSEL #1 was activated illuminating the corresponding cantilever #1. The motion of the reflected beam was monitored by the single PSD, and the detector output signal was sampled by an A/D converter at a rate of 1 kHz. To minimize noise, 50 samples were taken and the average value was recorded. The sequence was then repeated for VCSEL/cantilevers #2 through #12. The entire cycle of measuring and recording all 12 MCs (recall only 6 used for VOC analyses) takes less than one second; therefore a delay was added so that the cycles begin at one second

intervals. VCSEL control and data acquisition I/O were performed using a National Instruments NI-6014 DAQ card in an 800MHz Pentium III PC.

The data collected by the LabView program was transferred to an excel spreadsheet. The data was then plotted using excel to assist in determination of chromatographic parameters such as those listed below. Chromatographic retention and peak parameters were computed manually because integration software was not readily available. For example, efficiency (plate count, N) was calculated using  $N = 5.5 (t_R/w_{1/2})^2$  where  $t_R$  is the retention time of the peak and  $w_{1/2}$  is the peak width at half height. Also, peak asymmetry ( $A_s$ ) was calculated using  $A_s = B/A$  where B is peak center to peak tail at 10% peak height and A is peak front to peak center at 10% peak height.

In order to assess whether these different MCA response patterns enable analyte discrimination and quantification, a PCA[154-157] was utilized. Our PCA algorithm is based on a singular value decomposition (SVD)[158, 159], which also outputs a set of singular values. In this proof-of-concept approach these singular values serve as figure of merit to determine the number of linear independent patterns contained in a set of response patterns obtained in this work. The number of singular values  $\neq 0$  indicates the rank of the matrix containing the response vectors and thus the number of linear independent patterns. Due to measurement noise all singular values will be larger than zero and it needs to be determined later which are  $\approx 0$ . The inclusion of repeated measurements ensures the presence of linear dependent information which in turn allows an assessment of the level of a singular value  $\approx 0$  (“noise indicator”). Chemometric

computations were performed with software written in-house utilizing the Intel C++ compiler (version 9.1.038) for Linux.

### 5.3 RESULTS AND DISCUSSION

Figure 29 details the response magnitude of several differentially coated levers in the MCA to four analytes post GC separation. The response magnitudes demonstrate a great deal of diversity (molecular recognition contrast) from sensing phase to sensing phase and analyte to analyte. APTES and dealloyed MCs show no response to TCE, whereas TCE gives the largest response with the THPED coated lever. Also, the CuPC sensing phase responds to pentane by causing the MC to bend in the opposite direction of all other analytes. The larger amount of diversity in MCA response magnitudes bode well for elucidation of more complex VOC mixtures possibly containing co-eluting peaks. Our prior research explored the advantages of combining differentially coated MCAs with ANNs for detection of certain VOCs, singularly and in binary mixtures[116].

In order to determine whether there is sufficient information in the array response patterns of the figure to identify the four components if, for instance, they were not subjected to a separation, a PCA was performed. As mentioned above, this analysis is based on singular values determined from a PCA of the matrix containing 16 response patterns (four pure analytes repeated four times each). Since there are six cantilevers and 16 vectors this data matrix is of dimension  $6 \times 16$  and six =  $\min(6,16)$ <sup>5</sup> singular values are returned and analyzed for being  $\neq 0$  or being  $\approx 0$ .

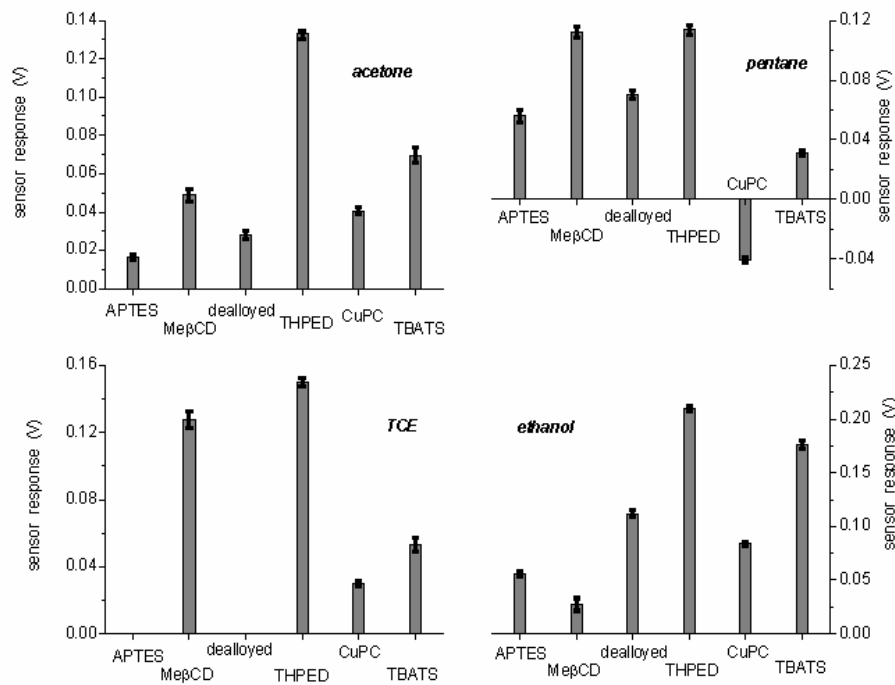


**Figure 29** The response variability (selectivity) is displayed for six differentially RP coated cantilevers to four (acetone, pentane, TCE, and ethanol) of the test VOC analytes after GC separation. With this MCAD, the deflection (static bending) of the tips of the 400  $\mu\text{m}$  long cantilevers is approximately one nm bending per mV of PSD output (responses are chromatographic peak heights). The error bars correspond to one standard deviation for four runs used to generate the bar graph.

As shown in Figure 30A the four analytes only result in three singular values that are clearly  $\neq 0$ . Hence, three analytes in the quaternary mixture were detected for sure; the fourth is questionable.

In the next step it is determined which analyte could possibly not be discriminated from a mixture of all four. For this purpose, one analyte after the other was removed from the PCA analysis. If the removed analyte reduces the number of relevant ( $\neq 0$ ) singular values by one, a linear independent pattern has been excluded. If, however, excluding a certain analyte does not change the number of relevant singular values, this analyte does not add a linear independent pattern to the data set. As shown in Figure 30B excluding acetone does not change the singular values as much as compared to the other analytes (see \*); thus, the acetone response pattern can be a linear combination of the other three. By means of a multivariate least squares regression[160-162] the coefficients of this linear combination are estimated; for this calculation the averaged pattern responses (Figure 29) have been used. From this analysis it appears that the array response (AR) for acetone can be fairly accurately modeled as follows by equation 11.

$$AR_{\text{acetone}} = -6.846 \times 10^{-2} AR_{\text{pentane}} + 0.3225 AR_{\text{ethanol}} + 0.4271 AR_{\text{TCE}}$$

(11)

The significance of this PCA analysis is that a MCA of the complexity

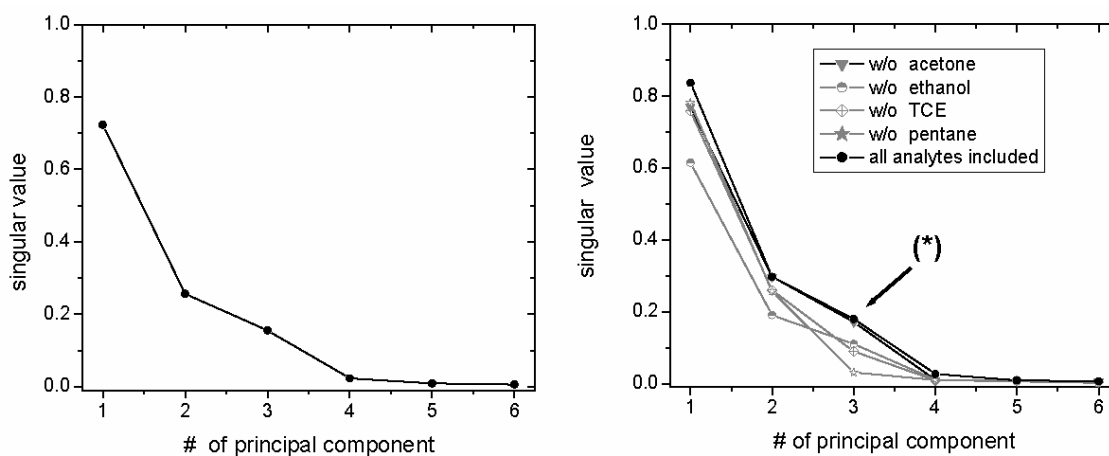


**Figure 30 [A]** Singular values obtained from the full calibration set, which contains four repeated measurement of four pure analytes; goal of this analysis is to determine how many linear independent patterns are present. Each singular value clearly  $\neq 0$  indicates a linear independent pattern – noise is represented by a singular value  $\approx 0$ . **[B]** The number of relevant singular values obtained from samples excluding either ethanol, TCE or pentane is decreased, i.e. the exclusion of one of these analytes reduces the number of linear independent signal patterns. With and without acetone included, however, the singular values are almost equal (\*).

used in this work (six different MCs with different RPs) could deal with a ternary mixture of the four VOCs studied, but the quaternary mixture may result in misclassification or concentration errors when performing qualitative and quantitative analysis. Given that minor co-elution often occurs even in properly designed GC experiments, but such massive co-elution is very unlikely (actually these four VOC are completely resolved in this work), the significance of the hyphenation of GC with a MCAD is clearly highlighted.

Figure 31A shows the MCAD response to a separation of a VOC mixture containing methanol and acetonitrile, which was not as thoroughly studied as the VOC mixture containing acetone, ethanol, and TCE. Figures 31B and 31C demonstrate the results of a calibration study through the response of TBATS coated cantilever for the latter VOC mixture. The elution order was as expected; the solvent pentane (bp 36 °C) eluted first, followed by acetone (bp 58 °C), ethanol (76 °C), and finally TCE (88 °C). The MCAD showed a linear response to concentrations of each component of the mixture over a range of two orders of magnitude. However, at 750 mmol/L concentrations of analyte the calibration curve showed nonlinearity. Ignoring the highest concentration, the  $r^2$  values for the plots are 0.995 for TCE, 0.972 for ethanol, and 0.997 for acetone. The nonlinearity at higher concentrations is probably indicative of saturation of the RP. The absolute limits of detection based on the 1.0  $\mu$ L injection ( $S/N = 3$ ) were 7nmol, 14nmol, and 14nmol for ethanol, TCE, and acetone, respectively. These are not impressive detection limits, however, in an optimized system it has been demonstrated that MC sensors can respond to gas phase aromatic



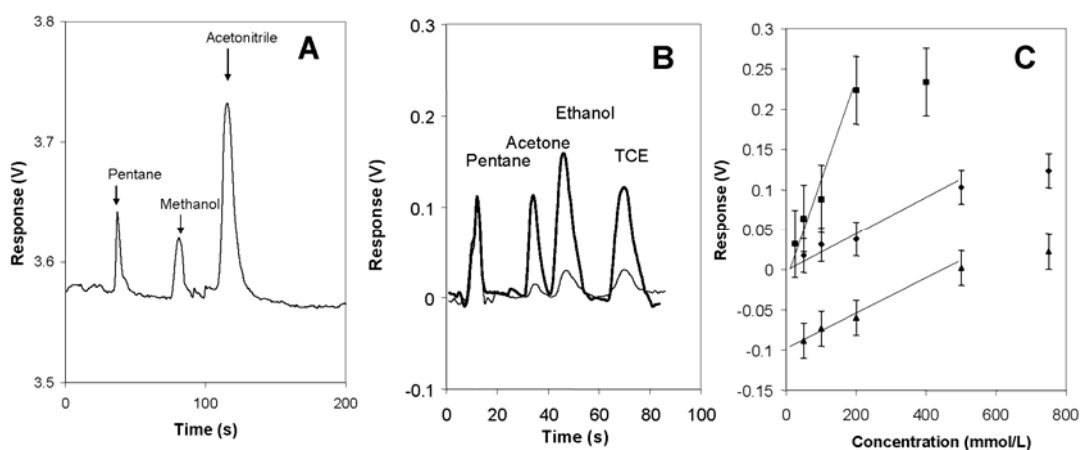


**Figure 31** [A] A separation of a VOC mixture containing methanol and acetonitrile in pentane. [B] Examples of GC-MCAD chromatograms (concentration based response of TBATS coated cantilever) at two different injected amounts (0.1 and 0.5  $\mu\text{mol}$ s). [C] Calibration curve based on the response curve of TBATS coated cantilever showing the responses are linear over the range of concentrations studied from 50mmol/L to 500mmol/L with r-squared values of 0.995, 0.972, and .997 for ( $\blacklozenge$ ) TCE, ( $\blacksquare$ ) Ethanol, and ( $\blacktriangle$ ) Acetone respectively.

compounds in sub-ppb concentrations and absolute masses at the picogram or low levels[101]. The potential for this sensitivity is therefore available in this system, but several conditions need to be optimized from this initial proof of concept configuration. For example, no effort was made in this initial work to optimize responses by optimizing the thickness of the coating on the cantilever or improving the nanostructuring procedure, which is known to enhance responses[31]. Additionally, measures such as thinning the MC or cooling the flow cell (see below) could be taken to improve the sensitivity of the MCA toward each analyte.

Reproducibility studies of the sensor array response for peak height and area were conducted. The RSDs for peak heights and areas for each analyte over several different sensing phases are included in Table 9. RSDs for peak height and area demonstrate that the MC sensor array responds reproducibly over a number ( $n = 4$ ) of injections during intra-assay studies. As expected, less reproducibility was demonstrated in the inter-assay studies, which represents responses compiled over a 3-day period. Although long-term reproducibility was not studied in this proof of concept, our other studies with this same MCA system and similar phases has demonstrated good long-term reproducibility[146].

While the effects of changing column temperature in GC are widely established, the determination of how these changes would impact the MCAD response is of interest. Figure 32A displays the response of a single TBATS coated lever in the MCA sensor at three separate column temperatures 90°C, 105°C, and 130°C to a mixture containing only acetone and

**Table 9** The reproducibility (%RSD) of peak heights and peak areas are demonstrated for inter- and intra-day experiments. The concentration of analyte for each experiment was 200 mmol/L.

<b>Reproducibility of Peak Area / Reproducibility of Peak Height</b>								
	Intra-assay reproducibility				Inter-assay reproducibility			
	Pentane	Acetone	Ethanol	TCE	Pentane	Acetone	Ethanol	TCE
THPED	2.4/2.3	2.1/1.7	3.9/2.9	3.5/2.7	23.8/17.4	15.0/20.4	19.3/20.0	7.4/7.4
TBATS	2.2/2.7	3.2/1.2	4.0/2.4	3.8/2.3	19.4/10.7	21.9/22.7	23.0/20.5	9.6/9.6
Me $\beta$ CD	3.7/1.8	3.6/1.9	3.6/2.5	2.2/2.9	24.3/20.6	25.2/25.6	18.9/22.1	10.8/10.8

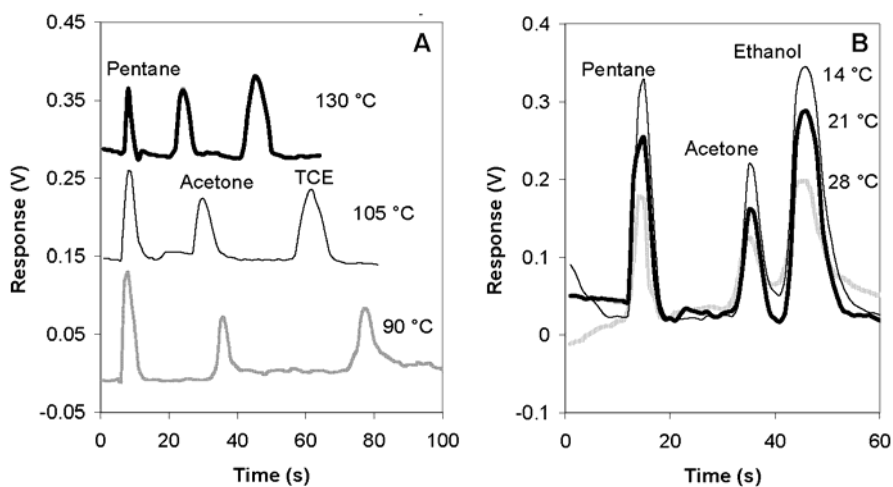


**Figure 32** Response of TBATS coated cantilever **[A]** to a mixture of pentane, acetone and TCE at three different column temperatures (90°C, 105°C, and 130°C) and **[B]** to a mixture of pentane, acetone and ethanol at three different array cell temperatures (14°C, 21°C, and 28°C) were studied to determine the effects of each parameter on the detection of each compound.

TCE in pentane. As expected, at the highest column temperature retention times are the smallest and as the column temperatures are decreased the retention times for each of the two compounds increased. There was only modest effect on the magnitude of response as the column temperature was altered. Thus, the effects of the column temperature on MCAD performance seem to be minimal.

When conducting GC experiments with hot gas flowing out of the column and with a MCAD connected to the end of the GC column, an important parameter to evaluate is temperature related changes in cantilever responses. The array flow cell used in these experiments not only allows for monitoring of the array flow cell temperature, but also control of that temperature by flowing cooled or heated water through a path in the brass body of the flow cell. Figure 32B shows the response of a single TBATS coated lever to a VOC mixture of acetone and ethanol in pentane separated by GC at different array flow cell temperatures. The temperature was altered from room temperature (21°C) to a lower temperature (14°C) and to a higher temperature (28°C, as monitored by a J type thermocouple). As the temperature of the array flow cell was increased to 28 °C the magnitude of response was decreased. However, as the temperature was decreased to 14°C the magnitude of response was largest. Other researchers have noted similar behavior of SAW sensors during temperature studies[163]. The increase in response at lower temperatures can be attributed, at least in part, to enhancements in the partitioning of the analyte into the RP on the active sides of the MCs as temperature is decreased. There maybe very slight increases in the tailing of the peaks at the lowest temperature (barely discernable in Figure 32B),

perhaps due to condensation. If that is an issue temperature programming of the flow cell itself (in addition to the column) may be beneficial.

The successful use of MCAs for informative qualitative and quantitative detection in GC requires that peak integrity (efficiency, symmetry etc.) for the separation be maintained during the detection process. The ability to distinguish between simple mixtures using MCA responses in conjunction with ANN methods has been established, however, and that may permit some loss in resolution with the MCAD approach without loss in the value of the detection approach. Peak volume issues are lessened for this initial report of hyphenating these techniques as we used a simple GC with a ¼" id packed column. With the system and conditions employed in this work, the TCD based peak volumes at the baseline were typically greater than 10 mL with an increase in peak volume for the MCAD mode of only 10-15% (data not shown). Band dispersion due to the volume of the connecting tubing and MCAD flow cell (totaling approximately 0.2 mL) should not be an issue with this large volume, packed column case. The experimental evidence of only small increases in peak volume and peak symmetry (MCAD versus TCD) also indicates that the internal volume in the GC plumbing after the TCD and the wash out characteristics of our flow cell are also not serious problems. The latter is discussed further below.

Data acquisition rates can also affect the ability of the detector to maintain peak integrity. The temporal widths of the peaks in this work were generally 10 seconds or greater at the baseline and the one Hz per cantilever acquisition rate did not seem to produce significant digitation-like distortion of the observed

peaks (see chromatograms herein). Moreover, the program delay and the number of A/D conversions that are averaged per datum could be easily altered (see Data Acquisition in Experimental Section) to increase the data acquisition rate to 10 Hz or greater in order to accommodate faster modes of GC separation. Whether flow cell volumes can be decreased and data acquisition rates increased sufficiently to meet the demands of small-bore capillary GC would need to be evaluated, and certainly would require the design of new MCAD systems.

The influence of flow rate on peak retention and profile parameters is presented in Table 10 for TCE. In addition to the digitation time issue discussed above, the ability of the RPs to equilibrate with the transient analyte band, and the translation of the induced stress caused by this into cantilever bending, are issues that could distort peak parameters. Peak heights should not depend on flow rate unless the MC can not keep up (sorption-desorption is too slow) with the transient band or the separation efficiency decreases with increasing flow. We expect to be in the resistance to mass transfer (C-term) dominated region of the operative van Deemter plate height plot under the conditions employed in this work.<sup>40</sup> Consequently, at the higher flow rate employed plate height is probably higher and analyte concentration at band center lower than at the slower flow rate. Both on-column efficiency and MCAD response kinetics may be causing the slightly higher peak heights at the faster flow rate (Table 10). Peak area should not depend on efficiency but should scale inversely with flow rate. The higher flow rate is not exactly the correct factor lower in area relative to the slow flow rate

**Table 10** The effects of column flow rate on GC-MCAD peak retention and profile parameters are given for TCE on two of the cantilevers

<b>RP</b>	<b>Flow Rate (ml/min)</b>	<b>Peak Height (V)</b>	<b>Peak Area</b>	<b>Adjusted Retention Time (s)</b>	<b>Efficiency (plates)</b>	<b>Asymmetry Factor</b>
THPED	35	0.018	0.18	98	530	1
THPED	65	0.019	0.11	52	410	1.2
Me $\beta$ CD	35	0.014	0.17	98	610	1.1
Me $\beta$ CD	65	0.016	0.11	52	430	1.3



(Table 10). This may simply relate to the inaccuracies in the manual treatment of the chromatograms for these parameters, particularly with different asymmetries observed at the two flow rates. The poor asymmetry factors at the higher flow rates (shorter temporal peak widths) could be due to some flow cell poorly swept areas or some pooling of RP on the MC surfaces. The flow cell in this case is low enough in volume, but it was not specifically designed for this application; the positioning of the inlet and outlet openings to the chamber holding the MCA are not conducive to efficient washout. The pooling of RP would exacerbate problems with slow sorption-desorption processes.

In summary, the facile coupling of a standard GC-TCD system and a MC sensor array for separation and detection of VOC mixtures is demonstrated. The MCA sensor displayed an excellent diversity in response of each sensing RP to the components of a VOC test mixture. PCA demonstrated that without separation, all of the components of a four component VOC mixture could not be identified with PCA alone. Calibration and reproducibility studies were performed to evaluate the performance of the MCAD. The array sensor demonstrated a linear response to varying concentrations over a range of two orders of magnitude. In addition to a linear response, the MCAD showed good intra-assay reproducibility with RSDs of peak area and peak height of 3 to 4%. Parameters such as GC column temperature, column flow rate, and flow cell temperature were studied and the MCAD was shown to maintain peak integrity reasonably well despite the fact that it was not modified for this application. The studies conducted herein represent a step forward in the elucidation of complex mixtures

using MCA sensors. It could be imagined that with the combination of pre-sensor separation, MCA detection, and pattern recognition of array response signatures, the components of complicated mixtures could be readily identified. Although not pursued in this proof of concept work, it should also be possible to take advantage of the diminutive size of MCAs to miniaturize and better integrate GC-MCAD systems.

## CHAPTER 6: CONCLUSIONS

In the field of MC sensors, great strides have been made in the development of detection schemes and strategies for increasing the sensitivity of the sensor. The research presented in this work represents strategies for enhancing the selectivity of MC sensors. Several different approaches were taken when attempting to improve the selectivity of the MC sensor. In chapter 2 research focused simply on demonstrating that MC sensors could be functionalized with thiolated SAMs. Once SAM formation was accomplished, these SAM coated cantilevers were used to detect metal ions in the liquid phase. Of particular importance, was the need to demonstrate that different thiolated ligand SAMs would respond differently to each metal ion. This fact was confirmed through the initial research, which not only demonstrated the moderate selectivity of SAMs to metal ions, but also the good sensitivity at which these metal ions could be detected.

The research detailed in chapter 2 paved the way for significant developments in MC sensor selectivity. The second phase of the research presented in chapter 3 represented the first time that MCAs were functionalized with SAMs having different ligand functionalities on one sensor chip. A capillary coating procedure was developed that allowed for individual coating of each cantilever. The ability to individually coat each cantilever gave rise to MCAs with each cantilever having a different ligand SAM. The MCA was exposed to different metal ions and the response signatures used in conjunction with pattern recognition algorithms to identify and quantitate the metal ion injected.

The metal ion array project demonstrated that by using an array and pattern recognition algorithms, a distributed selectivity could be generated in these MCAs. Another approach to producing selectivity in MC sensors was to couple the sensor to a chromatographic technique. By taking advantage of the ability of the chromatography to separate each analyte in a predictable manner, mixtures could be analyzed with the MC sensor. In addition to the selectivity enhancement given by a separation of components of a mixture, an MCA offering distributed selectivity could be used as the detector in chromatography allowing not only for measurement of a chromatographic peak, but identification of that peak. In an extension of the metal ion array research, the array used in this research was coupled to an IEC column for the separation and detection of metal ions. Unfortunately, an adequate flow cell was not designed that allowed for proper washout and sensitive detection of the metal ions after separation by an IEC column.

The second major division of research presented in chapter 4 of this work involves detection of analytes in the gas phase. In the first project related to gas phase detection, MCAs differentially coated with polymeric RPs by way of PVD. Small molecule gas phase analytes were detected by these polymer coated cantilevers, but the responses were similar for different gases. Experimental parameters such as temperature, humidity and injection methods were adjusted to determine if adjusting the parameters would impact the selectivity of the MCA response. In this work pattern recognition algorithms proved to be the most

significant means to differentiate between the responses of each gas phase analyte.

The final project detailed in chapter 5 of this work involved taking the former gas phase project a step further by invoking the use of GC to impart selectivity to the system. A standard GC system was connected to a flow cell housing a MCA and mixtures of VOCs were injected onto the GC column. The mixture was separated by the GC and detected by the MCA. The MCA showed good sensitivity to each analyte in the mixture. Pattern recognition algorithms were applied to the response signatures of each analyte and it was determined that all analyte's responses except for one analyte was significantly different from those of the other analytes tested. Demonstrating that chromatography coupled to pattern recognition algorithms would generate the largest amount of selectivity.

The research presented in this work presented interesting methods aimed at increasing the selectivity of MC sensors through a variety of approaches. The research presented represents one of many small steps that will be needed to push MC sensors to the forefront of sensor technology.

## **REFERENCES**

- [1] J. Janata, A. Bezegh, *Anal Chem*, 60 (1988) 62R.
- [2] V.M. Mecea, *Analytical Letters*, 38 (2005) 753.
- [3] G. Sauerbrey, *Zeitschrift fuer Physik*, 155 (1959) 206.
- [4] H. Wohltjen, R. Dessy, *Anal. Chem.*, 51 (1979) 1458.
- [5] H. Wohltjen, R. Dessy, *Anal. Chem.*, 51 (1979) 1465.
- [6] C. Mah, K.B. Thurbide, *Journal of Separation Science*, 29 (2006) 1922.
- [7] J.D.N. Cheeke, K. Shannon, Z. Wang, *Sensors and Actuators, B: Chemical*, B59 (1999) 180.
- [8] L.M. Dorozhkin, I.A. Rozanov, *Journal of Analytical Chemistry (Translation of Zhurnal Analiticheskoi Khimii)*, 56 (2001) 399.
- [9] F.T. Meehan, *Proc. Roy. Soc. (London)*, A115 (1927) 199.
- [10] D.J.C. Yates, *Proc. Roy. Soc. (London)*, A224 (1954) 526.
- [11] F.J. Norton, *Gas analyzing and control apparatus*, (General Electric Co.). US, 1943.
- [12] P.J. Shaver, *Review of Scientific Instruments*, 40 (1969) 901.
- [13] N.V. Lavrik, M.J. Sepaniak, P.G. Datskos, *Review of Scientific Instruments*, 75 (2004) 2229.
- [14] L.J.D. Frink, F. Van Swol, *Colloids and Surfaces, A: Physicochemical and Engineering Aspects*, 162 (2000) 25.
- [15] H. Ibach, *Journal of Vacuum Science & Technology, A: Vacuum, Surfaces, and Films*, 12 (1994) 2240.
- [16] R.E. Martinez, W.M. Augustyniak, J.A. Golovchenko, *Physical Review Letters*, 64 (1990) 1035.
- [17] R. Koch, *Journal of Physics: Condensed Matter*, 6 (1994) 9519.
- [18] R. Koch, *Applied Physics A: Materials Science & Processing*, 69 (1999) 529.
- [19] S. Alexander, L. Hellemans, O. Marti, J. Schneir, V. Elings, P.K. Hansma, M. Longmire, J. Gurley, *Journal of Applied Physics*, 65 (1989) 164.
- [20] G. Binnig, *Physical Review Letters*, 56 (1986) 930.
- [21] J.R. Barnes, R.J. Stephenson, M.E. Welland, C. Gerber, J.K. Gimzewski, *Nature (London)*, 372 (1994) 79.
- [22] E.A. Wachter, T. Thundat, *Review of Scientific Instruments*, 66 (1995) 3662.
- [23] R.d.S. Pereira, *Biochemical Pharmacology*, 62 (2001) 975.
- [24] A.M. Moulin, S.J. O'Shea, M.E. Welland, *Ultramicroscopy*, 82 (2000) 23.
- [25] T. Thundat, P.I. Oden, R.J. Warmack, *Microscale Thermophysical Engineering*, 1 (1997) 185.
- [26] H.G. Craighead, *Science (Washington, D. C.)*, 290 (2000) 1532.
- [27] R. Berger, C. Gerber, H.P. Lang, J.K. Gimzewski, *Microelectronic Engineering*, 35 (1997) 373.
- [28] R. Shuttleworth, *Proceedings of the Physical Society, London*, 63A (1950) 444.
- [29] G.G. Stoney, *Proc. Roy. Soc. Lond. (A)*, 82 (1909) 172.
- [30] J. Israelachvili, *Intramolecular and Surface Forces*, Academic Press, San Diego, CA, 1991.

- [31] N.V. Lavrik, C.A. Tipple, M.J. Sepaniak, P.G. Datskos, *Chemical Physics Letters*, 336 (2001) 371.
- [32] C.A. Tipple, N.V. Lavrik, M. Culha, J. Headrick, P. Datskos, M.J. Sepaniak, *Anal. Chem.*, 74 (2002) 3118.
- [33] D. Sarid, *Atomic Force Microscopy*, Oxford University Press, New York, 1991.
- [34] Y. Martin, C.C. Williams, H.K. Wickramasinghe, *Journal of Applied Physics*, 61 (1987) 4723.
- [35] G. Meyer, N.M. Amer, *Applied Physics Letters*, 57 (1990) 2089.
- [36] N. Abedinov, P. Grabiec, T. Gotszalk, T. Ivanov, J. Voigt, I.W. Rangelow, *Journal of Vacuum Science & Technology, A: Vacuum, Surfaces, and Films*, 19 (2001) 2884.
- [37] P.I. Oden, P.G. Datskos, T. Thundat, R.J. Warmack, *Applied Physics Letters*, 69 (1996) 3277.
- [38] Q.-M. Wang, L.E. Cross, *Ferroelectrics*, 215 (1998) 187.
- [39] R. Amantea, C.M. Knoedler, F.P. Pantuso, V.K. Patel, D.J. Sauer, J.R. Tower, *Proceedings of SPIE-The International Society for Optical Engineering*, 3061 (1997) 210.
- [40] C.L. Britton, R.L. Jones, P.I. Oden, Z. Hu, R.J. Warmack, S.F. Smith, W.L. Bryan, J.M. Rochelle, *Ultramicroscopy*, 82 (2000) 17.
- [41] R. Amantea, L.A. Goodman, F. Pantuso, D.J. Sauer, M. Varghese, T.S. Villani, L.K. White, *Proceedings of SPIE-The International Society for Optical Engineering*, 3436 (1998) 647.
- [42] G. Binnig, H. Rohrer, *IBM Journal of Research and Development*, 30 (1986) 355.
- [43] T.W. Kenny, W.J. Kaiser, J.A. Podosek, H.K. Rockstad, J.K. Reynolds, E.C. Vote, *Journal of Vacuum Science & Technology, A: Vacuum, Surfaces, and Films*, 11 (1993) 797.
- [44] L. Rottmann, K.G. Heumann, *Anal. Chem.*, 66 (1994) 3709.
- [45] A.G. Altenau, L.B. Rogers, *Anal. Chem.*, 36 (1964) 1726.
- [46] K. Sutton, R.M.C. Sutton, J.A. Caruso, *J. Chromatogr. A*, 789 (1997) 85.
- [47] S.J. Hill, T.A. Arowolo, O.T. Butler, S.R.N. Chenery, J.M. Cook, M.S. Cressar, D.L. Miles, *J. Anal. At. Spectrom.*, 17 (2002) 284.
- [48] S.W. Kang, C.M. Park, K.H. Cho, H.S. Han, *Bull. Korean Chem. Soc.*, 14 (1993) 59.
- [49] L.J.J. Janssen, L. Koene, *Chem. Eng. J.*, 85 (2002) 137.
- [50] E. Bakker, *Analytica Chimica Acta*, 350 (1997) 329.
- [51] T.S. Babu, J.B. Marder, S. Tripuranthakam, D.G. Dixon, B.M. Greenberg, *Environ. Toxicol. Chem.*, 20 (2001) 1351.
- [52] N.F. Starodub, N.I. Kanjuk, A.L. Kukla, Y.M. Shirshov, *Anal. Chim. Acta*, 385 (1999) 461.
- [53] M. Sarkar, M. Das, P.K. Datta, *J. Colloid Interface Sci.*, 246 (2002) 263.
- [54] D.A. Blake, R.M. Jones, R.C. Blake, A.R. Pavlov, I.A. Darwish, H.N. Yu, *Biosens. Bioelectron.*, 16 (2001) 799.



- [55] J.K. Gimzewski, C. Gerber, E. Meyer, R.R. Schlittler, *Chemical Physics Letters*, 217 (1994) 589.
- [56] N. Abedinov, P. Grabiec, T. Gotszalk, T. Ivanov, J. Voigt, I.W. Rangelow, *Journal of Vacuum Science & Technology a-Vacuum Surfaces and Films*, 19 (2001) 2884.
- [57] T. Thundat, E.A. Wachter, S.L. Sharp, R.J. Warmack, *Applied Physics Letters*, 66 (1995) 1695.
- [58] H.P. Lang, M.K. Baller, R. Berger, C. Gerber, J.K. Gimzewski, F.M. Battiston, P. Fornaro, J.P. Ramseyer, E. Meyer, H.J. Güntherodt, *Anal. Chim. Acta*, 393 (1999) 59.
- [59] R. Raiteri, H.J. Butt, M. Grattarola, *Electrochimica Acta*, 46 (2000) 157.
- [60] C.A. Tipple, N.V. Lavrik, M. Culha, J. Headrick, P. Datskos, M.J. Sepaniak, *Analytical Chemistry*, 74 (2002) 3118.
- [61] P.G. Datskos, S. Rajic, M.J. Sepaniak, N. Lavrik, C.A. Tipple, L.R. Senesac, I. Datskou, *Journal of Vacuum Science & Technology B*, 19 (2001) 1173.
- [62] R. Raiteri, G. Nelles, H.J. Butt, W. Knoll, P. Skladal, *Sensors and Actuators B-Chemical*, 61 (1999) 213.
- [63] A.M. Moulin, O.S. SJ, M.E. Welland, *Ultramicroscopy*, 82 (2000) 23.
- [64] K.M. Hansen, H.F. Ji, G.H. Wu, R. Datar, R. Cote, A. Majumdar, T. Thundat, *Analytical Chemistry*, 73 (2001) 1567.
- [65] C. Grogan, R. Raiteri, G.M. O'Connor, T.J. Glynn, V. Cunningham, M. Kane, M. Charlton, D. Leech, *Biosensors & Bioelectronics*, 17 (2002) 201.
- [66] P. Dutta, C.A. Tipple, N.V. Lavrik, P.G. Datskos, H. Hofstetter, O. Hofstetter, M.J. Sepaniak, *Analytical Chemistry*, 75 (2003) 2342.
- [67] J. Fritz, M.K. Baller, H.P. Lang, H. Rothuizen, P. Vettiger, E. Meyer, H.J. Guntherodt, C. Gerber, J.K. Gimzewski, *Science*, 288 (2000) 316.
- [68] G.H. Wu, H.F. Ji, K. Hansen, T. Thundat, R. Datar, R. Cote, M.F. Hagan, A.K. Chakraborty, A. Majumdar, *Proceedings of the National Academy of Sciences of the United States of America*, 98 (2001) 1560.
- [69] M. Sepaniak, P. Datskos, N. Lavrik, C. Tipple, *Analytical Chemistry*, 74 (2002) 568A.
- [70] R. Berger, C. Gerber, H.P. Lang, J.K. Gimzewski, *Microelectronic Engineering*, 35 (1997) 373.
- [71] M.K. Baller, H.P. Lang, J. Fritz, C. Gerber, J.K. Gimzewski, U. Drechsler, H. Rothuizen, M. Despont, P. Vettiger, F.M. Battiston, J.P. Ramseyer, P. Fornaro, E. Meyer, H.J. Guntherodt, *Ultramicroscopy*, 82 (2000) 1.
- [72] H.P. Lang, R. Berger, F. Battiston, J.P. Ramseyer, E. Meyer, C. Andreoli, J. Brugger, P. Vettiger, M. Despont, T. Mezzacasa, L. Scandella, H.J. Guntherodt, C. Gerber, J.K. Gimzewski, *Applied Physics a (Materials Science Processing)*, 66 (1998) S 61.
- [73] H.P. Lang, R. Berger, C. Andreoli, J. Brugger, M. Despont, P. Vettiger, C. Gerber, J.K. Gimzewski, J.P. Ramseyer, E. Meyer, H.J. Guntherodt, *Applied Physics Letters*, 72 (1998) 383.

- [74] P. Dutta, L.R. Senesac, N.V. Lavrik, P.G. Datskos, M.J. Sepaniak, *Sensor Letters*, 2 (2004) 1.
- [75] G.G. Stoney, *Proceedings of the Royal Society of London, A*, 82 (1909) 172.
- [76] N.V. Lavrik, C.A. Tipple, M.J. Sepaniak, P.G. Datskos, *Biomedical Microdevices*, 3 (2001) 33.
- [77] N.V. Lavrik, C.A. Tipple, M.J. Sepaniak, P.G. Datskos, *Chemical Physics Letters*, 336 (2001) 371.
- [78] J.J. Headrick, M.J. Sepaniak, N.V. Lavrik, P.G. Datskos, *Ultramicroscopy*, 97 (2003) 417.
- [79] P.G. Datskos, I. Sauers, *Sensors & Actuators B Chemical*, 61 (1999) 75.
- [80] T.A. Betts, C.A. Tipple, M.J. Sepaniak, P.G. Datskos, *Analytica Chimica Acta*, 422 (2000) 89.
- [81] H.-F. Ji, T. Thundat, R. Dabestani, G.M. Brown, P.F. Britt, P.V. Bonnesen, *Analytical Chemistry*, 73 (2001) 1572.
- [82] H.-F. Ji, E. Finot, R. Dabestani, T. Thundat, G.M. Brown, P.F. Britt, *Chemical Communications (Cambridge)* (2000) 457.
- [83] H.-F. Ji, T. Thundat, *Biosensors & Bioelectronics*, 17 (2002) 337.
- [84] S. Cherian, R.K. Gupta, B.C. Mullin, T. Thundat, *Biosensors & Bioelectronics*, 19 (2003) 411.
- [85] C. Grogan, R. Raiteri, G.M. O'Connor, T.J. Glynn, V. Cunningham, M. Kane, M. Charlton, D. Leech, *Biosensors & bioelectronics*, 17 (2002) 201.
- [86] J. Israelachvili, *Intermolecular and Surface Forces*, Academic Press, San Diego, 1991.
- [87] R. Zügler, J. Kambo-Dorsa, V.P.Y. Gadzekpo, *Talanta*, 61 (2003) 837.
- [88] H.-F. Ji, T. Thundat, *Biosensors & Bioelectronics*, 17 (2002) 337.
- [89] L.W. Chang, *Toxicology of Metals*, Lewis Publishers, Boca Raton, 1996.
- [90] L. Rottmann, K.G. Heumann, *Anal. Chem.*, 66 (1994) 3709.
- [91] A.G. Altenau, L.B. Rogers, *Anal. Chem.*, 36 (1964) 1726.
- [92] K. Sutton, R.M.C. Sutton, J.A. Caruso, *Journal of Chromatography, A*, 789 (1997) 85.
- [93] S.W. Kang, C.M. Park, K.H. Cho, H.S. Han, *Bulletin of the Korean Chemical Society*, 14 (1993) 59.
- [94] L.J.J. Janssen, L. Koene, *Chemical Engineering Journal (Amsterdam, Netherlands)*, 85 (2002) 137.
- [95] E. Bakker, *Analytica Chimica Acta*, 350 (1997) 329.
- [96] S.J. Hill, T.A. Arowolo, O.T. Butler, S.R.N. Chenery, J.M. Cook, M.S. Cresser, D.L. Miles, *Journal of Analytical Atomic Spectrometry*, 17 (2002) 284.
- [97] M. Sarkar, M. Das, P.K. Datta, *Journal of Colloid and Interface Science*, 246 (2002) 263.
- [98] T.S. Babu, J.B. Marder, S. Tripuranthakam, D.G. Dixon, B.M. Greenberg, *Environmental Toxicology and Chemistry*, 20 (2001) 1351.
- [99] N.F. Starodub, N.I. Kanjuk, A.L. Kukla, Y.M. Shirshov, *Analytica Chimica Acta*, 385 (1999) 461.

- [100] D.A. Blake, R.M. Jones, R.C. Blake, A.R. Pavlov, I.A. Darwish, H. Yu, *Biosensors & Bioelectronics*, 16 (2001) 799.
- [101] M.J. Sepaniak, P.G. Datskos, N. Lavrik, C.A. Tipple, *Anal Chem*, 74 (2002) 568A.
- [102] J.K. Gimzewski, C. Gerber, E. Meyer, R.R. Schlittler, *Chemical Physics Letters*, 217 (1994) 589.
- [103] T. Thundat, G.Y. Chen, R.J. Warmack, D.P. Allison, E.A. Wachter, *Anal. Chem.*, 67 (1995) 519.
- [104] H.P. Lang, M.K. Baller, R. Berger, C. Gerber, J.K. Gimzewski, F.M. Battiston, P. Fornaro, J.P. Ramseyer, E. Meyer, H.J. Guntherodt, *Analytica Chimica Acta*, 393 (1999) 59.
- [105] R. Raiteri, H.J. Butt, M. Grattarola, *Electrochimica Acta*, 46 (2000) 157.
- [106] R.N. Raiteri, G.; Butt, H. J.; Knoll, W.; Skladal, P, *Sensors and Actuators*, 61 (1999) 213.
- [107] K.M. Hansen, H.F. Ji, G. Wu, R. Datar, R. Cote, A. Majumdar, T. Thundat, *Anal Chem*, 73 (2001) 1567.
- [108] C. Grogan, R. Raiteri, G.M. O'Connor, T.J. Glynn, V. Cunningham, M. Kane, M. Charlton, D. Leech, *Biosensors & Bioelectronics*, 17 (2002) 201.
- [109] P. Dutta, C.A. Tipple, N.V. Lavrik, P.G. Datskos, H. Hofstetter, O. Hofstetter, M.J. Sepaniak, *Anal. Chem.*, 75 (2003) 2342.
- [110] J. Fritz, M.K. Baller, H.P. Lang, H. Rothuizen, P. Vettiger, E. Meyer, H. Guntherodt, C. Gerber, J.K. Gimzewski, *Science (New York, N.Y.)*, 288 (2000) 316.
- [111] G. Wu, H. Ji, K. Hansen, T. Thundat, R. Datar, R. Cote, M.F. Hagan, A.K. Chakraborty, A. Majumdar, *Proceedings of the National Academy of Sciences of the United States of America*, 98 (2001) 1560.
- [112] P. Dutta, P.J. Chapman, P.G. Datskos, M.J. Sepaniak, *Anal. Chem.*, 77 (2005) 6601.
- [113] N.V. Lavrik, C.A. Tipple, P.G. Datskos, M.J. Sepaniak, *Proceedings of SPIE-The International Society for Optical Engineering*, 4560 (2001) 152.
- [114] M.A. De Jesus, K.S. Giesfeldt, M.J. Sepaniak, *Applied Spectroscopy*, 57 (2003) 428.
- [115] R. Archibald, P. Datskos, G. Devault, V. Lamberti, N. Lavrik, D. Noid, M. Sepaniak, P. Dutta, *Analytica Chimica Acta*, 584 (2007) 101.
- [116] L.R. Senesac, P. Dutta, P.G. Datskos, M.J. Sepaniak, *Analytica Chimica Acta*, 558 (2006) 94.
- [117] C. Cortes, V.N. Vapnik, *Support Vector Networks, Machine Learning*, 20 (1995) 273.
- [118] V.N. Vapnik, *Statistical Learning Theory*, Wiley, New York, 1998.
- [119] C.A. Widrig, C. Chung, M.D. Porter, *Journal of Electroanalytical Chemistry and Interfacial Electrochemistry*, 310 (1991) 335.
- [120] M. Hara, Y. Saeki, N. Nomura, *Toyama Daigaku Kyoikugakubu Kiyo*, B: Rika-kei, 40 (1992) 43.
- [121] I.L. Bagbanly, I.K. Guseinov, A.K. Posadovskaya, S.I. Bagbanly, *Issled. Obl. Neorg. Fiz. Khim.* (1971) 218.

- [122] L. Chen, Z. Hu, Q. Wang, M. Liu, B. Fan, Z. Hu, Proc. Sino-West Ger. Symp. Chromatogr. (1983) 506.
- [123] J. Chwastowska, S. Szymczak, Chemia Analityczna (Warsaw, Poland), 14 (1969) 1161.
- [124] Z. Fang, J. Ruzicka, E.H. Hansen, Analytica Chimica Acta, 164 (1984) 23.
- [125] M. Griesbach, K.H. Lieser, Fresenius' Zeitschrift fuer Analytische Chemie, 302 (1980) 184.
- [126] M. Griesbach, K.H. Lieser, Fresenius' Zeitschrift fuer Analytische Chemie, 302 (1980) 181.
- [127] P. Janos, K. Stulik, V. Pacakova, Talanta, 38 (1991) 1445.
- [128] M.-C. Liu, B.-W. Fan, Z.-D. Hu, Gaodeng Xuexiao Huaxue Xuebao, 1 (1980) 61.
- [129] M. Lopez-Artiguez, A. Camean, M. Repetto, Atomic Spectroscopy, 17 (1996) 83.
- [130] A. Ono, N. Yamaguchi, R. Matsumoto, Bunseki Kagaku, 29 (1980) 644.
- [131] V.I. Orlov, A.A. Aratskova, A.R. Timberbaev, O.M. Petrukhin, Zhurnal Analiticheskoi Khimii, 47 (1992) 686.
- [132] N. Takai, T. Mizuno, Seisan Kenkyu, 39 (1987) 484.
- [133] J. Weiss, LaborPraxis, 11 (1987) 468.
- [134] J. Weiss, LaborPraxis, 11 (1987) 321.
- [135] D. Yan, G. Schwedt, Fresenius' Zeitschrift fuer Analytische Chemie, 327 (1987) 503.
- [136] A.A. Almeida, X. Jun, J.L.F.C. Lima, Analyst (Cambridge, United Kingdom), 123 (1998) 1283.
- [137] E. Santoyo, S. Santoyo-Gutierrez, S.P. Verma, Journal of chromatography. A, 884 (2000) 229.
- [138] J.M. Miller, Chromatography Concepts and Contrasts, John Wiley & Sons, New York, 2005.
- [139] M.F. L'Annunziata, Handbook of Radioactivity Analysis, Academic Press, Burlington, MA, 2003.
- [140] T. Thundat, R.J. Warmack, G.Y. Chen, D.P. Allison, Applied Physics Letters, 64 (1994) 2894.
- [141] A. Boisen, J. Thaysen, H. Jensenius, O. Hansen, Ultramicroscopy, 82 (2000) 11.
- [142] H.P. Lang, R. Berger, C. Andreoli, J. Brugger, M. Despont, P. Vettiger, C. Gerber, J.K. Gimzewski, J.P. Ramseyer, E. Meyer, H.J. Guntherodt, Applied Physics Letters, 72 (1998) 383.
- [143] H.P. Lang, R. Berger, F. Battiston, J.P. Ramseyer, E. Meyer, C. Andreoli, J. Brugger, P. Vettiger, M. Despont, T. Mezzacasa, L. Scandella, H.J. Guentherodt, C. Gerber, J.K. Gimzewski, Applied Physics A: Materials Science & Processing, 66 (1998) S61.
- [144] N. Fiedler, R. Laumbach, K. Kelly-McNeil, P. Liroy, Z.-H. Fan, J. Zhang, J. Ottenweller, P. Ohman-Strickland, H. Kipen, Environmental Health Perspectives, 113 (2005) 1542.

- [145] P.G. Datskos, S. Rajic, M.J. Sepaniak, N. Lavrik, C.A. Tipple, L.R. Senesac, I. Datskou, *Journal of Vacuum Science & Technology, B: Microelectronics and Nanometer Structures*, 19 (2001) 1173.
- [146] P. Dutta, L.R. Senesac, N.V. Lavrik, P.G. Datskos, M.J. Sepaniak, *Sensor Letters*, 2 (2004) 238.
- [147] B. Dhayal, W.A. Henne, D.D. Doorneweerd, R.G. Reifenberger, P.S. Low, *Journal of the American Chemical Society*, 128 (2006) 3716.
- [148] J.W. Grate, S.L. Rose-Pehrsson, D.L. Venezky, M. Klusty, H. Wohltjen, *Anal. Chem.*, 65 (1993) 1868.
- [149] M. Penza, G. Cassano, *Analytica Chimica Acta*, 509 (2004) 159.
- [150] R.E. Shaffer, S.L. Rose-Pehrsson, R.A. McGill, *Analytica Chimica Acta*, 384 (1999) 305.
- [151] T.A.P. Rocha Santos, A.C. Duarte, J.A.B.P. Oliveira, *Talanta*, 54 (2001) 383.
- [152] D. Williams, G. Pappas, *Field Analytical Chemistry and Technology*, 3 (1999) 45.
- [153] C.-J. Lu, J. Whiting, R.D. Sacks, E.T. Zellers, *Anal. Chem.*, 75 (2003) 1400.
- [154] H. Martens, T. Naes, *Multivariate Calibration*, John Wiley & Sons, New York, 1991.
- [155] I. Jolliffe, *Principal Component Analysis*, Springer, New York, 2002.
- [156] E. Malinowski, *Factor Analysis in Chemistry*, John Wiley & Sons, New York, 2002.
- [157] F. Vogt, K. Booksh, *Chemometric Methods for Data Analysis in Kirkothmer Encyclopedia of Chemical Technology*, John Wiley & Sons, New York, 2004.
- [158] W. Press, B. Flannery, S. Tuekolsky, W. Vettering, *Numerical Recipes in C++: The Art of Scientific Computing*, Cambridge University Press, Cambridge, UK, 2002.
- [159] J. Mandel, *American Statistician*, 36 (1982) 15.
- [160] A. Sen, M. Srivastava, *Regression Analysis: Theory, Methods, Applications*, Springer, New York, 1990.
- [161] N. Draper, H. Smith, *Applied Regression Analysis*, John Wiley & Sons New York, 1998.
- [162] S. Wiesberg, *Applied Linear Regression*, John Wiley & Sons, Hoboken, NY, 2005.
- [163] E.T. Zellers, M. Han, *Anal. Chem.*, 68 (1996) 2409.

## VITA

Peter James Chapman was born in Phoenixville, PA, on March 4<sup>th</sup>, 1981. He was raised in Wilmore, KY and went to grade school at Wilmore Elementary. He graduated junior high and high school from West Jessamine County High School in 1999. From there he went to Cumberland College where he earned his B.S. in chemistry in 2003.

Peter earned his doctorate in analytical chemistry at the University of Tennessee, Knoxville, TN, in May of 2008. Upon graduation he will begin a job as a PhD Advanced Development Chemist at Eastman Chemical Company.